2022

Chemical characterization of clastic cave sediments and insights into particle transport and storage in karst aquifers

Jill L. Riddell
West Virginia University, jlriddell@mix.wvu.edu

Chemical characterization of clastic cave sediments and insights into particle transport and storage in karst aquifers

Jill Leighanne Riddell

Dissertation submitted to the Eberly College of Arts and Sciences at West Virginia University

in partial fulfillment of the requirements for the degree of

Doctor of Philosophy
in
Geology

Dorothy J. Vesper, Ph.D., WVU, Chair
Christopher Russoniello, Ph.D., WVU
James Lamsdell, Ph.D., WVU
Louis M. McDonald, Ph.D., WVU
Ellen Herman, Ph.D., Bucknell University

Morgantown, West Virginia

Keywords: cave, sediment, karst, organic carbon, TOC, contaminant transport, microspheres, microplastics, sorption

Abstract

Chemical characterization of clastic cave sediments and insights into particle transport and storage in karst aquifers

Jill L. Riddell

Cave sediments can be divided into two groups: precipitates and clastics. Precipitates are speleothems, or lithologic or mineral features that are chemically precipitated in the cave environment. Clastic cave sediments are frequently described by depositional facies, sorting, and particle size (Bosch and White, 2004). Robust analytical chemical analyses of these sediments to quantify their physical and chemical components is rarely performed although some chemical characterization of mineralogy and paleomagnetism has become prevalent in recent years (Chess et al., 2010; Sasowsky et al., 2007). The organic carbon content of cave sediments can be representative of organic carbon concentrations in the larger karst system and concentrations of organic carbon in cave sediments can be used to estimate the potential retardation of organic contaminants through the entire karst system. The ability of karst sediments to be a sorbent for metals and organic contaminants, and store and transport contaminants is positively correlated with the amount of organic carbon in the sediment; yet these concentrations are rarely reported in karst sediments. This dissertation seeks to fill the gap in the mineralogy and chemical components of cave sediments; quantify the organic carbon content of cave sediments relative to depositional facies; and measure the adsorption of an organic microsphere onto a cave sediment to explore sediment-contaminant interactions.

A case study from Dropping Lick Cave in Monroe County, WV, is presented where a variety of analytical techniques were used to determine the active fraction (< 2mm) mineralogy and chemical components of the sediment The sediments were silt and sand-sized particles consisting of quartz, some clay or silicate minerals, dolomite, and amorphous materials. The particle size and total carbon was within the same range reported for the < 2mm fraction in other clastic cave sediments in this region, in the central United States, and in Puerto Rico. The preliminary mineralogy of the sediments is congruent with the mineralogy of surrounding siliciclastic rocks indicating that the source of the sediment is erosional products from nearby Peters Mountain and its slopes.

Particle size, TOC, and total nitrogen were measured in sediments representing different facies in Butler Cave, Virginia, USA. TOC concentrations ranged from 0.08 – 0.87 weight

percent and C:N molar ratio ranged from 3 – 15, indicating a possible terrestrial source of organic carbon in these sediments. TOC concentrations measured in Butler Cave were within the same range as those observed in above water, eogenetic clastic cave sediments from two caves in Puerto Rico. Estimated retardation factors calculated based on the TOC concentrations in the Butler Cave sediments indicate the range of TOC in this cave could be responsible for 39 – 987% increase in retardation of selected contaminants. This study highlights the importance of measuring the ranges of TOC in clastic cave sediments across different facies and their role in contaminant fate and transport. In this study,

The adherence of carboxylated and nonfunctionalized polystyrene microspheres onto a clastic cave sediment was quantified for microsphere dilutions in three water types – deionized water, a 25 mg/L $CaCO_3$ solution, and a karst spring water. Regardless of water type, both types of microspheres adhered to the sediment. Infrared absorbance data of different microsphere-solution-sediment mixtures indicated the potential presence of sediment minerals and microspheres in the solution. Analysis of solution pH and infrared spectra suggested pH and mineral constituents of the sediment are the most important factors in microsphere adherence. Using the adherence data, estimated K_{OC} values for both types of microspheres were calculated and were in the same ranges as phthalates, a known contaminant in karst aquifers that is also considered a plastic, like polystyrene. The chemical and physical commonalities between microspheres and organic and microplastic (MP) contaminants warrant further investigation of microspheres as a proxy for contaminants in sediment-contaminant experiments. The results of these experiments suggest that consideration of MPs adhered to sediments should be considered when quantifying MP contamination in karst systems.

Acknowledgements

This dissertation would not have been possible without the support and understanding of my advisor, Dr. Dorothy Vesper. Dorothy's mentorship throughout my pursuit of two degrees has developed me into the scientist and person I am today. She has always encouraged me to ask the hard questions, do the difficult tasks, and trusted my scientific judgement – especially when I didn't trust myself. More importantly, she was always willing to offer help and encouragement in times when I thought this dissertation would be impossible to finish. Dr. Vesper, thank you for everything. I would also like to thank my committee members Drs. McDonald, Herman, Russoniello, and Lamsdell for always offering scientific insight, guidance, and general life advice on this journey.

This research would not have been possible with the financial support of the West Virginia University Ruby Distinguished Doctoral Fellowship (thank you again to Dr. Vesper for nominating me), the NIEHS Superfund Research Project PROTECT, and the WVU Department of Geology and Geography. The Geology Department also gifted me with lifelong, invaluable friendships for which I will be forever grateful. Thank you, Autum, Shelby, Holly, Emily, Sofia, and Matt, for the love and laughs over the past five years.

Thank you to my family for encouraging me to always pursue my academic and professional interests, even when you didn't understand what I was doing or why I was doing it. Thank you to my dad Lonnie for instilling in me integrity and work ethic and to my mother Kathy for always telling me I could do or be whatever I wanted. Thank you to my sisters, Kelly and Sunny, for being beacons of reassurance and light on days when I wanted to give up.

Finally, a special thanks to my partner Corey who encouraged me to start this journey, never doubted me, and always made sure I had the resources necessary to do the best work possible. You've been my side through the highest highs and lowest lows during this pursuit and I truly could not have done it without you.

This work is dedicated to my sister Kelly and to Corey. For Kelly, who encouraged me to sign up for science club after school in junior high which started me on this path. And for Corey, who made sure I stayed on the path even when I wanted to leave it. Thank you for everything.

Table of Contents

Plato's "Allegory of the Cave" uses the concept of a cave to represent man's ignorance and unwillingness to become enlightened. The cave is darkness and only outside of the darkness, in the light, is truth and knowledge. He probably never imagined that the pursuit of knowledge would send some of us into that literal darkness.

After all…

"It takes a special point of view to see the same scientific value in a mud bank as in a cluster of stalagmites."
-William B. White

Introduction

The scientific exploration of cave systems dates to at least the 1680s with the first detailed geologic descriptions of caves in southern England (Shaw, 1992). Prior to the mid-1900s, cave-specific research was relegated to its contributions to other fields such as archaeology, geology and geography (Sasowsky and Mylroie, 2007). In recent history, cave science – or speleology – has sought to classify caves by size (depth and passage length), age, rock matrix, and structure (White, 1988). Contemporary cave science has begun to describe the geomicrobiology of caves (Barton and Jurado, 2007; E. Northup, 2001) and their ability to act as recorders of paleoenvironments (Hochstetler, 2006; Knapp et al., 2007; Musgrave and Webb, 2007; Sasowsky et al., 2007). Limestone caves, specifically, represent part of the larger karst landscape and provide a window to the karst system.

Karst landscapes are characterized by their solutional features and subterranean drainage systems which includes caves but also springs, sinkholes, and sinking streams (White, 1988). Aquifers can form in these systems. Due to the solutional nature, surface connectivity, and conduit flow of systems of karst systems, large amounts of water can be stored and transported in these aquifers. It is estimated that some 20% of the USA is underlain by karst features (Maupin and Barber, 2005) and some 25% of the world's population gets some amount of their drinking water from karst aquifers (Ford and Williams, 2007). Caves provide an interface with the karst aquifer and represent an intersection of the groundwater with the surface. Using caves as a proxy, the paleoclimate, hydrology, geomorphology, and storage and transport of water and sediment in the karst systems can be explored. Cave sediments offer a specific vehicle for exploring these topics.

Cave sediments can be divided into two groups: precipitates and clastics. Precipitates are speleothems, or lithologic or mineral features that are chemically precipitated in the cave environment. Clastics are sediments that have been transported into the cave from the surface or result from breakdown of the cave wall or rock matrix. These are the sediments that will be addressed in this dissertation. These sediments are often deposited in caves during high flow or threshold events and are left in place as karstification and continues and base levels are lowered. In some cases, entire passages can be filled with sediment. These can be discharged during subsequent (after deposition) threshold events or further processed by active streams. Clastic cave sediments are frequently described by depositional facies, sorting, and particle size (Bosch and White, 2004). Robust analytical chemical analyses of these sediments to quantify their physical and chemical components is rarely performed although some chemical characterization of mineralogy and paleomagnetism has become prevalent in recent years (Chess et al., 2010; Sasowsky et al., 2007).

The ability of karst sediments to act as a contaminant themselves, be a sorbent for metals and organic contaminants, and store and transport contaminants has long been recognized (Goeppert and Goldscheider, 2019; Loop and White, 2005; McCarthy and Zachara, 1989; Vesper et al., 2003). The adsorption of organic contaminants onto sediments and soil is positively correlated with the amount of organic carbon in the sediment yet these concentrations are rarely reported in karst sediments. The adsorption of these contaminants onto sediments can result in colloid-sized particles which can be stored or transported through a karst system depending on hydraulic condition (McCarthy and Zachara, 1989). The organic carbon content of cave sediments can be representative of organic carbon concentrations in the larger karst system. The concentrations of organic carbon in cave sediments can be used to estimate the potential retardation of organic contaminants through the system. Additionally, because cave sediments are abundant and ubiquitous, they can be used in laboratory experiments to explore their interactions with potential contaminants. Together, these analyses and experiments can provide insights into how sediments and particles interact and how particles are transported and stored in karst aquifers.

This dissertation contains three stand-alone manuscripts written for journal submission. Slight differences in formatting in each of the three chapters is due to the requirements of different target journals. The manuscripts seek to fill the gap in the mineralogy and chemical

components of cave sediments; quantify the organic carbon content of cave sediments relative to depositional facies; and measure the adsorption of an organic microsphere onto a cave sediment to explore sediment-contaminant interactions.

Chapter 1: Chemical characterization of clastic sediments from a cave in Monroe County, WV

This chapter represents a case study from Dropping Lick Cave in Monroe County, WV. Here, a composite sediment was collected where an active cave stream exits the cave passage. Sediments were collected from above the water. The composite sediment was subjected to six analytical techniques to quantify the particle size, mineralogy, elemental concentrations, and organic carbon content of the sediment. These parameters are not typically reported together, and the mineralogy of cave sediments remains unquantified in most caves. The selected techniques can be used to inform the interpretation of the results from the other techniques. The specific combination of techniques used here has, as far as the authors can determine, not been used on a composite clastic cave sediment previously. The data was compared to the known mineralogy of the surrounding lithologic units to speculate on the provenance of the clastic cave sediments.

Chapter 2: Total organic carbon concentrations in clastic cave sediments from Butler Cave, Virginia, USA: implications for contaminant fate and transport

In this chapter, the total organic carbon concentrations from two different cave sediment depositional facies were measured. Comparison of the organic carbon content across the facies provided insight into how the sediments are affected by depositional process. The organic carbon content of clastic cave and karst sediments is not well constrained; however, some comparison was possible to five other caves from the US, Puerto Rico, England, and Brazil. The organic carbon concentrations in Butler Cave were <1% but within the same range as reported in these other caves. Estimated retardation factors indicated that, even in low concentrations, this range of organic carbon could potentially result in an order of magnitude increase in retardation for selected contaminants.

Chapter 3: Adherence of nonfunctionalized and carboxylated polystyrene microspheres on a cave sediment: implications for organic contaminants and microplastics in karst systems

Here, the composite sediment characterized in Chapter 1, was used in batch adherence experiments with a polystyrene microsphere. Polystyrene microspheres have been used in tracer experiments in karst aquifers but resulted in exceptionally low recovery rates which were

attributed to adsorption of the microspheres onto mineral or components in the aquifer matrix. The adherence for two types of microspheres in three different water types was quantified. Both types of microspheres adhered to sediment in each water type and adherence was likely dominated by pH of the water, hydrophobicity of the structure of the polystyrene. Microsphere and sediment mixtures were also observed by scanning electron microscopy and spheres were observed on sediment surfaces. The choice of microsphere represents a potential proxy for organic contaminants and microplastics, as polystyrene is used in the manufacture of a variety of plastic and foam materials.

References

Barton, H. A., and Jurado, V., 2007, What's Up Down There? Microbial Diversity in Caves: Microbe, v. 2, p. 132-138.

Bosch, R. F., and White, W. B., 2004, Lithofacies and transport of clastic sediments in karstic aquifers, *in* Sasowsky, I. D., and Mylroie, J. E., eds., Studies of Cave Sediments: Physical and Chemical Records of Paleoclimate: New York, NY, Springer.

Chess, D. L., Chess, C. A., Sasowsky, I. D., Schmidt, V. A., and White, W. B., 2010, Clastic sediments in the Butler Cave -Sinking Creek System, Virginia, USA: Acta Carsologica, v. 39, no. 1, p. 17.

E. Northup, K. H. L. D., 2001, Geomicrobiology of Caves: A Review: Geomicrobiology Journal, v. 18, no. 3, p. 199-222.

Ford, D. C., and Williams, P. W., 2007, Karst Hydrogeology and Geomorphology, Hoboken, NJ, Wiley and Sons.

Goeppert, N., and Goldscheider, N., 2019, Improved understanding of particle transport in karst groundwater using natural sediments as tracers: Water Res, v. 166, p. 115045.

Hochstetler, B. I., 2006, Evolution of Clastic Cave Sediment Record Variability [Master of Science: The University of Akron, 298 p.

Knapp, E. P., Terry, D. O., Harbor, D. J., and Thren, R. C., 2007, Reading Virginia's paleoclimate from the geocheistry and sedimentology of clastic cave sediments, *in* Sasowsky, D. I. D., and Mylroie, J. E., eds., Studies of cave sediments: physical and chemical records of paleoclimate: New York, NY, Springer, p. 95 - 106.

Loop, C., M, and White, W., B, 2005, A Conceptual Model for DNAPL Transport in Karst Ground Water Basins: Groundwater, v. 39, no. 1.

Maupin, M. A., and Barber, N. L., 2005, Estimated withdrawsl from principal aquifers in the United States, 2000: Reston, VA, U.S. Geological Survey.

McCarthy, J. F., and Zachara, J. M., 1989, Subsurface transport of contaminants:mobile colloids in the subsurface environment may alter the transport of contaminants: Environmental Science and Technology, v. 23, no. 5, p. 7.

Musgrave, R. J., and Webb, J. A., 2007, Palaeomagnetic analysis of sediments on the Buchan Caves, Southeastern Australia, provides a pre-late Pleistocene date for landscape and climate evolution, *in* Sasowsky, I. D., and Mylroie, J. E., eds., Studies of cave sediments: physical and chemical records of paleoclimate: New York, NY, Springer, p. 47 - 70.

Sasowsky, I. D., Clotts, R. A., Crowell, B., Walko, S. M., LaRock, E. J., and Harbert, W., 2007, Paleomagnetic analysis of a long-term sediment trap, Kooken Cave, Huntingdon County, Pennsylvania, USA, *in* Sasowsky, I. D., and Mylroie, J. E., eds., Studies of cave sediments: physical and chemical records of paleoclimate: New York, NY, Springer, p. 71-82.

Sasowsky, I. D., and Mylroie, J. E., 2007, Studies of cave sediments: physical and chemical records of paleoclimate, New York, NY, Springer.

Shaw, T. R., 1992, History of cave science, Sydney Speleological Society, 338 p.:

Vesper, D., J, Loop, C., M, and White, W. W., 2003, Contaminant transport in karst aquifers: Speleogenesis and Evolution of Karst Aquifers, v. 1, no. 2, p. 11.

White, W. B., 1988, Geomorphology and Hydrology of Karst Terrains, New York, New York, Oxford University Press.

CHAPTER ONE

Chemical characterization of clastic sediments from a cave in Monroe County, West Virginia

Jill L. Riddell[1*] and Dorothy J. Vesper[1]

1 West Virginia University, Morgantown WV

*Corresponding author

ORC ID

Jill Riddell: 0000-003-3485-2896

Dorothy J. Vesper: 0000-0002-29607548

Target Journal: Journal of Cave and Karst Studies

Target Submission Date: August 2022

Abstract

The mineralogy and chemical components of clastic cave sediments are comparatively unknown when compared to other types of sediments or rocks. These sediments are ubiquitous in fluvial cave and karst aquifers. Previous studies on clastic cave sediments have focused on their role in the karstification process and their usefulness in providing a record of paleoclimate. The larger role of cave and karst sediments in contaminant fate and transport is an emerging area of study, especially with regard to organic contaminants and microplastics. However, the microscopic surface chemical interactions of clastic cave sediments with contaminants cannot be fully understood without quantifying the mineralogy and chemical components of the sediments. Here, a case study from Dropping Lick Cave in Monroe County, WV, is presented where a variety of analytical techniques were used to determine the active fraction (< 2mm) particle size, total and organic carbon, elemental chemistry, and mineralogy of a composite sample from two sediment banks near the access point of the cave at land surface. The sediments were mostly silt and sand-sized particles consisting of quartz, some clay or silicate minerals, dolomite, and amorphous materials. The particle size and total carbon was within the same range reported for the < 2mm fraction in other clastic cave sediments in this region, in the central United States, and in Puerto Rico. The preliminary mineralogy of the sediments is congruent with the mineralogy of surrounding siliciclastic rocks indicating that the source of the sediment is erosional products from nearby Peters Mountain and its slopes. This investigation illustrates the importance in using different analytical techniques to describe sediment mineralogy and the greater role this data has in exploring clastic cave sediment chemistry.

Keywords clastic, cave sediments, mineralogy, karst, West Virginia

Highlights A case study of the chemical and physical characteristics of the clastic sediments from a cave in Monroe County, WV, using multiple analytical techniques revealed high concentrations of quartz and low concentrations of carbonate, silicate, and clay minerals. The results indicate the provenance of the sediment is Peters Mountain. This work has implications for the origins of clastic sediments in caves, illustrates the importance of robust analytical techniques in cave sediment chemistry, and has implications for particle transport and storage in karst systems.

1.0 Introduction

Cave sediments can be divided into two groups- precipitates, or those sediments that are chemically precipitated inside the cave, also called speleothems and clastics, or those sediments that are transported into the cave from the surface or resultant from the breakdown of the cave matrix (Bosch and White, 2004; Hochstetler, 2006; Sasowsky, 2007; Springer, 2019). The mineralogy and formation of speleothems has been extensively studied (Cacchio et al., 2004; Davis et al., 1991; Dhami et al., 2018; Dreybrodt, 1999; Ercole et al., 2007; Melim et al., 2008; Melim et al., 2001; Northup et al., 2000) but the mineralogy and chemical components of clastic cave sediments has received comparatively less attention. Clastic cave sediments play an important role in the hydrology and karstification of cave systems, preserving paleoclimate records, and providing insight into past geomorphological processes that contributed to cave development (Asanidze et al., 2017; Bosch and White, 2004; Chess et al., 2010; Hart, 2021; Hochstetler, 2006; Lane et al., 2018; Sasowsky, 2007; Springer, 2019; Springer and Kite, 1997). Identifying and quantifying the chemical components and the provenance of clastic cave sediments is paramount in understanding the overall role of these sediments in karst processes.

Clastic cave sediments are an amalgam of minerals, amorphous materials, and natural organic matter. Clastic sediments that enter the cave from the surface are transported and deposited by the cave fluvial system. Sediments can be mobile or immobile depending on grain size and hydraulic conditions (Mahler, 1999; Sasowsky, 2007). Sediments can enter a cave system through injection at sinkholes or sinking streams or by percolation through the overlying soil and epikarst layers (Bosch and White, 2004; Sasowsky, 2007). Sediment injection can be gradual (like percolation) or episodic due to threshold events like floods and hurricanes. During these events, large amounts of sediment can be mobilized into cave systems and existing sediments can be re-mobilized and ejected at springs or other karst-surface interfaces (Doehring and Vierbuchen, 1971; Herman et al., 2008; Mahler et al., 1998a; Mahler et al., 2007; Mahler et al., 1998b). During speleogenesis, passages can experience pipe-full flow and become filled with sediment during threshold events. These sediments can then be transported or reprocessed during baseflow. As karstification continues and the base level is lowered, conduits can become abandoned and the sediment deposits within them preserve a record of the last depositional environment (Schmidt, 1982).

Clastic cave sediments are often described physically in-situ based on their grain size and sorting. A facies classification exists to describe these facies and is based on various facies description from sedimentology, glaciology, and other cave systems (Bosch and White, 2004; Gillieson, 1986; Pickle, 1985; Springer and Kite, 1997). The facies are backswamp, thalweg, slackwater, channel, and diamicton and are best described by Bosch and White (2004). Briefly, backswamp facies are fine grained, poorly sorted, and show minimal stratification; thalweg facies are large grained and well sorted; slackwater facies are fine grained, well-sorted clays and silts with some stratification; channel facies are moderately sized, moderately well sorted silts and sands that are deposited and re-worked by active cave streams; and diamicton facies are chaotic injections of sediments that exhibit very little sorting and contain a large range of grain sizes. These sediments are less frequently described chemically, and chemical analyses of their components has been limited to paleomagnetic signatures (Chess et al., 2010; Hochstetler, 2006; Knapp et al., 2007; Musgrave and Webb, 2007; Sasowsky et al., 2007), x-ray diffraction on select minerals or grain sizes (Chess et al., 2010; Lynch et al., 2007), and isotopic signatures (Hart 2021).

Sediment deposits in caves can be considered "data repositories" (Sasowsky and Mylroie, 2007) as caves represent environments that are protected from surface erosional and degradation processes. Clastic sediments from caves in Australia and Pennsylvania, Virginia, and West Virginia, USA, have all been dated using paleomagnetic techniques to date sediments to the last paleomagnetic reversal, 780,000 ya. In Butler Cave, VA, USA, sediments with reverse polarity were overlain by sediments with normal polarity indicating deposition during two periods of opposing polarity, one within 780,000 years and one at least 990,000 ya (Chess et al., 2010). In northern Monroe County, WV, the paleomagnetic signatures of clastic cave sediments from Scott Hollow Cave and Hunt Cave had normal polarity while in a third nearby cave, Union Cave, sediments exhibited reverse polarity (Hochstetler, 2006), indicating deposition during two different polarities. In Bathers Cave, VA, USA, (Knapp et al., 2007) and Buchan Caves, Australia, (Musgrave and Webb, 2007) clastic sediments had normal polarity and, in conjunction with other evidence, indicated much more recent deposition. In Kooken Cave, PA, USA, normal polarity and observations of the stratigraphic section of clastic cave sediments indicate deposition within the last 1,000 – 10,000 years (Sasowsky et al., 2007). Quantitative mineralogy by x-ray diffraction (qXRD) has been employed to determine the provenance of clay minerals in

Barton Springs (part of the Edwards Aquifer) in TX, USA (Lynch et al., 2007). This study found that the origin of the clay minerals in the clastic karst sediments were from soil some ten kilometers away from the spring discharge rather than the aquifer matrix or overlying soil and lithologic units (Lynch et al., 2007). Isotopic signatures from a clastic sediment in Capshaw Cave, TN, USA employed cesium isotopes and total lead concentrations to determine that urbanization in the area since the 1960s lead to increased flooding and decreased sedimentation rates (Hart, 2021).

Clastic cave sediments are ubiquitous in fluvial cave and karst systems. Previous research has illustrated the importance of clastic cave sediments in recreating paleoclimatic conditions, determining the origin of sediments, and understanding anthropogenic effects on cave and karst systems. Yet, few studies have combined robust analytical chemical analysis of a single clastic deposit to thoroughly quantify its components. The mineralogy and chemical components of soils, surface sediments, and rock types has long been pursued by geologists as a fundamental characterization of different geologic media, yet this characterization has been largely ignored for clastic cave sediments. A detailed characterization of clastic cave sediments using multiple techniques will provide greater insight into the origins and transport of clastic sediments in caves.

This study seeks to begin to fill that gap by presenting a case study from Dropping Lick Cave in Monroe County, WV. Clastic sediments were collected from two banks near where the cave passage emerges at the surface and the cave stream exits the cave passage. These sediments were combined to create a single composite sample of the sediments in the entrance of the cave. The < 2mm fraction of sediments were analyzed for particle size, total carbon, and preliminary mineralogy using qXRD, EDS, and FTIR analyses. The sediments were mostly silt and sand sized particles consisting of quartz, some clay or silicate minerals, dolomite, and amorphous materials. The < 2mm fraction of the composite sample had particle size and total carbon in the same range reported for the active fraction of other clastic cave sediments in this region (Riddell et. al., unpublished – Chapter Two of this dissertation). The preliminary mineralogy of the sediments is congruent with the mineralogy of surrounding siliciclastic rocks indicating that the source of the sediment is erosional products from nearby Peters Mountain and its slopes. This investigation illustrates the importance in using different analytical techniques to describe

sediment mineralogy and the greater role these data have in exploring clastic cave sediment chemistry.

2.0 Site description and sample collection

Dropping Lick Cave, also called McClung Zenith Cave (WVASS, 2017), was chosen for this analysis due to previous characterization of sediments from this cave; the abundance of clastic sediments in the cave; and the relative ease of access compared to other caves in the region. Dropping Lick Cave is located in southern Monroe County, WV (Fig. 1a). Monroe County is in two physiographic provinces of the Appalachian Mountains, the Appalachian Plateau and the Valley and Ridge. The Appalachian Plateau Province occupies the northern and western portion of the county, and the Valley and Ridge occupies the eastern and southern part of the county (Sturms, 2008). In Monroe County, these two provinces are delineated by the St. Clair thrust fault (Fig. 1b) which represents the boundary of the Allegheny structural front (Sturms, 2008). The fault also creates the ridge of Peters Mountain in the far southeastern section of the county. The thrust fault and subsequent weathering of overlying units resulted in the exposure of Ordovician dolostone and limestone units. Whereas in the Appalachian Plateau section, the exposed limestone units are the Mississippian Greenbrier Group (WVASS, 2017). These different units and structural settings create two distinct karst regions in Monroe County. The Valley and Ridge karst region is structurally constrained by the St. Clair thrust fault and Peters Mountain. The caves and springs in this region receive recharge by runoff from the slopes of Peters Mountain as well as direct recharge from precipitation (Bausher, 2018; Richards 2006).

Dropping Lick Cave is in the Ordovician-aged carbonates of the Valley and Ridge karst region. The karst forming unit in this area is the Beekmantown Group which has a lithology of dolostone and limestone interbedded with chert. The outcrop of the Beekmantown Group (O_b) in this region is approximately 40 miles long and contains 52 documented caves and 23 springs (WVASS, 2017). Dropping Lick Cave is a single passage, linear cave with approximately 1,500 ft. of mapped passage (WVASS, 2017) and is formed along east trending joints at N-50-W (WVASS, 2017). The cave is characterized by an active cave stream, which flows WSW (Fig. 1c). A dye-trace from Evelyn Miller Cave, one mile ENE of Dropping Lick Cave, was detected in Dropping Lick Cave (WVASS, 2017). The cave passage eventually reaches the surface at a limestone cliff and the stream continues underground at the base of the cliff (Fig. 1c). The stream resurges at Dropping Lick Spring approximately 70 feet east of the cliff. The cliff serves as the

point of access into Dropping Lick Cave. There is sediment deposition and breakdown throughout the cave (Fig. 1c). The clastic sediments were likely transported or deposited by the stream during alternating periods of high and low flow.

Clastic sediments were collected from two sediment banks near the cliff entrance of the cave (Fig. 2) and composited to create a single representative sediment. The first bank was approximately eight feet tall, and sediment was collected from the top of the bank where it meets the cave ceiling and from the bottom three feet of the bank (Fig. 2a). The second bank was not measured for height but was observed to be taller than the first. Sediment was collected from approximately the middle of the bank down to the cave stream (Fig 2b, c). All sediments were above of the active cave stream at the time of sampling. Sediments were air dried in a dark room for ~72 hours and combined by gentle breaking part of clumps, grinding in an agate mortar and pestle, and sieving to < 2mm. This process was chosen to minimize chemical alteration of the sediments while simultaneously creating a uniform sediment with which to conduct experiments and analyses.

3.0 Analytical methods

Sediment samples were subjected to six analytical methods (particle size analysis, quantitative mineralogy, dissolved element chemistry, infrared spectroscopy, total carbon analysis, and elemental dispersive spectroscopy) to quantify the physical and chemical components of the active fraction (< 2mm). This size fraction is sometimes referred to as the "fine-earthed fraction" (Owens and Rutledge, 2005) and contains sand, silt, and clay-sized particles. This fraction controls the physical properties and chemical behavior of sediment and soils due to increased surface area relative to the coarse fraction, > 2 mm (Hillel, 2008). The sand (0.02 – 2 mm) and silt (0.002 – 0.02 mm) fractions are dominated by primary minerals from the parent material and commonly consist of quartz, feldspars, and zircons (Hillel, 2008). The clay-size particles (< 0.002 mm) typically consist of secondary minerals which include aluminosilicates and hydrated oxides. Bulk and surface chemical analyses of the composite sediment provide data on the mineralogy, elemental distributions, and organic components of the sediment. Using multiple analytical techniques provides a more robust characterization of the sediment as the results from each technique can be used to inform the interpretation of the results from the other techniques.

3.1 Physical characterization: particle size analysis and quantitative mineralogy

Particle size analysis provides a volume percent of each particle size group in a sample, in this case sand, silt, and clay sizes. Quantitative mineralogy by x-ray diffraction (XRD) analyzes the crystalline structure of a sample to identify the presence of different crystalline materials, in this case minerals. When combined, particle size and quantitative mineralogy provide insights into the dominant minerals in a sediment sample. Although typically dominated by quartz, other minerals exist in the sample. The relative distribution of particle size can be an aid when analyzing mineralogical data of a sample since different minerals exist in different size fractions (Hillel, 2008; Owens and Rutledge, 2005).

Nine replicates of the composite sediment were analyzed for particle size of the < 2 mm fraction. The replicates were further air-dried in a fume hood, mixed in a 1:1.5 sediment to 5% Calgon® mass ratio solution, and shaken on a rotary shaker for ~24 hours at 70 rotations per minute (RPM). Particle size was measured at Bucknell University on a Beckman Coulter single wavelength LS13-320 particle size analyzer measuring from 0.4 μm – 2,000 μm. The raw data were organized in R and processed using the GRADISTAT program (Blott and Pye, 2001) to determine the volume percent of sand, silt, and clay in each replicate.

Six replicates of the cave sediment were analyzed for preliminary quantitative mineralogy using XRD. Samples were analyzed in bulk at the Stanford Synchrotron Light Source (SSRL) beamline 11-3 at Stanford University in Stanford, California. Samples were ground to < 50 μm via milling with zirconium oxide ceramic ball mill for twenty minutes and mixed with a corundum internal standard in a 1:4 mass ratio. The XRD data were collected in transmission mode at wavelength 0.9765 Å and calibrated using a lanthanum hexaboride standard. Data were converted from synchrotron wavelengths to Cu-Kα radiation. Mineral percentages were quantified using X'Pert HighScore Plus (Malvern PANAnalytical) software using Rietveld refinement. Mineral percentages were then normalized to exclude the corundum standard.

3.2 Bulk chemical characterization: digested elemental concentrations, infrared spectroscopy, and total carbon

Bulk analysis of the elemental concentrations of the composite sample can be used to support the quantitative mineralogical analysis. From these data, molar ratios such as Ca:Mg can be calculated which are useful in determining if calcite or dolomite is the dominating carbonate mineral in the sample. Elemental concentrations can also be used to identify any trace elements

or the relative portions of elements that are common in secondary mineral structures like Si, Al, Fe, Ca, and K. Infrared spectroscopy is commonly used to identify vibrational modes of covalent bonds in organic materials. Recent research has employed Fourier transform infrared spectroscopy (FTIR) to identify covalent bond vibrations of minerals in sediments and clay (Craddock et al., 2017; Jozanikohan and Abarghooei, 2022). Total carbon analysis provides a preliminary determination of the type of carbon in a sample (organic or inorganic) as well as the relative abundance of each type of carbon. These analyses provide further insight into the organic and inorganic components of the sediment and support the interpretation of the mineralogical data.

Eight replicates of the homogenized sediment were analyzed for digested element chemistry following an Aqua Regia digestion. Approximately three grams of the composite < 2mm sediment were digested in an Aqua Regia solution (a 1:3 ratio of reagent grade nitric and hydrochloric acid). The resulting aqueous material was filtered through 1-µm Whatman filtered and diluted to 100 mL using 0.5 M nitric acid. Samples were analyzed at Geoscience Laboratories (GeoLabs) in Sudbury, Ontario, CA and analyzed for major elements using inductively-coupled plasma atomic-emission spectroscopy (ICP-AES) according to method IAL-100. Elemental concentrations were reported in parts per million (ppm).

Four replicates of the solid sieved sediments were freeze dried and mixed in a 1:200 sample to KBr ratio for Fourier transform infrared spectroscopy (FTIR) on a Nicolet Magna-IR 560 spectrometer at the University of Arizona. Pure KBr was used as background. Samples were pressed into pellets and scanned across the spectral range of 400 – 4, 000 cm^{-1} in transmittance mode. Transmittance was converted to absorbance using OMNIC processing software and peaks were identified using the same software. IR band assignments were given based on reported band assignments in spectroscopy, sedimentology, and mineralogy literature.

Seven replicates of the homogenized sediment were oven-dried at 60 C for 24 hours for analysis of total carbon (TC) and total inorganic carbon (TIC) at the University of Florida Stable Isotope Mass Spectroscopy Laboratory in Gainesville, Florida. TC and TIC were measured on a Carlo Erba NA 1500 CNHS elemental analyzer and TOC was calculated as the difference in TC and TIC. All parameters are reported as weight percent (wt %) sample.

3.3 Surface chemical characterization: energy dispersive X-ray spectroscopy

Energy dispersive x-ray spectroscopy (EDS) uses an x-ray technique to determine the elemental composition of the surface material. This technique quantifies different elements in a sample and can be used to interpret the presence of oxide coatings or different minerals in a sample. Unlike the ICP-AES analysis which provides bulk elemental data, this technique only provides information about the surface of a sample.

Back-scattered electron images (BSE) and element chemistry via EDS were collected from the sediments on a Hitachi S-4800 cold-field emission gun scanning electron microscope (FE-SEM) equipped with a Thermo-Noran Si(Li) EDS spectrometer at the Kuiper Imaging Facility at the University of Arizona in Tucson, AZ. An accelerating voltage of 15.0 kV and a working distance of 8 mm were used to obtain BSE images and EDS maps of the sediment. Samples were freeze dried and coated in 5 nm of platinum by ion sputter to generate conductivity. EDS is reported in wt % and atomic % of identified elements from atomic number six (carbon) and up – the technique cannot identify light elements, like hydrogen. Because of this, EDS is considered qualitative or semi-quantitative.

This combination of analytical techniques provides a robust characterization of the chemical components of the composite sediment as each technique can aid in the interpretation of the results of another. The strength of this characterization allows for an intensive investigation into the provenance of the sediments in Dropping Lick Cave.

4.0 Results

4.1 Physical characterization

The particle size analysis of the active fraction of the bulk sediment had only sand and silt size particles, no clay size particles were detected in any of the replicates (Fig. 3). The samples were classified as poor to poorly sorted. Sand sized particles ranged from 34.9 – 60.5% and silt size particles ranged from 39.4 – 65.0% (Table 1). Samples with less than 50% sand were classified as very fine sandy very coarse silts and samples with greater than 50% sand were classified as very coarse silty very fine sand.

Quantitative XRD analysis identified quartz, dolomite, K-feldspar (orthoclase), and amorphous material in each of the six replicates. Chlorite was identified in four out of the six replicates and calcite was identified in one replicate. Quartz was the dominant mineral in each

sample, contributing 52.3 – 77.1% of each sample, followed by amorphous material (5.86 – 35.1%), and dolomite (3.7 – 9.11%). The low percentages of dolomite and lack of calcite identified in the analysis is consistent with the known sources of clastic sediments – material derived from outside of the cave environment with only minor contributions from cave breakdown. The large percentage of sand-sized particles and the geology (and thus weathering products) of surrounding rock units (shales, limestones with chert, and sandstones) supports the existence of weathered quartz grains in these samples.

4.2 Chemical characterization

The digestion method for major element chemistry detected 33 total cations, although many of these were only detected in one replicate. The elements of interest (Al, Ca, Fe, K, Mg, Si, and Ti) were detected in all eight replicates. These elements are the most abundant elements in common rock forming minerals and sedimentary rocks and will be the focus of the discussion. Although Na is among the most common elements in earth's crust and in rock forming minerals, it was not detected in any replicate by this analysis. The most abundant elements detected by this method were Al, Mg, and Ca, followed by K and Si, and finally Fe and Ti (Table 1). The range of concentration among the replicates was low and standard deviations were an order of magnitude smaller than the average concentration of each element.

In total 21 IR absorbance bands were identified among the replicates. However, every band was not identified in every sample, thus, only bands that were identified in three or more samples will be analyzed here, leaving thirteen bands (Table 2). The mixed nature of the sediment sample (inorganic minerals, amorphous material, and NOM) makes band assignment and identification challenging, especially without standard mineral data. Yet, the low organic carbon wt % indicate the samples are mostly inorganic so a mineralogical interpretation of the FTIR data will be presented for the "fingerprint region", or those bands occurring between 600 – 1500 cm^{-1} (Nandiyanto et al., 2019; Socrates, 2001). Each sample had a strong band at approximately 1024 cm^{-1} with shoulders at 1070 cm^{-1}, 1000 cm^{-1}, and 913 cm^{-1} (Fig. 4). A doublet is observed at 798 cm^{-1} and 778 cm^{-1} which is common in the quartz IR spectra (Bandopadhyay, 2010; Bertaux et al., 1998). Together, these bands represent Si-O stretching associated with quartz or silicate minerals (Bandopadhyay, 2010; Bertaux et al., 1998; Jozanikohan and Abarghooei, 2022; Madejova, 2002; Nayak and SIngh, 2007). Bands at 913 cm^{-1}, 694 cm^{-1}, and 669 cm^{-1} (Fig. 2) possibly represent Al-OH, Al-O, Si-bending (Bertaux et al., 1998; Nandiyanto et al., 2019)

which may correspond to the presence of clay and silicate minerals in the samples. Bands at 3698 cm^{-1}, 3621 cm^{-1}, and 3380 cm^{-1} represent O-H stretching in the interlayer of the silicate minerals (Farmer, 2000). Bands at 1623 cm^{-1} may represent the bending of water molecules or iron and aluminum hydroxides (amorphous materials, Socrates, 2001). A prominent band is also observed at 1384 cm^{-1} and may represent C-N stretching or atmospheric CO_2 (Socrates, 2001). Overall, the peaks observed in these spectra indicate the presence of quartz and silicate clay-forming minerals which is supported by the qXRD data. The characteristic IR peaks of calcite and dolomite were not observed in these spectra (Hsiao et al., 2019; Ji et al., 2009).

Concentrations of TC, TOC, and TIC ranged from 1.07 – 1.18 wt %, 0.57 – 0.91 wt %, and 0.16 – 0.60 wt %, respectively (Table 1). TOC ranges reported for these sediments are within the same range as those reported for other clastic cave sediments (Bottrell, 1996; de Paula et al., 2020; de Paula et al., 2016; Downey, 2020; Panno et al., 2004). Reaction time of the TIC analyses indicated that dolomite or another slow reacting carbonate was present (J. Curtis, personal communication, March 23, 2020) in the samples which is consistent with the dolostone containing rock unit in which the cave formed.

The SEM-EDS method detected a total of sixteen different elements in six different sediment images ranging in magnification from 5,000x – 7,000x. These sediments were contaminated with a known carbon-based particle; thus carbon was excluded from the interpretation of the results. In this analysis, Ti was detected in only one sample whereas in the digestion method, Ti was detected in every sample (Table 1). Na was detected in this analysis but not in the digested analysis. The most abundant element detected in by this technique was Si, followed by Al, Fe, K, Mg, Ca, and Ti. Here, concentrations had a much larger range and standard deviations than the digested method. Standard deviations were often on the same order of magnitude as concentration for some elements. EDS maps of a representative replicate show some correlation in the concentration of Al, Si, and K (Fig. 5) which may indicate the presence of some aluminosilicate or other clay mineral.

5.0 Discussion

5.1 Chemical components of the clastic sediments

The composite sediment sample from Dropping Lick Cave consists mostly of quartz grains with some dolomite, clay or aluminosilicate minerals, and amorphous material also

present. This is supported by the results of the grain size analysis where the replicates were in the silt and sand size range. The digested elemental data identified Al, Ca, and Mg as the most abundant elements, not Si, indicative of the limitation of this method to characterize samples with quartz. The EDS data did identify Si as the most abundant element with Al, Fe, and K as the next most abundant elements. This supports the qXRD findings that quartz is the most abundant mineral in this sediment. The other elements support the presence of secondary minerals and/or amorphous materials like aluminosilicates or hydrated Fe or Al oxides. The infrared spectroscopy analysis identified IR bands consistent with quartz and potentially hydroxide minerals. The carbon content of this sediment is less than 2 wt % and is represented by organic and inorganic carbon. The analysis suggested the presence of dolomite or other slow reacting carbonates. These data can be compared to mineralogical and chemical data from the surrounding rock units to interpret the potential source of the clastic sediments in Dropping Lick Cave.

5.2 Potential sources of clastic sediments

Clastic sediments in caves and karst systems are injected into the system from the surface via sinking streams and sinkholes or percolate through the overlying soils and epikarst into the system. The sediment transported during these processes is largely a result of erosion of rock units higher in the stratigraphic section than the karst-bearing units. In the Appalachian Plateau and Valley and Ridge provinces, these rocks are often sandstones and shales which form the ridges (whereas the limestone and carbonate rocks form the valleys). In the case of Dropping Lick Cave, the clastic sediments are likely a mixture of eroded material from the surrounding units. The Beekmantown Group (O_b), the unit in which Dropping Lick Cave is formed, is one of the oldest rock units in the area. It is an Ordovician-aged dolomite or dolostone with interbedded chert nodules. Above it lies two more layers limestone – the New Market Limestone (O_{nm}) and Trenton Black River Limestone (O_{tbr}). The carbonate units in this sequence were deposited in a shallow to ocean/carbonate bank setting. The siliciclastic units in this sequence consist of the Reedsville Shale (O_r) and two sandstones that create the slopes and resistant caprocks in the area – the Juniata Sandstone (O_{jo}) and the resistant quartz-rich Tuscarora Sandstone (S_t, S_{tc}), Fig. 6. and forms the ridge of Peters Mountain. These carbonate and shale units were deposited in a shallow sea or terrestrial environment as the paleo-sea receded and a series of orogenies began. These units have been subjected to low degrees of metamorphism due to folding and faulting

during mountain building. Although extensive mineralogical and petrological investigations do not exist for each unit listed above, a general description of their mineralogy can provide clues to the source of the clastic sediments in Dropping Lick Cave and the potential mineralogy present in these sediments.

The mineralogy of the Beekmantown group is mostly dolomite (Sturms, 2008), a carbonate rock with chemical formula $CaMg(CO_3)_2$, with interbedded chert nodules which is a silica (SiO_2) rich microcrystalline rock. The Ca:Mg ratio of elements in sediment, rock, and water is often used to determine if the carbonates present are more dolomitic or more calcitic. A dolomitic chemical signature will have Ca:Mg ~ 1 whereas a calcitic chemical signature will have Ca:Mg >>> 1. For Dropping Lick Cave Ca:Mg ratios were calculated from the digestion method elemental data. Ca:Mg ratios ranged from 0.85 – 0.95 with an average value of 0.89 ± 0.03. These ratios, indicate the presence of dolomite in the sediments which is likely a weathering product of the Beekmantown Group and overlying carbonate units. The qXRD data identified calcite in only one of the replicates and dolomite was identified in every replicate, but at small ranges, 3.70 – 9.11 wt %. Further, the total carbon analysis revealed very low weight percent of total carbon (1.07 – 1.18 wt %), the majority of which was organic carbon. Inorganic carbon, which is assumed to be carbon associated with carbonate minerals, contributed only 0.16 – 0.60 wt % and the analysis indicated that dolomite or another slow reacting carbonate was present. Finally, in the FTIR analyses of these data, the signature peaks of dolomite and calcite were absent. Thus, the dominate carbonate mineral in these clastic sediments is dolomite.

The mineralogy of the Reedsville Shale has been described throughout its outcroppings in Pennsylvania and through the analyses of core data. An XRD analysis of outcrops of this formation in Pennsylvania found an average of 36.6 wt % quartz, 32.30 wt % muscovite, and 6.42 wt % chlorite (Cooney, 2013). The lithology and mineralogy of the Juniata Sandstone is a graywacke, consisting mostly of siliciclastic rock grains, quartz, clay minerals – possibly illite or chlorite, iron oxides, and feldspar (Blue, 2011; Thompson, 1969; Weaver, 1953). The Tuscarora sandstone is variable throughout the entire Appalachian Mountain Range, but in West Virginia it presents as a sandstone or quartzite matrix and is primary ridge-former throughout the Valley and Ridge (Folk, 1960). Mineralogically, this portion of the Tuscarora is nearly purely quartz (Folk, 1960). Lower portions of the Tuscarora and some portions of the Reedsville shale have

been documented as containing some hematite (Folk, 1960; Weaver, 1953) and occasionally some minor feldspar grains (Folk, 1960).

The sediments in this study contained an average of 67.2% quartz, 4.29% chlorite, and 5.55% K-feldspar according to the qXRD analysis. The FTIR analysis had peaks consistent with the Si-O stretch and bend of quartz and silicate minerals. The major element chemistry done by EDS identified Si as the most abundant element in the images scanned, however the major element chemistry done by digestion identified Al and Ca as the most abundant minerals. Combined, these analyses and mineralogy of the surrounding rock units indicate that the erosion of silica rich rocks like chert, shales, and sandstones are contributing measurable amounts of quartz to the clastic sediment in Dropping Lick Cave. Small amounts of clay minerals are also present and may account for the concentrations of Al, Fe, and K observed in the major element chemistry.

The soils in Monroe County may be contributing some clay minerals to the clastic sediments in Dropping Lick Cave. The soil series that overlay the lithologic units on Peters Mountain and its slopes are the Frederick and Dunmore series, the Litz series, and the Murrill colluvial series (USDA, 1965). These soils are classified as various types of loams and are noted for the large rock fragments they contain (USDA, 1965). The soils have low organic carbon concentrations and carbonates, but thin clay films have been observed (USDA, 1965). The soil overlying the Beekmantown Group is the Dunmore and Bodine series (USDA, 1965). These are well drained cherty soils where the clay material is high in kaolinite. Although clay sized particles were not identified in the particle size analyses and the clay mineral identified in the qXRD analyses was chlorite, the overlying soils may be contributing some clay material to the clastic sediments. The identification of chlorite in the qXRD analyses may be due to the presence of amorphous materials disrupting the XRD pattern of the < 10 Å clays and the error in the Reitveld refinement technique (personal communication, Dr. B. Moravec, July 26, 2019).

The EDS maps show some corresponding areas of K, Al, and Si which supports the potential presence of some clay mineral in these sediments. Both the qXRD data analysis and the FTIR analysis both indicated the presence of amorphous materials. Amorphous materials in soils and sediments are frequently in the form of Fe and Al hydroxides. The oxidized state of these elements ($Fe^{3+,}$ $Al^{3+)}$ form the semi-solid material $Fe(OH)_3$ and $Al(OH)_3$ in aqueous

environments. These materials could have formed when the clastic sediments interacted with the cave stream or other water source during their transport or deposition.

The clastic sediments of Dropping Lick Cave contain mostly quartz that is likely an erosional product of the surrounding siliciclastic rock units. Small amounts of clay and silicate minerals are also present and likely also resultant from the erosion of the siliciclastic rock units or soils. The presence of small amounts of dolomite are derived from the breakdown of the cave matrix. Amorphous materials are also present and could have formed from the interaction of the sediment with the cave stream.

5.3 Comparison to other Valley and Ridge caves

A previous study by Shokri (2017) characterized the physical and chemical properties of several cave sediments in Monroe County and other parts of southern West Virginia. Dropping Lick Cave was a part of this study. Particle size analysis of the sediments collected during that study had approximately 9% clay, 38% silt, and 50% sand. The 2017 study used a wet sieving method to separate sand and larger sized particles and only silt and clay sized particles were analyzed in the same way as the sediments described in the current study. However, in both studies, the particle size of the sediments was majority sand, regardless of method.

Concentrations of Ca, Mg, Fe, and Mn in Dropping Lick Cave from the 2017 study were 0.22 mol/L, 0.24 mol/L, 0.27 mol/L, and 4.9 x 10^{-4} mol/L, respectively. Ca, Fe, and Mg were within the same order of magnitude as the averages reported in the current study, but Al was much higher in the current study than in 2017. Average molar ratios of Ca:Mg from the 2017 in Dropping Lick Cave were 0.89, the same as the average reported here. This is strong evidence that dolomite is the dominant carbonate mineral in these clastic sediments. Although Ca:Mg ratios never reach 1 in either study, small amounts of Mg from other clay minerals are also likely present in the aqueous digestions analyses which decreases the overall ratio.

Miss Effie Cave is another cave that was included in the 2017 study and is near Dropping Lick Cave with similar geology. It is also located in the Beekmantown Formation. Particle size data from Miss Effie Cave had 6% clay, 23% silt, and 70% sand making these sediments slightly sandier than the sediments observed in Dropping Lick. Concentrations of Ca, Mg, Fe, and Al in Miss Effie Cave were 0.12 mol/L, 0.15 mol/L, 0.24 mol/L and 4.1 x 10^{-4} mol/L as determined by digestion. Overall these are lower than the concentrations observed at Dropping Lick in 2017 or this current study, especially Al. This could be due to different preparations and analysis

methods of the sediment in the two different studies. The Ca:Mg molar ratio at Miss Effie Cave was 0.77 indicating another important source of Mg in these sediments besides dolomite. No mineralogical data was collected during the 2017 study so no comparisons or inferences can be made regarding mineralogy in these sediments.

A nearby cave in Bath and Highland Counties, VA that has been extensively studied and is similar in geology and formation to Dropping Lick Cave is Butler Cave. Butler Cave is formed in Helderberg Group, a Silurian- Devonian age limestone but is flanked by ridges that are also capped by the Tuscarora sandstone and slopes formed by shale and mudstone units (Swezey, 2017). Particle size data collected in the same method as the data presented here had 0 – 13% clay, 6 – 84% silt, and 16 – 91% sand (Riddell et al., unpublished). These sediments were collected from diamicton and channel depositional facies and with increasing distance for sediment input which is responsible for the large range of grain size percentages. These sediments have, generally, more clay than the Dropping Lick sediments but similar ranges of silt and sand. A mineralogical investigation of the Butler Cave sediments showed that the light fraction of sediments consisted predominantly of quartz and rock fragments and the heavy minerals consisted rom rutile, zircons, and iron oxides(Chess et al., 2010). Although rutile (TiO_2) was not observed in the Dropping Lick sediments, Ti was detected in some samples by the digestion method and on the EDS maps. This indicates that possibility of rutile in the Dropping Lick sediments. Zirconium was not detected in the digestion method of major element analysis in the Dropping Lick sediments but was detected on the EDS maps. Other investigations into cave sediment chemistry in Puerto Rico also detected zirconium (Downey, 2020). The origin of the sediments in Butler Cave was determined to be erosional products from the flank of the major mountain in the area, Jack Mountain, which is capped by the Tuscarora sandstone. The similar geology, grain size, and preliminary mineralogy of the clastic cave sediments of Dropping Lick also indicate their provenance is from erosional products related to the siliciclastic rocks in the region, namely Peters Mountain and the Tuscarora sandstone (Fig. 7a).

The transport of sediments in Dropping Lick Cave originates in at least Evelyn Miller Cave, as the cave stream has been traced to this cave by dye tracing. Sediments may also percolate through the epikarst layer. The composite sediment collected as part of this study is a representative of sediment that has been transported into the larger karst system and deposited at

the cave stream outlet. Figure 7b provides a schematic for the possible origins and transport of clastic sediments in Dropping Lick Cave.

6.0 Conclusions

The mineralogy and other chemical components of clastic cave sediments remains unquantified for many caves. The chemical and physical components of these sediments reveal details of their origins and transport which is essential to understanding how sediments and other particles are carried through karst systems. By using cave sediments as a proxy for understanding the large karst aquifer, detailed mineralogical analyses can be made which allows for the interpretation of the provenance of clastic sediments in caves. In this study, a combination of analytical techniques were used to quantify the particle size, mineralogy, elemental concentrations, and total carbon content of a composite clastic sediment from Dropping Lick Cave in Monroe County, WV. The qXRD analysis indicated quartz was the dominant mineral in the sediment and this was supported by FTIR analysis. Digested elemental analysis and EDS indicated the presence of elements that are common in silicate minerals and amorphous material which was supported by the qXRD data. The sediments had organic carbon concentrations in the same range for the < 2mm fraction as other clastic caves sediments in Virginia, USA (Riddell, unpublished) and Puerto Rico (Downey, 2020). This combination of analyses allowed for comparison to the lithologic and soil units that may be contributing to the injection of clastic sediments in Dropping Lick Cave. The provenance of these sediments are erosional products from Peters Mountain and its slopes with possibly minor contributions from overlying soil layers. Quartz is a relatively resistant to weathering compared to other minerals in the lithology and rock units in this area. Its dominance in these sediment samples suggests that other minerals have been eroded or weathered beyond detection or transported out of the cave system. This work illustrates the importance of using a combination of analytical techniques when analyzing cave sediments. Future work regarding cave sediments as a proxy for understanding sediment transport and storage in karst systems should consider the mineralogy and provenance of clastic sediments when interpreting the chemistry and mechanics of transport.

7.0 References

Asanidze, L., Chikhradze, N., Lezhava, Z., Tsikarishvili, K., Polk, J., and Chartolani, G., 2017, Sedimentological Study of Caves in the Zemo Imereti Plateau, Georgia, Caucasus

Region: Open Journal of Geology, v. 7, no. 4, p. 13. https://www.doi.org/10.4236/ojg.2017.74032

Bandopadhyay, A. K., 2010, Determination of quartz content for Indian coals using an FTIR technique: International Journal of Coal Geology, v. 81, no. 1, p. 6. https://www.doi.org/10.1016/j.coal.2009.10.018

Bausher, E. A., 2018, Qualitative and quantitative analysis of carbonate waters in the Peters Mountain Region of Monroe County, WV [Master of Science, 137 p. https://researchrepository.wvu.edu/cgi/viewcontent.cgi?article=4707&context=etd

Bertaux, J., Frohlich, F., and Ildefonse, P., 1998, Multicomponent analyss of FTIR spectra: quantification of amorphous and crystallized mineral phases in synthetic and natural sediments: Journal of Sedimentary Research, v. 68, no. 3, p. 8. https://doi.org/10.2110/jsr.68.440

Blott, S. J., and Pye, K., 2001, GRADISTAT: a grain size distribution and statistics package for the analysis of unconsolidated sediments: Earth Surface Processes and Landforms, v. 26, no. 11, p. 1237-1248. https://doi.org/10.1002/esp.261

Blue, C. R., 2011, Stratigraphic architecture and paleography of the Juniata Formation, Central Appalachians, Master of Science: Virginia Polytechnic Institute and State University, 117 p. https://vtechworks.lib.vt.edu/bitstream/handle/10919/31683/Blue_CR_T_2011.pdf?sequence=1&isAllowed=y

Bosch, R. F., and White, W. B., 2004, Lithofacies and transport of clastic sediments in karstic aquifers, *in* Sasowsky, I. D., and Mylroie, J. E., eds., Studies of Cave Sediments: Physical and Chemical Records of Paleoclimate: New York, NY, Springer.

Bottrell, S. H., 1996, Organic carbon concentrations profiles in recent cave sediments: Records of agricultrual pollution or diagenesis?: Environmental Pollution, v. 91, no. 3, p. 8. https://doi.org/10.1016/0269-7491(95)00064-x

Cacchio, P., Contento, R., Ercole, C., Cappuccio, G., Martinez, M. P., and Lepidi, A., 2004, Involvement of Microorganisms in the Formation of Carbonate Speleothems in the Cervo Cave (L'Aquila-Italy): Geomicrobiology Journal, v. 21, no. 8, p. 497-509. https://doi.org/10.1080/01490450490888109

Chess, D. L., Chess, C. A., Sasowsky, I. D., Schmidt, V. A., and White, W. B., 2010, Clastic sediments in the Butler Cave -Sinking Creek System, Virginia, USA: Acta Carsologica, v. 39, no. 1, p. 17. https://doi.org/10.3986/ac.v39i1.109

Cooney, M. L., 2013, The Utica Shale play in Pennsylvania: A characterization of the Reedsville, Anges, Utica, and Point Pleasant Formations, Bachelor's of Science: Allegheny College, 95 p.

Craddock, P. R., Herron, M. M., and Herron, S. L., 2017, Comparison of Quantitative Mineral Analysis By X-Ray Diffraction and Fourier Transform Infrared Spectroscopy: Journal of Sedimentary Research, v. 87, no. 6, p. 23. https://doi.org/10.2110/jsr.2017.34

Davis, D. G., Palmer, M. V., and Palmer, A. N., 1991, Extraordinary subaqueous speleothems in Lechuguilla Cave,New Mexico: The National Speleological Society Bulletin, v. 52, p. 70-86.

de Paula, C. C. P., Bichuette, M. E., and Seleghim, M. H. R., 2020, Nutrient availability in tropical caves influences the dynamics of microbial biomass: Microbiologyopen, v. 9, no. 7, p. e1044. https://doi.org/10.1002/mbo3.1044

de Paula, C. C. P., Montoya, Q. V., Rodrigues, A., Bichuette, M. E., and Seleghim, M. H. R., 2016, Terrestrial filamentous fungi from Gruta do Catão (São Desidério, Bahia, Northeastern Brazil) show high levels of cellulose degradation: Journal of Cave and Karst Studies, v. 78, no. 3, p. 208-217. https://doi.org/10.4311/2016mb0100

Dhami, N. K., Mukherjee, A., and Watkin, E. L. J., 2018, Microbial Diversity and Mineralogical-Mechanical Properties of Calcitic Cave Speleothems in Natural and in Vitro Biomineralization Conditions: Frontiers in Microbiology, v. 9. p. 22. https://doi.org/10.3389/fmicb.2018.00040

Doehring, D. O., and Vierbuchen, R. C., 1971, Cave development during a catastrophic storm in the Great Valley of Virginia: Science, v. 174, p. 3.

Downey, A. R., 2020, Physical and chemical properties of clastic sediments from two caves in the northern karst region of Puerto Rico, M.Sc. Graduate Theses, Dissertations, and Problem Reports: West Virginia University. 157 p.

Dreybrodt, W., 1999, Chemical kinetics, speleothem growth and climate: Boreas, v. 28, no. 3, p. 347-356. https://doi.org/10.1111/j.1502-3885.1999.tb00224.x

Ercole, C., Cacchio, P., Botta, A. L., Centi, V., and Lepidi, A., 2007, Bacterially Induced Mineralization of Calcium Carbonate: The Role of Exopolysaccharides and Capsular Polysaccharides: Microscopy and Microanalysis, v. 13, no. 01, p. 42-50. https://doi.org/10.1017/s1431927607070122

Farmer, V. C., 2000, Transvere and longitudinal crystal modes associated with OH stretching vibrations in single crystals of kaolinite and dickite: Spectrochimica Acta Part A, v. 56, p. 4. https://doi.org/10.1016/S1386-1425(99)00182-1

Folk, R. L., 1960, Petrography and origin of the Tuscarora, Rose Hill, and Keefer Formations, Lower and Middle Silurian of eastern West Virginia: Journal of Sedimentary Petrology, v. 30, no. 1, p. 58. https://doi.org/10.1306/74D709C5-2B21-11D7-8648000102C1865D

Gillieson, D., 1986, Caved sedimentation in the New Guinea Highlands: Earth Surface Processes and Landforms, v. 11, p. 11. https://doi.org/10.1002/esp.3290110508

Hart, E., 2021, Dating and interpretation of recent clastic sediments in an urban cave: Journal of Cave and Karst Studies, v. 83, no. 1, p. 20-28. https://doi.org/10.1002/esp.3290110508

Herman, E. K., Toran, L., and White, W. B., 2008, Threshold events in spring discharge: Evidence from sediment and continuous water level measurement: Journal of Hydrology, v. 351, no. 1, p. 98-106. https://doi.org/10.1016/j.jhydrol.2007.12.001

Hillel, D., 2008, Soil physical attributes, Soil in the Environment: Burlington, MA, Elsevier, p. 55 - 77. https://doi.org/10.1016/B978-0-12-348536-6.50010-1

Hochstetler, B. I., 2006, Evolution of Clastic Cave Sediment Record Variability, Master of Science: The University of Akron, 298 p.

Hsiao, Y.-H., Wang, B., La Plante, E. C., Pignatelli, I., Krishnan, N. M. A., Le Pape, Y., Neithalath, N., Bauchy, M., and Sant, G., 2019, The effect of irradiation on the atomic structure and chemical durability of calcite and dolomite: npj Materials Degradation, v. 3, no. 1, p. 1 - 9. https://doi.org/10.1038/s41529-019-0098-x

Ji, J., Ge, Y., Balsam, W., Damuth, J. E., and Chen, J., 2009, Rapid identification of dolomite using a Fourier Transform Infrared Spectrophotometer (FTIR): A fast method for identifying Heinrich events in IODP Site U1308: Marine Geology, v. 258, no. 1-4, p. 9. https://doi.org/10.1016/j.margeo.2008.11.007

Jozanikohan, G., and Abarghooei, M. N., 2022, The Fourier transform infrared spectroscopy (FTIR) analysis for the clay mineralogy studies in a clastic reservoir: Journal of

Petroleum Exploration and Production Technology, p. 14. https://doi.org/10.1007/s13202-021-01449-y

Knapp, E. P., Terry, D. O., Harbor, D. J., and Thren, R. C., 2007, Reading Virginia's paleoclimate from the geocheistry and sedimentology of clastic cave sediments, *in* Sasowsky, D. I. D., and Mylroie, J. E., eds., Studies of cave sediments: physical and chemical records of paleoclimate: New York, NY, Springer, p. 95 - 106.

Lane, S. B., Bishop, M. R., Dore, M. J., and Sasowsky, I. D., Scott Hollow Cave, *in* White, W. B., ed., Caves and Karst of the Greenbrier Valley in West Virginia, Springer International Publishing.

Lynch, F. L., Mahler, B. J., and Hauwert, N. N., 2007, Provenance of suspended sediment discharged from a karst aquifer determined by clay mineralogy, *in* Sasowsky, I. D., and Mylroie, J. E., eds., Studies of cave sediments: physical and chemical records of paleoclimate: New York, NY, Springer, p. 83 - 94.

Madejova, J., 2002, FTIR techniques in clay mineral studies: Vibrational Spectroscopy, v. 31, p. 1 - 10. https://doi.org/10.1016/S0924-2031(02)00065-6

Mahler, B. J., Bennett, P. C., and Zimmerman, M., 1998a, Lanthanide-labeled clay: a new method for tracing sediment transport in karst: Groundwater, v. 36, no. 5, p. 835 - 844. https://doi.org/10.1111/j.1745-6584.1998.tb02202.x

Mahler, B. J., Valdes, D., Musgroves, M., and Massei, N., Nutrient migration in carbonate aquifers in response to storms: a comparison of two geologically contrasting aquifers, *in* Proceedings 2007 GSA Denver Annual Meeting.

Mahler, B. J., Winkler, M., Bennett, P. C., and Hillis, D. M., 1998b, DNA-labeled clay: a sensitive new method for tracing particle transport: Geology, v. 26, no. 9, p. 831 - 834. https://doi.org/10.1111/j.1745-6584.1998.tb02202.x

Mahler, B. J. L., L; Bennett, P.C., 1999, Mobile sediment in an urbanizing karst aquifer: implications for contaminant transport: Environmental Geology, v. 39, no. 1, p. 14. https://doi.org/10.1007/S002540050434

Melim, L. A., Northup, D. E., Spilde, M. N., Jones, B., Boston, P. J., and Bixby, R. J., 2008, Reticulated filaments in cave pool speleothems: Microbe or mineral?: Journal of Cave and Karst Studies, v. 700, no. 3, p. 135-141. https://doi.org/10.7939/R3J38KZ7V

Melim, L. A., Shinglman, K. M., Boston, P. J., Northup, D. E., Spilde, M. N., and Queen, J. M., 2001, Evidence for microbial onvolvement in pool finger precipitation, Hidden Cave, New Mexico: Geomicrobiology Journal, v. 18, p. 311-329. https://doi.org/10.1080/01490450152467813

Musgrave, R. J., and Webb, J. A., 2007, Palaeomagnetic analysis of sediments on the Buchan Caves, Southeastern Australia, provides a pre-late Pleistocene date for landscape and climate evolution, *in* Sasowsky, I. D., and Mylroie, J. E., eds., Studies of cave sediments: physical and chemical records of paleoclimate: New York, NY, Springer, p. 47 - 70.

Nandiyanto, A. B. D., Oktiani, R., and Ragadhita, R., 2019, How to Read and Interpret FTIR Spectroscope of Organic Material: Indonesian Journal of Science and Technology, v. 4, no. 1, p. 22. https://doi.org/10.17509/ijost.v4i1.15806

Nayak, P. S., and SIngh, B. K., 2007, Instrumental characterization of clay by XRF, XRD, and FTIR: Bulletin of Materials Science, v. 30, no. 3, p. 4.

Northup, D. E., Dahm, C. N., Melim, L. A., Spilde, M. N., Crosse, L. J., Lavoie, K. H., Mallory, L. M., Boston, P. J., Cunningham, K. I., and Barns, S. M., 2000, Evidence of geomicrobiological interactions in Guadalupe Caves: Journal of Cave and Karst Studies, v. 62, no. 2, p. 80-90.

Owens, P. R., and Rutledge, E. M., 2005, Morphology, *in* Hillel, D., ed., Encyclopedia of Soils in the Environment: New York, NY, Elsevier, p. 511 - 520. https://doi.org/10.1016/B0-12-348530-4/00002-3

Panno, S. V., Curry, B. B., Wang, H., Hackley, K. C., Liu, C.-L., Lundstrom, C., and Zhou, J., 2004, Climate change in southern Illinois, USA, based on the age and δ13C of organic matter in cave sediments: Quaternary Research, v. 61, no. 3, p. 301-313. https://doi.org/10.1016/j.yqres.2004.01.003

Pickle, J. D., 1985, Dynamics of Clastic Sedimentation and Watershed Evolution Within a Low-Relief Karst Drainage Basin, Mammoth Cave Region Kentucky. Doctor of Philosophy: University of New Mexico.

Richards, B.G., 2006, Aqueous geochemistry of springs in Monroe County, WV, Master of Science in Geology, West Virginia University, p. 72.

Sasowsky, I. D., 2007, Clastic sediments in caves - imperfect recorders of processes in karst: Time in Karst, v. 1, p. 8.

Sasowsky, I. D., Clotts, R. A., Crowell, B., Walko, S. M., LaRock, E. J., and Harbert, W., 2007, Paleomagnetic analysis of a long-term sediment trap, Kooken Cave, Huntingdon County, Pennsylvania, USA, *in* Sasowsky, I. D., and Mylroie, J. E., eds., Studies of cave sediments: physical and chemical records of paleoclimate: New York, NY, Springer, p. 71-82.

Sasowsky, I. D., and Mylroie, J. E., 2007, Studies of cave sediments: physical and chemical records of paleoclimate, New York, NY, Springer.

Schmidt, V. A., 1982, Magnetostratigraphy of sediments in Mammoth Cave, Kentucky: Science, v. 217, p. 827 - 829.

Shokri, M., 2017, Determination of physiochemical characteristics of cave sediments for the assessment of the impact of electrokinetic remediation of karst groundwater, Master's of Science: West Virginia University, 96 p.

Socrates, G., 2001, Infrared and Raman characteristic group frequencies: tables and charts, West Sussex, England, Wiley and Sons.

Springer, G. S., 2019, Clastic sediments in caves, *in* White, W. B., Culver, D., and Pipan, T., eds., Encyclopedia of Caves, Elsevier, p. 277-284.

Springer, G. S., and Kite, J. S., 1997, River-derived slackwater sediments in caves along Cheat River, West Virginia: Geomorphology, v. 18, no. 2, p. 91-100. https://doi.org/10.1016/S0169-555X(96)00022-0

Sturms, J. M., 2008, Surficial mapping and kinematic modeling of the St. Clair Thrust Fault, Monroe County, West Virginia , Master of Science in Geology: West Virginia University, 91 p.

Thompson, A. M., 1969, Clay-mieral diagensis in redbed sequence, Juniata Formation, central Pennsylvania, AAPG Bulletin, Volume 53, American Association of Petroleum Geologists, p. 2. https://doi.org/10.1306/5D25C7CB-16C1-11D7-8645000102C1865D

USDA, S. C. S., 1965, Soil Survey, Monroe County, West Virginia, *in* Agriculture, U. S. D. o., ed., Volume 1960: Washington, D.C., U.S. Government Printing Office, p. 119.

Weaver, C. E., 1953, A lath shaped non-expanded dioctahedral 2:1 clay mineral: American Mineralogist, v. 338, no. 3-4, p. 11.

WVASS, 2017, The Caves and Karst of Monore County West Virginia: National Speological Society.

Acknowledgements

The authors would like to acknowledge Dr. Jon Chorover, Dr. Robert Root, Dr. Yaniv Olshansky, and Dr. Bryan Moravec, all of the University of Arizona, for their help in preparing and analyzing samples for FTIR, qXRD, and SEM-EDS analysis. We especially acknowledge Dr. Yaniv Olshansky and Dr. Robert Root for instruction and guidance on instrumentation. We would also like to acknowledge Autum Downey for her assistance in sample collection and processing the particle size data and Dr. Ellen Herman and the Bucknell University for allowing us to use their instrumentation.

Data availability

For the purposes for this dissertation, data can be found in Appendix A. Upon publication, data will be made publicly available in the GitHub repository for this project, https://www.gitbub.com/jlriddell12/DroppingLick

Author Declarations

This work was supported by the National Institute of Environmental Health Sciences Superfund Research Program project PROTECT (Puerto Rico Testsite for Exploring Contamination Threats) PTE Federal Award Number 5P42ES017198-12, the West Virginia University Ruby Distinguished Doctoral Fellowship, and the NIEHS KC Donnelly Externship program.

The authors have no relevant competing financial or non-financial interests to disclose.

All authors contributed to the study conception and design. Material preparation, data collection, and analysis were performed by Jill Riddell. The first draft of the manuscript was written by Jill Riddell and all authors commented on previous versions of the manuscript. All authors read and approved the final manuscript.

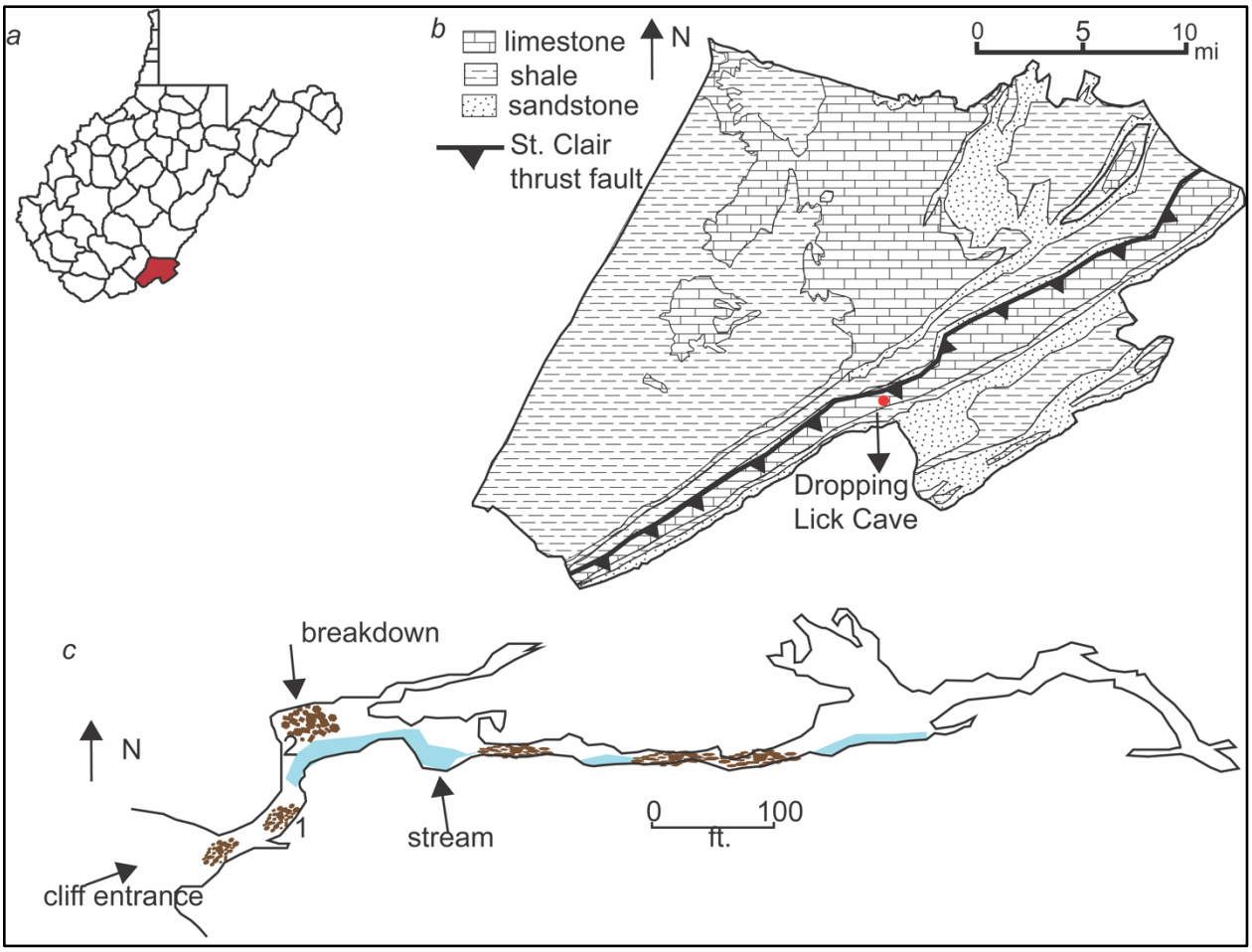

Fig. 1. Location of Monroe County, WV highlighted in red (a). Major lithologic units, thrust fault, and location of Dropping Lick Cave within Monroe County (b). Map of Dropping Lick Cave passage and stream. The stream often disappears under breakdown and reemerges. The stream sinks under the cliff entrance of the cave and emerges some distance west as a spring outside of the cave. Numbers 1 and 2 indicate where clastic samples were collected for this study (c).

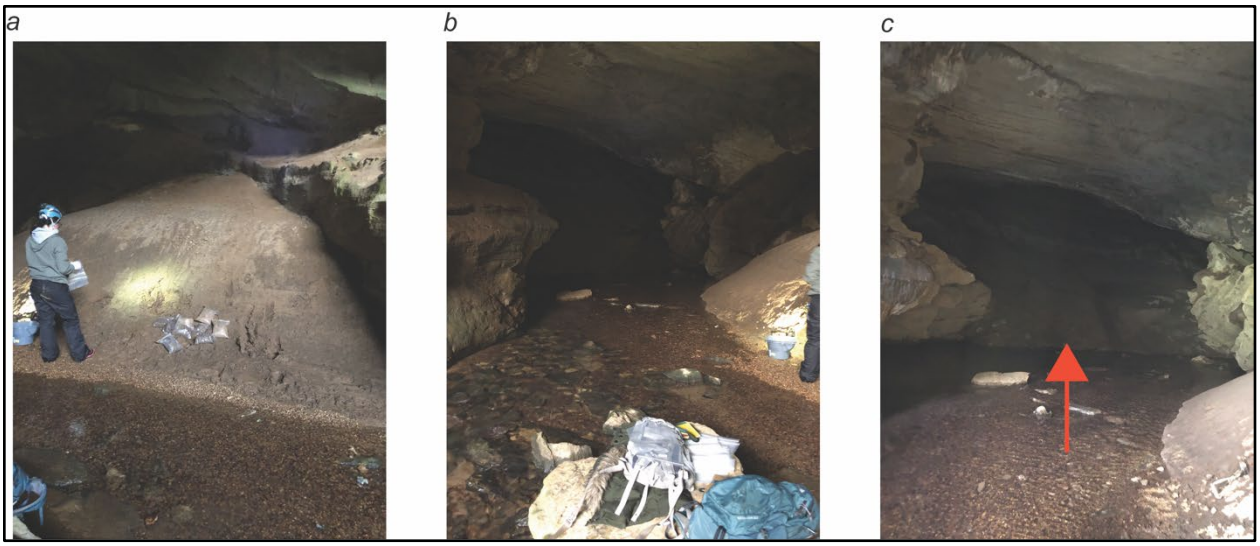

Fig. 2. Sampling location 1 in a clastic bank just inside the cliff entrance (a). Looking back from the cliff entrance toward sampling location two. The cave stream sinks below the cliff just behind the photographer (b). Sampling location two indicated by red arrow. Just to the right of this bank, the passage bends and becomes almost fully submerged by the cave stream (c).

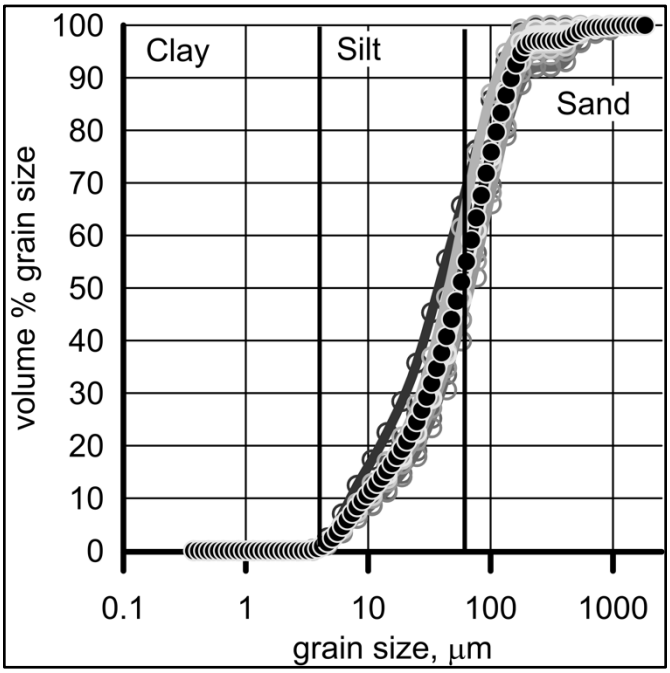

Fig. 3. Cumulative grain size of the nine replicates analyzed for particle size (< 2mm). The samples are mostly silt and sand sized. The darkest black circles indicate the average of the nine replicates. Grain size is plotted on a log scale.

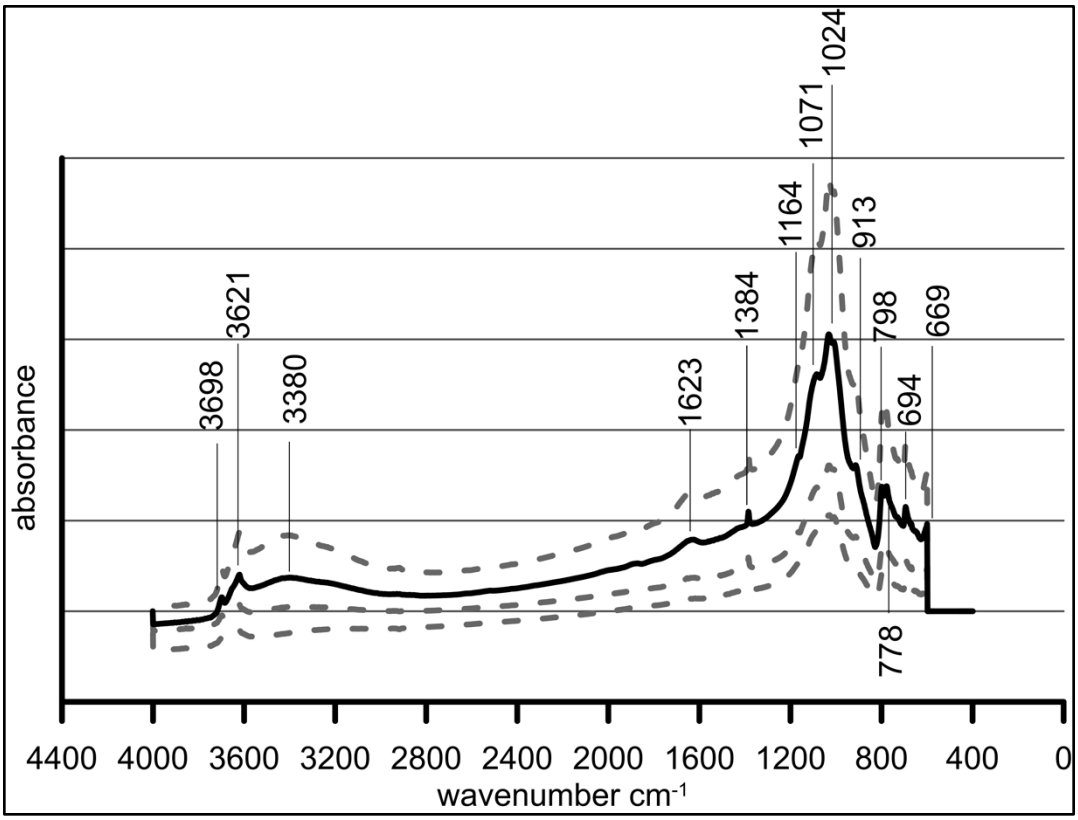

Fig. 4. Infrared spectra from the FTIR analyses of four replicates of the freeze dried and < 2mm sediment. The dotted lines represent the replicates (two replicates were nearly identical in results and plot on top of each other and are represented by the top dotted line). The solid line represents the average calculated absorbance at each wavenumber from the four replicates. Peaks identified by the OMNIC processing software are labeled.

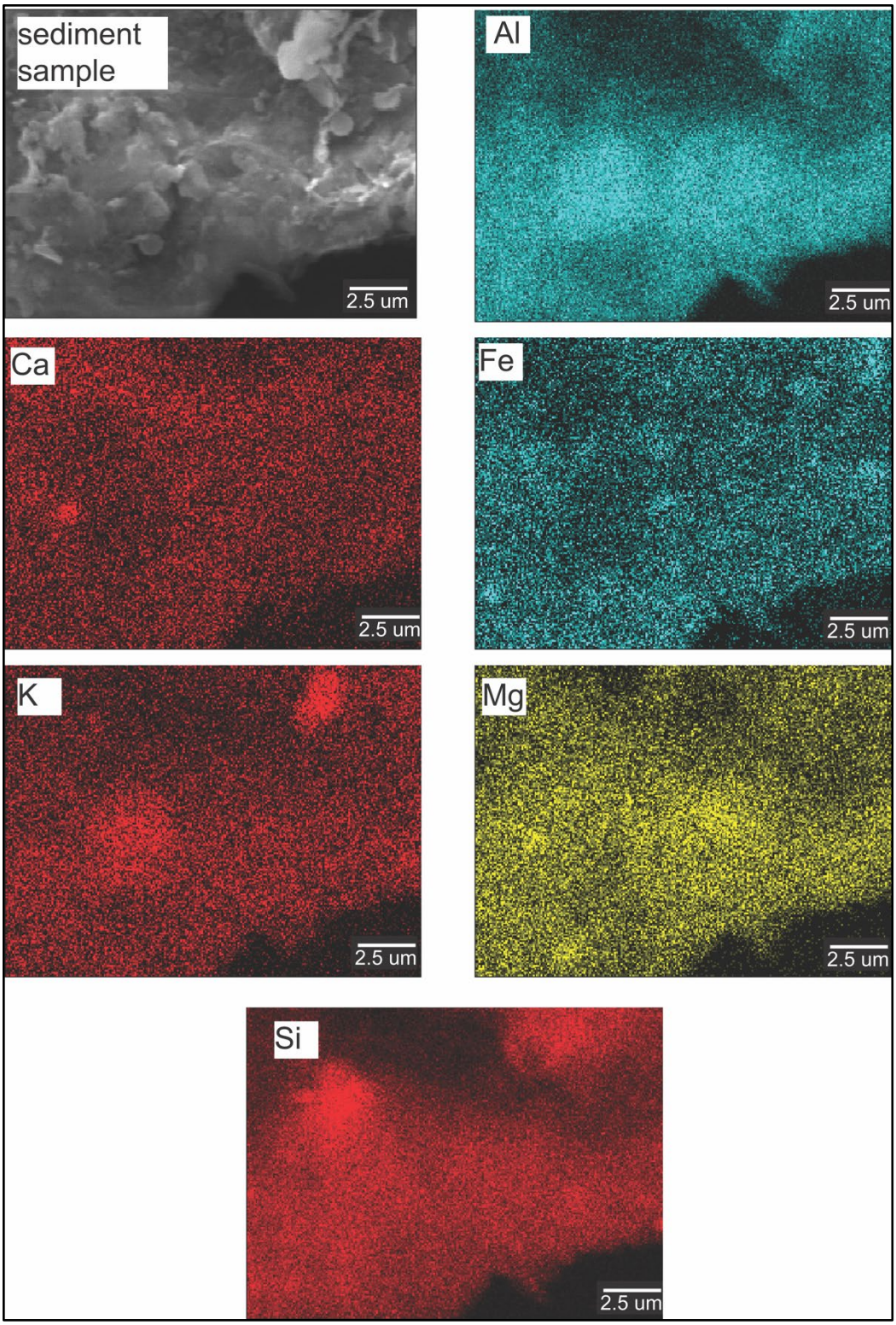

Fig. 5. Example of SEM image of sediment sample and EDS maps at 7,000x magnification (a). Representative elements are shown, Ti was not detected in this image. The two spherical objects in (a) are known contamination from a carbon-based microparticle. K and Al show a higher concentration in similar regions that is also appears to be somewhat correlated with high concentrations of Si. No correlation is observed between the remaining elements.

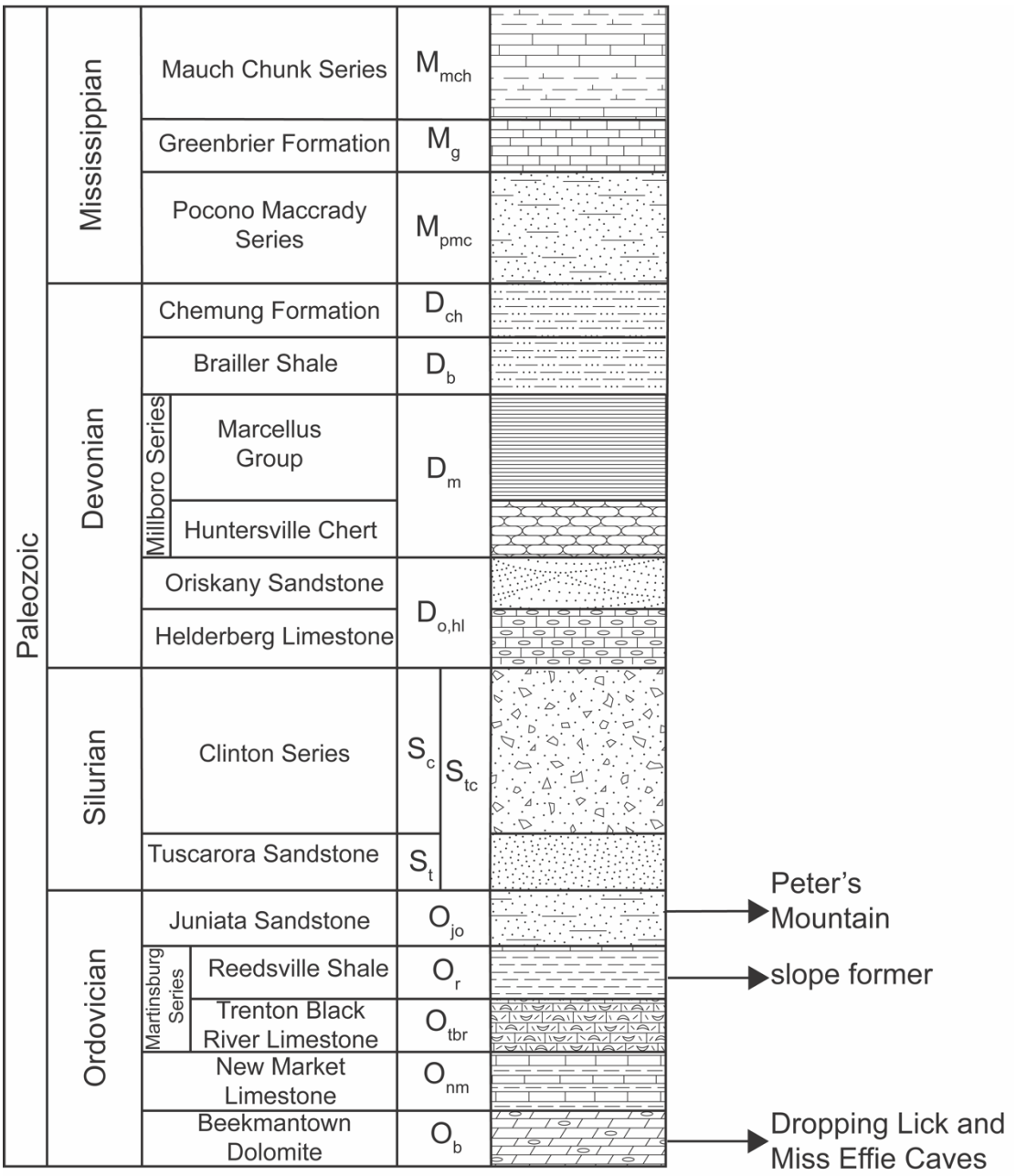

Fig. 6. Generalized stratigraphic section of Monroe County, WV adapted from Sturms (2008) and Bausher (2018). The unit of occurrence of important geologic features in this study are indicated.

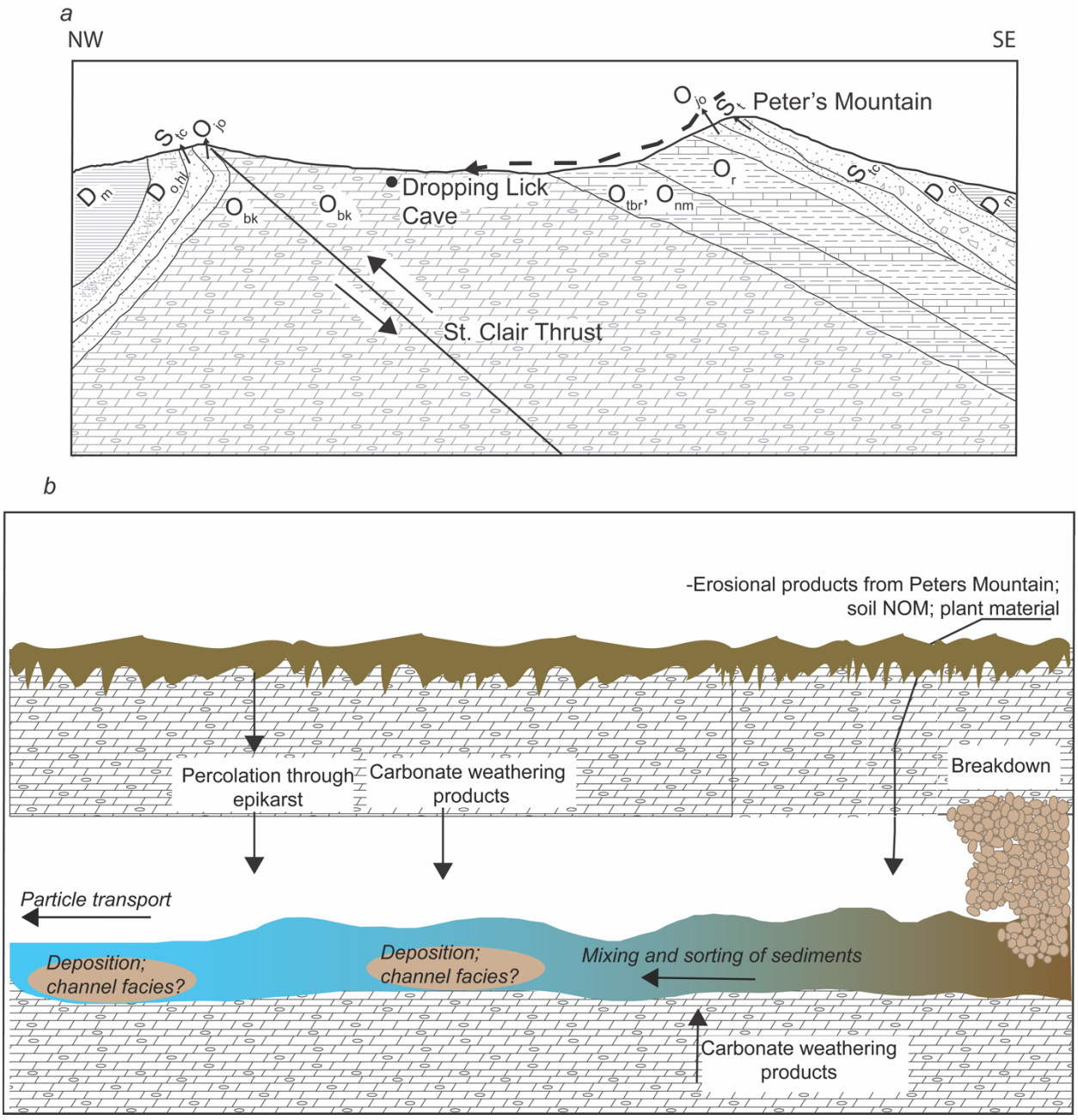

Fig. 7. Generalized geologic cross section of Monroe County, WV adapted from Bausher (2018), Richards (2006), and Sturms (2008) showing the lithologic units of Dropping Lick Cave, Peters Mountain, and its slopes (a). Theoretical schematic of clastic sediment input, types, and transport in Dropping Lick Cave (b).

Table 1. Physical and chemical components of active fraction of sediment (< 2mm)

Parameter	Minimum	Maximum	Average
Particle Size (volume %) (n=9)			
Sand	34.9	60.5	50.2 ± 7.9
Silt	39.4	65.0	49.7 ± 7.9
qXRD (wt %) (n=6)			
Chlorite	3.27	5.62	4.29 ± 0.9
Quartz	52.3	77.1	67.2 ± 7.6
Dolomite	3.70	9.11	5.89 ± 1.7
Calcite	8.39	8.39	N/A**
K-feldspar	3.22	7.17	5.55 ± 1.5
Amorphous material	5.86	35.1	17.1 ± 9.5
Element chemistry, digestion (mol/L) (n=8)			
Al	0.217	0.255	0.231 ± 0.02
Ca	0.184	0.217	0.203 ± 0.02
Fe	$1.26x10^{-4}$	$1.57x10^{-4}$	$1.40x10^{-4} \pm 1.6x10^{-5}$
K	$1.43x10^{-2}$	$1.62x10^{-2}$	1.53x10-2 $\pm$ $5.8x10^{-4}$
Mg	0.211	0.247	0.229 ± $1.1x10^{-2}$
Si	$1.00x10^{-2}$	$2.66x10^{-2}$	$2.05x10^{-2} \pm 6.4x10^{-3}$
Ti	$7.39x10^{-4}$	$8.31x10^{-4}$	$7.97x10^{-4} \pm 3.2x10^{-5}$
Total carbon (wt %) (n=7)			
TC	1.07	1.18	1.13 ± 0.04
TOC	0.57	0.91	0.72 ± 0.1
TIC	0.16	0.60	0.41 ± 0.1
Element chemistry, EDS (atomic %) (n=8)			
Al	1.77	7.29	5.28 ±1.8
Ca	0.11	0.78	0.49 ± 0.3
Fe	1.09	2.92	2.05 ± 0.7
K	0.34	2.54	1.42 ± 0.7
Mg	0.17	0.73	0.50 ± 0.2
Si	10.8	25.3	19.2 ± 5.8
Ti	0.3	0.3	N/A*

Physical and chemical components of the dried and sieved sediments. Only selected elements of interest are shown for major element chemistry, remaining identified elements can be viewed in the supplemental data portion of this research. *In the EDS analysis Ti was only detected in one sample. This analysis also had known contamination of carbon containing particles in the sediment, so C was not evaluated as part of this work. **Calcite was only identified in one sample during qXRD analysis. Differences in n are due to sample size and available sediment.

Table 2. IR band assignments of freeze-dried sediments

Vibration frequency (cm^{-1})	Absorbance
3698	O-H stretch[1,2,3]
3621	O-H stretch[1,2,3]
3380	O-H stretch[1,2,3]
1623	H-O-H or Fe-O, Al-O amorphous hydroxides[4,5]
1384	C-N stretching or CO_2 (atmospheric)[5,6]
1164	Si-O stretch[3,4,7,8]
1071	Si-O stretch[3,4,7,8]
1024	Si-O stretch[3,4,7,8]
913	Al-OH bending[3,5]
798	Si-O stretch (quartz doublet)[7,8]
778	Si-O stretch (quartz doublet)[7,8]
694	Si-O stretch[3,5]
669	Si-O, Al-O stretch[5,7]

IR band assignments for the freeze-dried sediments. Vibrational frequencies are averages across the four replicates. Mineral interpretation of the sediments is provided given the low amount of organic carbon in the sediments and to confirm the qXRD analysis. The bands are characteristic of quartz and clay minerals. The IR bands of calcite and dolomite are not observed (Hsiao et al., 2019; Ji et al., 2009).

[1]Farmer (2000); [2]Jozanikohan and Abarghooei (2022); [3]Madejova (2002): [4]Nayak and Singh (2007); [5]Nandiyanto et al., (2019); [6]Socrates (2001); [7] Bertaux et al., (1998); [8]Bandopadhyay, (2010).

CHAPTER TWO

Total organic carbon concentrations in clastic cave sediments from Butler Cave, Virginia, USA: implications for contaminant fate and transport

Jill L. Riddell[1,*], Autum R. Downey[2], Dorothy J. Vesper[1], an Ingrid Y. Padilla[3]

1 West Virginia University Department of Geology and Geography 98 Beechurst Avenue, Morgantown WV 26508

2 University of Washington Department of Earth and Space Sciences 4000 15th Avenue NE, Seattle WA 98195

3 University of Puerto Rico Mayagüez, Department of Civil Engineering and Surveying, PO Box 9000, Mayagüez, PR 00681

*Corresponding author

Email: jlriddell@mix.wvu.edu

ORCID

Jill L. Riddell: 0000-003-3485-2896

Autum R. Downey: 0000-0002-8050-799X

Dorothy J. Vesper: 0000-0002-29607548

Ingrid Y Padilla: 0000-0001-8460-167

Target Journal: Environmental Earth Sciences

Submitted: May 6, 2022

Abstract

Clastic cave deposits are representative of sediments throughout fluvial karst aquifers and thus are an abundant and accessible resource through which to study the chemistry of karst aquifer. Clastic cave sediments are attributed to depositional facies based on sortin, and particle size. These facies settings may influence different chemical parameters of the sediments, like concentrations of total organic carbon (TOC). The TOC concentrations in clastic cave sediments have not been well constrained nor has the role of clastic sediments in contaminant fate and transport through karst systems been well described. In this study, particle size, TOC, and total nitrogen were measured in sediments representing different facies in Butler Cave, Virginia, USA. TOC concentrations ranged from 0.08 – 0.87 weight percent and C:N molar ratio ranged from 3 – 15, indicating a possible terrestrial source of organic carbon in these sediments. The diamicton facies was sandier and but had similar TOC concentrations compared to the channel facies. TOC concentrations measured in Butler Cave were within the same range as those observed in above water, eogenetic clastic cave sediments from two caves in Puerto Rico. Estimated retardation factors calculated based on the TOC concentrations in the Butler Cave sediments indicate the range of TOC in this cave could be responsible for 39 – 987% increase in retardation of selected contaminants. This study highlights the importance of measuring the ranges of TOC in clastic cave sediments across different facies and their role in contaminant fate and transport.

Keywords karst, cave, TOC, sediment, contaminant transport

Acknowledgements

The authors acknowledge the Butler Cave Conservation Society (BCCS) for encouraging scientific pursuits in Butler Cave, providing access to the cave property, and acting as tour guides through the cave. The authors specifically thank BCCS members Bryan Crowell, Rose-Anna Behr, and Christopher Swezey for their assistance. Finally, the authors acknowledge and thank Matthew Bell and Corey O'Malley for assisting in sample collection, preparation, and the manufacturing of tools used during sample collection.

1.0 Introduction

The presence, nature, and concentration of natural organic matter in aquifer systems plays a critical role in carbon processing, nutrient cycling, and contaminant storage and transport. Natural organic matter is contained within the soil and sediments of aquifer systems and is measured as total organic carbon (TOC), yet the TOC concentrations of aquifer sediments are not as thoroughly quantified or described as the TOC for other types of sediments, such as marine or lacustrine. The amount of subsurface TOC generally decreases with depth through the soil zone and is even lower in aquifer sediments (Hicks et al. 2018), however it is important to quantify and characterize the TOC of aquifer sediments to better understand how this carbon is participating in and effecting other processes, such as contaminant fate and transport. While all aquifers are susceptible to contamination, karst aquifers and their sediments are of particular interest given the well documented vulnerability of these aquifers to contamination (Ewers et al. 1991; Vesper 2008; White 2018; Williams and Farmer 2003), their connectivity to surface inputs, and their capacity to store and transport large amounts of sediment depending on hydraulic conditions (Herman et al. 2008). Further, relatively little attention has been paid to the role of sediment in contaminant fate and transport. Karst aquifer sediments with relatively high TOC may act as a reservoir for organic contaminants via adsorption of contaminants onto sediments (Schwarzenbach et al. 2003) and as a source for reintroduction of contaminants to the surface if hydraulic conditions initiate sediment transport (Herman et al. 2008; Vesper et al. 2003). To understand the role of aquifer sediments in contaminant fate and transport, a more comprehensive data set is necessary.

Sediments deposited in caves are relatively accessible and approximately analogous to sediments stored throughout the karst aquifer. Cave sediments include material generated chemically (precipitates) or physically (clastic). Precipitates include speleothems which are primarily inorganic in composition and contain minor amounts of TOC (Dreybrodt 1999). Clastic sediments consist of breakdown and surface derived material (White 1988) originating from collapse structures like sinkholes, injection during storms or floods, or incoming recharge (Hart and Schurger 2005). Caves are considered an oligotrophic environment with typically < 2 mg/L TOC (Barton and Jurado 2007) yet the diverse microbial communities in caves (Banks et al. 2010; Barton et al. 2004; Barton and Northup 2007; Kosznik-Kwasnicka et al. 2022; Suarez-

Moo et al. 2022) may be responsible for critical generation and transformation of organic carbon in the system (Kosznik-Kwasnicka et al. 2022; Suarez-Moo et al. 2022).

In clastic cave sediments and karst systems, the spatial and temporal distribution of TOC, the range of concentrations, and the chemical and biological pathways by which this carbon is transformed are poorly constrained (Husic et al. 2017; Simon et al. 2010; Simon et al. 2007). Recent efforts have been made to characterize and measure the flux of dissolved organic matter and TOC in subsurface fluvial karst systems (Husic et al. 2017; Simon et al. 2010; Simon et al. 2007). These studies focus on sediment flux along with the dissolved and particulate organic carbon content in cave streams. In cases where the TOC concentration of clastic cave sediments has been reported, ranges of TOC vary widely depending on the climatic conditions and surface connectivity of the cave system. Tropical caves have more microbial biomass and are more microbially active (de Paula et al. 2016) and, as a result, are assumed to have higher concentrations of sediment TOC; however, in the limited data reported for clastic cave sediments, this is not the case. The amount of TOC in clastic cave sediments appears to depend on their age, connectivity of the system to the surface, and geologic and geomorphologic history of the system (Bottrell 1996; de Paula et al. 2020; de Paula et al. 2016; Downey 2020; Panno et al. 2004).

The TOC concentration of any sediment or soil positively correlates to the soil adsorption coefficient of that material and its ability to act as a sorbent for organic compounds (Schwarzenbach et al. 2003). These parameters are often reported in different types of soil and sediments but rarely reported for clastic cave sediments or karst aquifer sediments. In karst systems, few connections have been made regarding the introduction of contaminants into these systems via sediment pulses or the transport of these contaminants to the surface or downstream receptors (springs, etc.) during subsequent storms. It is well documented that cave and karst systems can store and transport sediments (Bretz 1942; Ford and Williams 2007; Herman et al. 2008; Mahler et al. 2007; Mahler 1999) and any contamination associated with incoming sediments can be stored and transported as well. Contaminants can also enter the aquifer independently through runoff and percolation through the soil and epikarst. This has been documented for volatile organic compounds and other emerging and legacy contaminants in the northern karst aquifers of Puerto Rico (Ghasemizadeh et al. 2015; Padilla et al. 2011). However, the amount of TOC in these sediments and whether it is a controlling factor in storage and

transport has not been constrained. Therefore, measuring the range of TOC in clastic sediments is important for understanding and exploring the role of cave and aquifer sediments in contaminant fate and transport. Clastic cave sediments are protected from surface erosional processes but may undergo physical or chemical transformations within the cave. Land-use, geomorphology, and climatic changes will influence the amount of sediment being injected and its potential reworking in the cave. The origin, chemistry, and chemical behavior of clastic cave sediments receives little attention or analysis compared to speleothems and cave precipitates. The role of these clastic sediments may play a pivotal role in contaminant storage and transport (Mahler 1999) and supporting the cave ecosystem (Barton and Jurado 2007; Husic et al. 2017) as well as providing clues as to the paleohydrology and paleoclimate during the deposition of these sediments.

The purpose of this investigation is to physically describe clastic cave sediment deposits and measure the range of TOC concentration, total nitrogen (TN) concentration, and particle size distribution in Butler Cave, Virginia, USA with respect to cave sediment depositional facies and distance from sediment input. TOC concentrations ranged from 0.08 – 0.87 weight percent and TOC:N ranged from 3 – 15. The diamicton facies was sandier and had a similar TOC concentration to the channel facies, although the core samples in the channel facies had more TOC than core samples in the diamicton facies. TOC concentrations measured in Butler Cave were within the same range as those observed in unsaturated, eogenetic clastic cave sediments in Puerto Rico and Brazil. Estimated retardation factors calculated based on the TOC concentrations in the Butler Cave sediments indicate the range of TOC in this cave could be responsible for 39 – 987% increase in retardation of selected phthalates and volatile organic compounds.

2.0 Site description and methods

Butler Cave was chosen for this study because the cave sediments are abundant and have been previously studied in regard to physical characteristics and mineral content. Butler Cave, located in Bath County Virginia (VA), USA is in a karst valley known as the Burnsville Cove (Fig.1). Structurally, the valley contains a series of southwest-northeast trending folds formed during the Alleghenian Orogeny (325 – 270 million years ago) which resulted in layers of limestone being folded and faulted, resulting in units thick enough to support major cave development (Swezey et al. 2017). The Chestnut Ridge Anticline is the main fold axis in the

valley, and it is flanked by the White Oak Syncline to the southeast and Sinking Creek Syncline to the northwest. The main trunk of Butler Cave formed along the Sinking Creek Syncline with secondary passages forming along dip on the western side of the syncline (Swezey et al. 2017). The Tonoloway Formation, a Devonian limestone with interbedded sandstones, is the rock unit which forms the cave (Fig. 1).

The sediments in Butler Cave consist of speleothems and clastic deposits. The clastic deposits, the focus of this investigation, were likely washed into the cave during various flooding events and range in size from clays to boulders (White 2015). Some of the sediments of Butler Cave have been reworked and transported by the active cave stream. The sediments were described and placed into a facies classification by Bosch and White (2004) and later White (2015). The classification system consists of five different facies based on particle size, particle sorting, and potential fluvial deposition conditions of the deposit. The framework for the facies names and descriptions are based on depositional studies of sediments in other caves and in other settings, such as glacial (Gillieson 1986; Pickle 1985; Springer and Kite 1997; Valen et al. 1997). The facies described for Butler Cave by Bosch and White (2004) include 1) backswamp facies – fine grained, poorly sorted muds and silts that show minimal stratification and are not deposited or reworked by active cave streams; 2) thalweg facies – large grained, well sorted boulders, gravels, and cobbles from which fine grained material has been winnowed away; 3) slackwater facies – fine grained, well sorted clays and silts often with layering, deposited by settling out of turbid flood waters; 4) channel facies- moderately size, moderately sorted interbedded silts and sands that often show stratification and are deposited by active cave streams; and, 5) diamicton facies – a poorly sorted, chaotic dump of cobble to silt size particles resultant from large debris flows into the cave, also described by Gillieson (1986). Channel and diamicton facies are well represented and described in Butler Cave and represent two extremes of clastic sediment working in caves – large pulses from outside events like floods (diamicton) and sediment transport and reworking within caves (channel). The mineralogy of the Butler Cave sediments is dominated by quartz, with iron oxides, zircons, rutile, and other trace minerals (Chess et al. 2010). Paleomagnetic analysis of channel deposits in Butler Cave showed normal polarity while sediments from dip passages had reversed polarity, indicating deposition dates prior to 780,000 years before present.

For this investigation, six locations (Fig. 1) were chosen for sediment sampling. Grab samples were obtained from a sediment bank using pre-cleaned stainless-steel instruments; core samples were obtained by inserting a ~ 5 x 30.5 cm polyethylene tube into the barrel of a stainless-steel split-spoon corer and using a sliding hammer to drive the tube into the sediment bank. If the tube was filled before failure, a second tube was inserted, and sampling continued until failure. The grab samples were stored in plastic bags or amber glass jars; core samples were capped and tightly wrapped in their core sleeves. All samples were stored on ice during transportation to laboratory. Upon arrival at the laboratory, samples were refrigerated and kept out of direct light until preparation and analysis. Physical description of the sediments was completed for the sediment deposits in the field and for the grab and core samples in the laboratory. Core samples were subsampled based on observed changes in color or grain size. In total, 33 samples were collected for particle size distribution and chemical analysis (Table 1). Samples were analyzed for particle size, total carbon (TC), TN, and total inorganic carbon (TIC). Sediment samples were prepared for particle size analysis by air drying in a fume hood for approximately 48 hours and then in an oven at 60 C for approximately 24 hours. The sediments were then sieved to < 2 mm to separate the active fraction (0.2 μm – 2,000 μm) of the sediments which consists of clay (< 2 μm), silt (2 – 50 μm), and sand (0.05 – 2.0 mm). This fraction controls the physical and chemical processes of the sediment due to the high surface area relative to the coarser particles (> 2 mm). The samples were then mixed in a 1: 1.5 sediment to 5% Calgon® mass ratio solution and shaken at 70 rotations per minute on a rotary shaker for ~ 24 hours to fully disperse the particles. Particle size was measured using a Beckman Coulter single wavelength LS13-320 particle size analyzer, measuring from 0.4 μm – 2,000 μm. The particle size data are reported in volume percent; the raw data was organized in R and processed using the GRADISTAT program (Blott and Pye 2001) to determine volume percent of sand, silt, and clay.

For TC and TN analysis, samples were air-dried for 24 hours, lightly homogenized using an agate mortar and pestle, sieved to < 2 mm, and then oven-dried at 60 C for 24 hours. TC and TN were measured on a Carlo Erba NA1500 CNHS elemental analyzer at the University of Florida Stable Isotope Mass Spectroscopy Laboratory in Gainesville, Florida. This instrument flash combusts the sample and the resultant gas is passed through a reduction column where oxygen is removed, and water is trapped. The remaining gas is passed through a 125 C

chromatography column that separates the CO_2 and N_2 gases. TIC was measured by acidifying the sediment in an N_2 environment and quantifying the degassed CO_2 using an UIC 5017 CO_2 coulometer. TOC is determined as the difference between TC and TIC. TC, TN, and TOC are reported as a weight percent (wt %) by sample.

3.0 Results

3.1 Physical description

Sample location 001 was collected from a diamicton facies (Bosch and White 2004) at the end of a passage known as Dave's Gallery (Fig. 1). One core sample was collected from the top of sediment bank with a recovery of 26 cm and three grab samples were collected from the face of the sediment bank between the bottom of the core toward the cave floor (Fig. 2a). The sediment bank consisted of a finer grained sandy cap over a thicker, gravel sized deposit (Fig. 2a). Based on field observations, the coarser sediments were poorly sorted, angular to subangular, and unsaturated. The core sample was split open in the laboratory and appeared to be consistent in grain size and color (brownish yellow, 10 YR 6/6 on the Munsell color chart. Although no visible change in grain size or color was observed, the core was subsampled in two sections of roughly equal length for analyses (Fig. 2a). Sample location 002 was collected from the dry stream bed in a passage known as Sand Canyon. Although the stream was dry at the time of sampling, it is known to flow intermittently. Two consecutive cores with total recovery of 43 cm and one grab sample from the top of the cored area were collected. The core samples were subsampled in four sections based on visible change in grain size. The color of the core samples was dark yellowish brown (10 YR 4/5 Munsell color chart), and no distinct stratification or layering was observed. Sample location 003 was collected from the same bank deposit as 002 but slightly downstream and higher (relative to the stream bed) in the deposit stratigraphy than location 002. One core sample with 22 cm of recovery was collected and one grab sample from the bottom of the core was collected. Overall, the core sample was observed to be yellowish brown in color (10 YR 5/6 on the Munsell color chart). Sample location 004 was collected from an approximately 225 cm tall bank around the bend from Sand Canyon. Two consecutive core samples were collected from the top of the bank with total recovery of 45 cm. Five grab samples were collected from the face of the bank moving down to represent the entire bank from top to bottom, save for the last ~ 50 cm which consisted of large gravels and small boulders. The

sediments appeared to be well sorted but varied in grain size from sand to large boulders (Fig. 2b). The core samples were subsampled in 10 total sections. The top 20 cm of the core had distinct layers of sand and silt sized particles that were light yellowish brown (10 YR 6/4) and dark yellowish brown (10YR 4/4), respectively. The bottom 17 cm of the core was mostly sandy with a smaller, clay-like layer between 14 – 16 cm (Table 1). The sandier bands were much thicker than the smaller particle size bands and were light yellowish brown (10 YR 6/4) while the smaller particle band was dark yellowish brown (10 YR 4/4). Sample locations 002 through 004 represent the channel facies (Bosch and White, 2004). Sample location 005 was collected from a sediment bank consisting of mostly sand sized particles capped by a smaller silt or clay-like textured sediment. One grab sample of the sand and one of the clay-like sediment were collected. This location has not been previously categorized according to the facies classification system but may represent channel or slackwater facies. Finally, sample location 006 was collected from a sediment bank further back in the cave and close to an active stream. One core sample of 23 cm recovery was collected and subsampled in four sections. While above water at the time of sampling, this core contained much more moisture when split open than other sediment cores collected in during this sampling event. This location was also not previously categorized in the facies classification scheme but may represent slackwater facies. The total list of samples and sample naming schema is listed in Table 1.

3.2 Particle size and carbon analysis: active fraction, < 2mm

All samples were sieved < 2 mm to obtain the active size fraction and these materials were analyzed for particle size. All samples at locations 001, 002, 003, 004, and 005 were classified as some type of sand (Table 1), ranging from fine to coarse, except for four samples at locations 001 and 002 that were classified as fine to coarse silts (Table 1). All the samples from location 006 were classified as course silts (Table 1). The volume percent for all the samples ranged from 16.2% – 91.4% sand, 6.1% – 83.8% silt, and 0% – 12.7% clay. The highest sand content was at location 003 and the lowest was at location 006 (Fig. 3).

The TC concentrations ranged from 0.08 – 0.87%: the lowest concentration was at location 006 and the highest at 003. TOC also ranged from 0.08 – 0.87 % because some samples had zero measurable TIC concentrations. Location 002, in the active cave stream, had the highest average TOC while location 004 (the location with the largest grain size) had the lowest. A linear regression between TC and TOC data including all samples had slope = 0.91 ($R^2 = 0.92$),

indicating that most of the carbon in all the samples was TOC. Location 001 had the largest range of TOC with slight positive skew while location 004 had a smaller range of TOC with close to normal distribution. Location 003 had the highest median TOC and location 006 had lowest median TOC (Fig. 4a).

Microbial uptake of nitrogen is a driver of organic carbon decomposition in surface leaf and root litter (Ravn, 2020); however, in caves total nitrogen is often low (and as a result the C:N ratio is low), thus slowing down the rate of organic carbon decomposition. (Ravn, 2020). Reporting TOC and N concentrations can provide information on how microbial activity may be supported in the caves and how this may contribute to carbon processing in caves. TOC:N ratios were compared to the average C:N ratios of amino acids, 3.15, (Jover et al. 2014) and C:N range of humic and fulvic acids, 6.23 - 147, (Rice and MacCarthy 1991), respectively. The C:N ratio of amino acids generally represents a microbially-based source of organic carbon (Jover et al. 2014) whereas humic and/or fulvic acids represent the heterogenous, molecular organic components of soil organic matter (Rice and MacCarthy 1991). The TOC:N molar ratio range across the six locations was 3 – 15 with the highest and lowest concentrations represented at locations 006 and 003, respectively. Location 001 and location 003 have the largest range of TOC:N but location 003 has the highest median and average of TOC:N. Location 006 has the lowest median TOC:N (Fig. 4b). Most of the TOC:N data fall above the average amino acid ratio and slightly below or well within the humic and fulvic acid range (Fig. 5). This could possibly indicate that the TOC in these samples is largely a result of soil organic matter that has been washed into the cave. Interestingly, three out of the four samples collected from the core at location 006 had a TOC:N ratio at or below 3.5 and this location also had the lowest average TC and second lowest average TOC. This could possibly indicate that the further away from source input a sample is, the less likely terrestrial OC is to be washed that deep and that microbial signatures of TOC dominate any TOC that is present even if TOC concentrations are comparatively lower.

Some of the sample locations had a positive linear relationship between the percentage of silt-sized particles and TOC but this was not true across the entire sample set. A positive linear relationship was observed in each of the diamicton facies (location 001) and channel facies (location 004) between the silt-sized fraction and TOC but not between the clay-sized fraction and TOC. For the channel facies, when the core and grab samples were compared individually, the core samples had a linear relationship in silt-sized particles and TOC, but the grab samples

did not. At location 006 where silt was the dominant sized fraction, a negative linear relationship was observed between the silt-sized fraction and TOC, but a positive linear relationship was observed between the clay-sized fraction and TOC. It should be noted that small sample sizes and data clusters around high silt-size percentages and low clay-size percentages could be skewing these relationships. The data presented here show that large ranges organic carbon content can occur in clastic cave sediments across grain sizes and lithofacies.

3.3 Comparison of channel and diamicton facies, < 2 mm fraction

The samples collected at locations 001 and 004 were selected to compare the diamicton (poorly sorted, chaotic dump of cobble to silt size particles resultant from large debris flows into the cave) and channel facies (moderately sized, moderately sorted interbedded silts and sands that often show stratification and are deposited by active cave streams). These locations were chosen based on previous mapping and descriptions (Bosch and White 2004) and each represent a potential different mechanism of clastic sediment deposition and processing in caves.

For the active fraction of the diamicton facies (location 001), the samples mostly consisted of sand-sized grains although the three grab samples had slightly more silt than the core samples (Fig. 6a). In the diamicton facies, TOC ranged from 0.08 – 0.37 % (Fig. 6b) and TOC:N ranged from 4 – 7.4 (Fig. 6b). There was an increase in TOC and TOC:N with depth from the top of the bank with the exception of location 1E (the bottom of the bank) which had a marked decrease in TOC and TOC:N (Fig. 6c, d). This could be due to the overall large grain size dominating the sample, based on field observations. Most of the TOC:N ratios fell between the average amino acid range but below the range of humic and fulvic acids (except for 1D). Given the inferred source of a diamicton facies, these samples are likely dominated by terrestrial TOC. There is a decrease in grain size with depth of sample (Fig. 6c) with sand making up 86% of the active fraction at the top of the bank and decreasing to only 45% at the bottom. The observed overall grain size at the bank (sand to boulder) was observed to increase from the top of the bank to the bottom of the bank. However, since this facies represents a large, chaotic injection of sediment, it is not advised to interpret this as a depositional feature with regard to depth in the same way one would consider it in a surface sedimentological setting.

Welch's t-test was performed to compare the means values of the sand, silt, clay, TOC, and TOC:N between the grab (n = 2) and core (n = 3) samples at location 001. The result showed a significant difference ($\alpha = 0.05$) in the mean for the sand and silt size fractions ($p < 0.05$)

where the mean sand-size percentage was greater in the core samples and the mean silt-size percentage was greater in the grab samples. The remaining variables have no significant difference in means. However, because each sample size is small, these results should be interpreted with caution since Type I or Type II errors can be common in low sample size populations.

In the channel facies at location 004, the bank is capped by a sandy deposit approximately 47 cm thick and then increases in grain size down the bank from gravel to boulder. The samples are mostly sand sized with some core samples being slightly siltier than the grab samples (Fig. 7a). The core samples have alternating high percentages of sand and silt with depth in the first 20 cm which is consistent with described interbedded sands and silts that are descriptive of channel facies. The grab samples had a more consistent grain size with depth which is likely due to an overall larger grain size (cobble and boulder) dominating the deposit as observed during sample collection. The TOC ranged from 0.1 – 0.26 % and TOC:N ranged from 4.7 – 8.7 (Fig. 7b) with six samples in the humic and fulvic acid range and nine samples between the humic and fulvic acid range and the amino acid average (Fig. 7b). The TOC source in these samples is likely terrestrial. The core samples show an alternating pattern of increasing and decreasing TOC concentrations and TOC:N ratios with depth (Fig. 7c, d) which is indicative of the interbedded sands and silts characteristic of channel facies. Results from Welch's t-test between the core and grab samples at location 004 also showed a significant difference (α = 0.05) in the means of the sand and silt size fractions ($p < 0.05$) where the mean sand percentage was greater in the grab samples and the mean silt percentage was greater in the core samples. Differences in the core and grab samples could be due to the overall differences in grain size or exposure of the grab samples to the ambient cave environment.

A significant difference ($\alpha = 0.05$) was observed between the core samples at location 001 and 004 for the means of sand, silt, and TOC; the mean sand percentage was greater in the diamicton facies (001), but the mean TOC and silt percentage was greater in the channel facies (004). Since organic carbon is often associated with smaller size fractions, it is reasonable that a siltier sediment (004) will have more TOC than a less silty sediment, which is supported by these statistics. Grab samples between the diamicton and channel facies had a statistical difference (α = 0.05) only in the sand and silt size fractions where the mean sand percentage was greater at in the channel facies and mean silt was greater in the diamicton facies. It is possible error is present

in this analysis due to the large difference in sample size (location 004 had three times more samples collected than location 001) and the overall low number of samples available at 001. The observed differences in the data suggest there could be a difference in the active fraction particle size and chemistry of these two sediment lithofacies. The differences in core and grab samples could be due to the sampling method, where coring is more likely to capture smaller particles than grab sampling. However, the core samples in the diamicton facies were sandier (coarser) than the grab samples.

4.0 Discussion

4.1 Comparison to other clastic cave sediments

Tropical caves, like those in Puerto Rico or Brazil, present an interesting comparison to temperate caves, like Butler Cave. Tropical caves in eogenetic karst settings, such as in the Caribbean, frequently receive large injections of sediments from tropical storms and hurricanes (van Hengstum et al. 2014). In 2018 and 2019, sediment samples were collected from two different caves in Puerto Rico: El Tallonal (TAL) Cave and Cueva Clara - Rio Camuy (CAM) Cave (Downey 2020). TAL cave is a privately owned cave with an active stream. Cueva Clara is part of the dry section of the Rio Camuy Cave system. It is in the Parque Nacional de las Cavernas del Rio Camuy in Quebrada, Puerto Rico and is a show and wild cave that is open for tours to the public. Rio Camuy experienced large sediment injections during Hurricane Maria in 2017 (Miller, 2018) and some of these sediments were collected as part of the study by Downey (2020). The TAL sediments in this study consisted of both saturated and unsaturated sediments found, respectively, below and above the level of the stream. Downey (2020) reported that TOC in unsaturated sediments ranged from 0.13 – 0.73% (Downey 2020), which is comparable to the Butler Cave samples collected in this study. Downey reported that the TOC in saturated sediments ranged from 0.11 – 2.36%. Most of the carbon in these TAL samples was organic in form. The TOC:N ratio for all the Puerto Rico sediments ranged from 0 – 34 (Downey 2020) with most samples falling in the typical range for humic and fulvic acids (6.23 – 147, Rice and MacCarthy 1991). Several of the CAM sediments were at or below the amino acid average (3.15, Jover et al. 2014). The CAM sediments were deposited during Hurricane Maria (they were located on the paved public tour pathways) and thus are younger than the sediments from TAL. The Butler Cave sediments described here have a similar range of TOC:N to the unsaturated

TAL sediments but much lower overall TOC concentrations than the unsaturated TAL sediments (Fig. 8). In general, microbial activity in tropical sediments and soils is likely to be much higher (de Paula et al. 2020) than in temperate sediments and soils, such as Butler Cave. This is likely why the Puerto Rico sediments have much higher TOC content overall, even though the Butler Cave sediments are also unsaturated. The similar TOC:N ratios result from overall low N concentrations in both the temperate (Butler Cave) and tropical caves (Puerto Rico), which is a common feature of oligotrophic environments. Based on Welch's t-test, a significant ($\alpha = 0.05$) difference was observed between the mean TOC concentration of Butler Cave and the mean TOC concentration of the saturated and unsaturated El Tallonal sediments, the Rio Camuy sediments, and all the Puerto Rico cave sediments as a group: Butler Cave had a significantly lower mean TOC concentration than all of the other groups.

The TOC for the Butler Cave clastic cave sediments fall within the range of TOC reported for several caves in Brazil, 0.004 – 1.31% (de Paula et al. 2020; de Paula et al. 2016) for various locations and through wet and dry seasons. In the Brazil caves in which N was reported, concentrations ranged from $8x10^{-7}$ – $1.95x10^{-5}$ wt % (de Paula et al. 2020), much lower than what is reported for the Butler Cave or Puerto Rico cave sediments. This may indicate possible microbial N immobilization – the conversion of inorganic N to organic N- in the Brazil sediments. Microbial biomass was isolated from the Brazil cave sediments and samples were incubated to promote reproduction. Respiration rates were estimated by quantifying CO_2 released from the incubated samples. Respiration rates were observed to be higher in the wetter seasons and a positive correlation was observed between microbial biomass carbon and sediment TOC in both wet and dry seasons (de Paula et al. 2016). The Butler Cave sediments have TOC concentrations within the range of both tropical settings (although overall, the Brazilian samples had much lower TOC concentrations on average than the Butler Cave or Puerto Rico cave sediments), less N than the Puerto Rico cave sediments, and more N than the Brazilian cave sediments. This indicates that multiple climatic (humidity, temperature) and geologic factors (saturation, surface connectivity) are controlling the sediment processing in caves in different regions.

Similar TOC concentrations (Table 2) have been reported for comparable temperate caves in England (Bottrell 1996) and in Illinois, USA (Panno et al. 2004). Bottrell (1996) reported an overall decrease in TOC with core depth, similar to in Butler Cave but the greater

range of TOC reported by Bottrell (1996) could be due to the short length of the time of those sediments had been underground (<7 years). However, the generally held notion that tropical caves contain more organic carbon may not be necessarily true given the comparisons between the tropical and temperate settings described here. Welch's t-test showed that mean TOC concentration at Butler Cave was significantly ($\alpha = 0.05$) higher than the TOC concentration reported by Panno et. al. (2004) in Illinois cave sediments but lower than the mean TOC concentration reported Bottrell et al. (1996) in England (Table 2b). Of the studies compared using Welch's t-test, the highest to lowest mean TOC were England (1.12 %, Bottrell 1996), TAL (0.78 %, Downey 2020), CAM (0.42 %, Downey 2020), Butler Cave (0.22, this study), and Illinois (0.12%, Panno et al. 2004). Based on these limited data, the highest TOC concentrations were observed in the most recently deposited sediments. The CAM sediment samples (highest TOC = 3.43%) were deposited within two years of collection and the England cave sediments (highest TOC = 3.37%) were deposited within seven years of collection (Bottrell 1996). Generally, between sites, higher TOC concentrations were observed in saturated or wetter sediments vs. unsaturated or drier sediments and for those sediments where ages were available, older sediments had less TOC than younger sediments (Table 2). Although more data are needed to confirm this, it is likely that saturation and sediment age (beginning from time underground) may be more important in determining sediment TOC concentration than climate/geographic location.

4.2 Data implications for contaminant fate and transport, paleoclimate, and microbial activity

The ability of aquifer sediment to store or mobilize contaminants is controlled largely by the TOC of the sediments. The fraction of organic carbon (f_{OC}) of a sediment is positively correlated to the adsorption of an organic molecule (K_D) via the organic carbon sorption coefficient (K_{OC}) where:

$$f_{OC} = \frac{K_D}{K_{OC}} \qquad \text{Equation 1.}$$

Simplified, an increase in organic carbon content generally results in greater adsorption of an organic chemical onto the sediment (Schwarzenbach et al. 2003). Even at very low f_{OC}, sorption of organic compounds onto sediments and soil is a dominant mechanism in the storage of these contaminants (Schwarzenbach et al. 2003). Common organic contaminants in karst aquifers include volatile organic compounds (VOCs), chlorinated volatile organic compounds (CVOCs), and phthalates (Ghasemizadeh et al. 2015; Padilla et al. 2011). All of these contaminants can

adsorb onto sediments in the aquifer matrix which retards their movement through an aquifer. Retardation factors (R_F) can be calculated if the K_D, bulk density (ρ), and effective porosity (n_e) of the sediment are known. For the Butler Cave sediments, estimated R_F values for various contaminants were calculated for the minimum (0.08%) and maximum (0.87%) TOC concentrations reported in Butler Cave (Table 3). Bulk density (ρ) and effective porosity (n_e) were averaged from values reported for sandy sediments by Aberson et al. (2011), Grabowski et al. (2011), Stringer et al. (2016), and Woessner and Poeter (2020). Retardation factors ranged from 1.04 for dichloromethane (DCM) to 22,950 for di(2-ethylhexyl)phthalate (DEHP). DEHP has a K_{OC} value three to five orders of magnitude higher than the other contaminants which contributes to its high R_F. Excluding DEPHP, the average R_F for the minimum TOC value was 2.73 and average RF for the maximum TOC value was 19.8 (Table 3). The TOC concentrations in Butler Cave were < 1%, however this is responsible for a 39 – 987 % increase in RF for the selected contaminants, highlighting not only the importance of low TOC concentrations in cave sediments and karst aquifers with respect to contaminant fate and transport, but also why it is necessary to know the TOC.

Contaminants adhered to sediments are considered immobile in granular aquifers given the low transmissivity of solid particles through granular systems, thereby resulting in storage and retardation of contaminants (Schwarzenbach et al. 2003). Recent research on colloidal-sized (1 nm – 0.1 μm) particles in contaminant fate and transport has shown the enhanced ability of these particles to move through aquifers (Frimmel et al. 2007; Toran and Palumbo 1992) and carry contaminants via adsorption (McCarthy and Zachara 1989). However, in karst aquifers, particles of any size can be mobilized through fractures and conduits, where the aperture threshold for turbulent flow (and thus the capacity to transport sediment) is between 0.5 and 5 cm (White 1988). These sediments may then be deposited in the aquifer or cave setting or flushed out via springs (Mahler 1999). Organic carbon content of soil and sediment is generally associated with clay and silt-sized particles, but recent studies have shown that organic carbon can be stored on the sand size fraction before the clay and silt size particles are saturated with organic carbon (Yang et al. 2016). Future research into the contaminant transport ability of cave and karst sediments should be careful to consider the organic carbon content across the active fraction, even in low concentrations.

The source of organic carbon in caves and karst aquifers is largely considered to be introduced from ex-situ as a result of pulses of soil and sediment entering the cave from the surface (Mahler 1999). However, dissolved organic carbon carried into a system via recharge water can adsorb onto in-situ sediments in the cave or aquifer. Mahler et. al. (1999) suggested that the amount of organic carbon across a karst system (from surface soil, epikarst, cave sediments, spring discharge, and sinkholes) in conjunction with the sediment mineralogy could be useful in determining the in-situ and ex-situ components of the TOC of the system. Essentially, the highest organic carbon content is in the surface sediments and the lowest is in the cave sediments and that the relative amount of feldspar in the system is positively correlated to surface sediments. Thus, if a cave sediment has a TOC concentration similar or close to the TOC concentration of the surface sediment and a relatively higher feldspar content, it was likely washed in relatively recently compared to cave or aquifer sediments with lower TOC concentrations and feldspar content. Mahler (1999) used a threshold of 0.4% TOC or higher to consider a sediment to be recently deposited, while any value lower was associated with paleo-fill deposits. While surface samples or mineralogical characterization was not within the scope of this Butler Cave study, concentrations of TOC ranged from 0.08 – 0.87% and previous mineralogical studies showed that some feldspar is present in the Butler Cave sediments, but it is not the dominant mineral (Chess et al. 2010). This indicates that the source of organic carbon in Butler Cave is likely older but with some modern input related to the ephemeral cave stream since the highest TOC reported in this study were in the active stream portion at location 002. However, this feldspar-TOC relationship should be approached with caution in geological settings where feldspar containing rocks (like volcanics) are adjacent to the karst system, such as in Puerto Rico.

If most organic carbon in cave systems is introduced from the surface, and diverse microbial populations exists in caves, it is likely that these ecosystems source the organic carbon content in cave systems as a nutrient or energy source (Barton and Jurado 2007; Barton and Northup 2007; E. Northup 2001; Northup et al. 2000). de Paula et. al. (2016) isolated several genera of bacteria and fungi in clastic cave sediments and showed that ca. 90% of isolates were metabolically active - not only proving the existence of microbiota in the system but that is also actively participating in the cave ecosystem. In Butler Cave, the organic carbon content of the clastic sediments is lower than what would be expected at the surface, so it is possible that

microbial activity has been re-processing the organic carbon content of the sediments. The majority of the TOC:N ratios of the Butler Cave sediments indicate a terrestrial source of organic carbon, but some samples did have TOC:N in the amino acid average range, indicating some microbial activity may be present. Because the breakdown of organic carbon by organisms results in a net release of CO_2 (and TOC generation from chemolithotrophs in oligotrophic environments also contributes to a net release in CO_2), the TOC of clastic sediments and active microbial populations of cave and karst systems should be considered when evaluating the overall carbon budget of the system.

5.0 Conclusions

The concentrations of organic carbon in deposited cave sediments have remained largely unquantified. The data presented here show that a significant difference exists in the grain size and TOC concentrations in the active fraction of diamicton and channel facies in Butler Cave. The diamicton facies sediment was overall sandier and had less TOC in the core samples but more TOC overall compared to the channel facies sediment. Butler Cave represents a cave in a temperate climate with little modern sediment injection and most of the TOC likely resultant from paleo-filling. The Butler Cave sediments are within the same range of TOC in tropical and temperate caves. Although the amount of data is limited, the comparisons between facies and different caves suggest that higher concentrations of TOC may be associated with younger sediments and influenced by flowing water rather than climatic conditions (tropical vs. temperate). Continued sampling of cave systems from a variety of climates with different sediment sources and should continue to determine the range of organic carbon that is stored in cave sediments and karst systems. The data presented here also show that TOC can occur across a range of grain sizes; this should be considered when evaluating the role of cave and karst sediments in contaminant fate and transport. Even small TOC concentrations, like those reported for Butler Cave, could potentially be responsible for increases in retardation of organic contaminants through the system and long-term storage of contaminants. Finally, the source and amount of organic carbon can be an indicator of paleoclimate conditions and microbial activity in oligotrophic environments.

6.0 References

Aberson MJR, Bolam SG, Hughes RG (2011) The dispersal and colonisation behaviour of the marine polychaete Nereis diversicolor (O. F. Müller) in south-east England. Hydrobiologia 672:3-14. https://doi.org/10.1007/s10750-011-0752-y

Banks ED, Taylor NM, Gulley J, Lubbers BR Giarrizzo, JG, Bullen HA, Hoehler TM, Barton, HA (2010) Bacterial calcium carbonate precipitation in cave environments: a function of calcium homeostasis. Geomicrobiol J 27:444-454. https://doi.org/10.1080/01490450903485136

Barton H, Taylor M, Pace N (2004) Molecular phylogenetic analysis of a bacterial community in an oligotrophic cave environment. Geomicrobiol J 21:11-20. https://doi.org/10.1080/01490450490253428

Barton HA, Jurado V (2007) What's up down there? Microbial diversity in caves. Microbe 2:132-138. http://hdl.handle.net/10261/61951

Barton HA, Northup DE (2007) Geomicrobiology in cave environments: past, current and future perspectives. J Cave and Karst Stud 69:163-178.

Blott SJ, Pye K (2001) GRADISTAT: a grain size distribution and statistics package for the analysis of unconsolidated sediments. Earth Surf Processes 26:1237-1248. https://doi.org/10.1002/esp.261

Bosch RF, White WB (2004) Lithofacies and transport of clastic sediments in karstic aquifers. In: Sasowsky ID, Mylroie JE (eds.) Studies of cave sediments Springer, Boston, MA, 22 pp. 1-22. https://doi.org/10.1007/978-1-4419-9118-8_1

Bottrell SH (1996) Organic carbon concentrations profiles in recent cave sediments: Records of agricultrual pollution or diagenesis? Environ Pollut 91:325-332. https://doi.org/10.1016/0269-7491(95)00064-x

Bretz JH (1942) Vadose and phreatic features of limestone caverns. J Geol 50:675-811. https://doi.org/10.1086/625074

Chess DL, Chess CA, Sasowsky ID, Schmidt VA, White WB (2010) Clastic sediments in the Butler Cave -Sinking Creek System, Virginia, USA. Acta Carsologica 39:11-26. https://doi.org/10.3986/ac.v39i1.109

de Paula CCP, Bichuette ME, Seleghim MHR (2020) Nutrient availability in tropical caves influences the dynamics of microbial biomass. Microbiologyopen 9:1:13. https://doi.org/10.1002/mbo3.1044

de Paula CCP, Montoya QV, Rodrigues A, Bichuette ME, Seleghim MHR (2016) Terrestrial filamentous fungi from Gruta do atão (São Desidério, Bahia, Northeastern Brazil) show high levels of cellulose degradation. J Cave and Karst Stud 78:208-217. https://doi.org/10.4311/2016mb0100

Downey AR (2020) Physical and chemical properties of clastic sediments from two caves in the northern karst region of Puerto Rico. MS Thesis, West Virginia University, Morgantown, West Virginia, USA. https://researchrepository.wvu.edu/etd/7716

Dreybrodt W (1999) Chemical kinetics, speleothem growth and climate. Boreas 28:347-356. https://doi.org/10.1111/j.1502-3885.1999.tb00224.x

EPA Superfund Soil Screening Guidance Part 5: Chemical Specific Parameters. Report Number 9355.4-14FSA. Retrieved February 7, 2022 from https://www.epa.gov/superfund/superfund-soil-screening-guidance

Ewers RO, Duda AJ, Estes EK, Idstein PJ, Johnson KM (1991) The transmission of light hydrocarbon contaminants in limestone (karst) aquifers. Third Conference on Hydrology, Ecology, Monitoring, and Management of Ground Water in Karst Terranes, Nashville, TN.

Ford DC, Williams PW (2007) Karst Hydrogeology and Geomorphology 2nd ed. Wiley and Sons, Hoboken, NJ

Frimmel FH, von der Kammer F, Flemmin HC, (2007) Colloidal Transport in Porous Media. Springer, New York, NY

Ghasemizadeh R, Yu X, Butscher C, Hellweger F, Padilla I, Alshawabkeh, A (2015) Equivalent porous media (EPM) simulation of groundwater hydraulics and contaminant transport in karst aquifers. PLoS One 10:1-21 e0138954. https://doi.org/10.1371/journal.pone.0138954

Gillieson, D (1986) Cave sedimentation in the New Guinea Highlands. Earth Surf Processes 11:533-543. https://doi.org/10.1002/esp.3290110508

Grabowski RC, Droppo IG, Wharton G (2011). Erodibility of cohesive sediment: the importance of sediment properties. Earth-Science Reviews 105:101-120. https://doi.org/10.1016/j.earscirev.2011.01.008

Hart EA, Schurger SG (2005) Sediment storage and yield in an urbanized karst watershed. Geomorphology 70:85-96. https://doi.org/10.1016/j.geomorph.2005.04.002

Herman EK, Toran L, White WB (2008) Threshold events in spring discharge:eEvidence from sediment and continuous water level measurement. J Hydrol 351:98-106. https://doi.org/10.1016/j.jhydrol.2007.12.001

Hicks CE, Sulman BN, West C, O'Neill C, Poppleton E, Porras RC, Castanha C, Zhu B, Wiedemeier DB, Torn, MS (2018) Root litter decomposition slows with soil depth. Soil Biol Biochem 125:1-12. https://doi.org/10.1016/j.soilbio.2018.07.002.

Husic A, Fox J, Agouridis C, Currens J, Ford W, Taylor C (2017) Sediment carbon fate in phreatic karst (Part 1): conceptual model development. J Hydrol 549:179-193. https://doi.org/10.1016/j.jhydrol.2017.03.052

Jover LF, Effler TC, Buchan A, Wilhelm SW, Weitz JS (2014) The elemental composition of virus particles: implications for marine biogeochemical cycles. Nat RevMicrobiol 12:519-528. https://doi.org/10.1038/nrmicro3289

Kosznik-Kwasnicka K, Golec P, Jaroszewicz W, Lubomska D, Piechowicz L (2022) Into the unknown: microbial communities in caves, their tole, and potential use. Microorganisms 10:2-18. https://doi.org/10.3390/microorganisms10020222

Mahler BJ, Valdez D, Musgroves M, Massei N (2007) Nutrient migration in carbonate aquifers in response to storms: a comparison of two geologically contrasting aquifers. Geological Society of America, Annual Meeting. Denver, Colorado, USA.

Mahler BJ, Lynch L, Bennett PC (1999) Mobile sediment in an urbanizing karst aquifer: implications for contaminant transport. Environ Geol 39:25-38. https://doi.org/10.1007/s002540050434

McCarthy JF, Zachara JM (1989) Subsurface transport of contaminants:mobile colloids in the subsurface environment may alter the transport of contaminants. Environ Sci Technol 23:496-502. https://doi.org/10.1021/es00063a001

Miller T (2018) Karst notes from the stricken land: Hurricane Maria and the Camuy Caverns. NSS News February 4-8.

National Center for Biotechnology Information (2022). PubChem Compound Summary for CID 8343, Bis(2-ethylhexyl) phthalate. Retrieved February 7, 2022 from https://pubchem.ncbi.nlm.nih.gov/compound/Bis_2-ethylhexyl_-phthalate

Northup DE, Dahm CN, Melim LA, Spilde MN, Crosse LJ, Lavoie KH, Mallory LM, Boston PJ, Cunningham KI, Barns SM (2000) Evidence of geomicrobiological interactions in Guadalupe Caves. J Cave Karst Stud 62:80-90.

Northup DE, Lavoie KH (2001) Geomicrobiology of caves: a review. Geomicrobiol J 18:199-222. https://doi.org/10.1080/01490450152467750

Padillab IY, Irizarry C, Steele K (2011) Historical contamination of the groundwater resources in the north karst aquifers of Puerto Rico. Rev Dimens 3:7-12.

Panno SV, Curry BB, Wang H, Hackley KC, Liu CL, Lundstrom C, Zhou J (2004) Climate change in southern Illinois, USA, based on the age and δ13C of organic matter in cave sediments. Quaternary Res 61: 301-313. https://doi.org/10.1016/j.yqres.2004.01.003

Pickle JD (1985) Dynamics of clastic sedimentation and watershed evolution within a low-relief karst drainage basin, Mammoth Cave region Kentucky. Doctoral Thesis, University of New Mexico.

Rice JA, MacCarthy P (1991) Statistical evaluation of the elemental composition of humic substances. Org Geochem 17:635-648. https://doi.org/10.1016/0146-6380(91)90006-6

Schwarzenbach RP, Gschwend PM, Imboden DM (2003) Environmental Organic Chemistry. Second ed. Wiley and Sons, Hoboken, New Jersey

Simon K, Pipan T, Ohno T, Culver D (2010) Spatial and temporal patterns in abundance and character of dissolved organic matter in two karst aquifers. Fund Appl Limnol 177:81-92. https://doi.org/10.1127/1863-9135/2010/0177-0081

Simon KS, Pipan T, Culver DC (2007) A conceptual model of the flow and distribution of organic carbon in caves. J Cave Karst Stud 69:279-284.

Springer GS, Kite JS (1997) River-derived slackwater sediments in caves along Cheat River, West Virginia. Geomorphology 18:91-100. https://doi.org/10.1016/S0169-555X(96)00022-0

Stringer CE, Trettin CC, Zarnoch SJ (2016) Soil properties of mangroves in contrasting geomorphic settings within the Zambezi River Delta, Mozambique. Wetl Ecol Manag 24:139-152. https://doi.org/10.1007/s11273-015-9478-3

Suarez-Moo P, Remes-Rodriguez CA, Marquez-Velazquez NA, Falcon LI, Garcia-Maldonado JQ, Prieto-Davo A (2022) Changes in the sediment microbial community structure of coastal and inland sinkholes of a karst ecosystem from the Yucatan Peninsula. Sci Rep 12:1-11. https://doi.org/10.1038/s41598-022-05135-9

Swezey CS, Lucas PC, Lambert RA (2017) Geologic controls on cave development in Burnsville Cove, Bath and Highland Counties. In: Bailey CM, Jaye S (eds). From the Blue Ridge to the Beach: Geological Field Excursions across Virginia. Geological Society of Americ,. Virginia, USA. 35pp. 89-123. https://doi.org/10.1130/2017.0047(04)

Toran L, Palumbo AV (1992) Colloid transport through fractured and unfractured laboratory sand columns. J Contam Hydrol 9:289-303. https://doi.org/10.1016/0169-7722(92)90009-4

Valen V, Lauritzen SE, Lovlie R (1997) Sedimentation in a high-latitude karst cave: Sirijordgrotta, Nordland, Norway. Norsk Geol Tidsskr 77:233-250.

van Hengstum PJ, Donnelly JP, Toomey MR, Albury NA, Lane P, Kakuk B (2014) Heightened hurricane activity on the Little Bahama Bank from 1350 to 1650 AD. Cont Shelf Res 86:103-115. https://doi.org/10.1016/j.csr.2013.04.032

Vesper DJ, Loop CM, White WW (2003) Contaminant transport in karst aquifers. Speleogenesis and Evolution of Karst Aquifers 1:101-111.

Vesper DJ (2008) Karst resources and other applied issues. In: Martin JM, White WB (eds). Frontiers of Karst Research. Karst Waters Institue, Leesburg Virginia, USA. 9pp. 65-73.

White WB (1988) Geomorphology and Hydrology of Karst Terrains. Oxford University Press, New York, New York

White WB (2015) The Caves of Burnsville Cove, Virgnia. Springer International, Cham, Switzerland. https://doi.org/10.1007/978-3-319-14391-0

White WB, Herman JS, Herman EK, Rutigliano M (2018) Karst Groundwater Contamination and Public Health. Springer International, Cham, Switzerland. https://doi.org/10.1007/978-3-319-51070-5

Williams SD, Farmer JJ (2003) Volatile organic compound data from three karst springs in Middle Tennessee, February 2000 to May 2001. U.S. Geological Survey, Open-File Report 03-355. 77pp. 1-69.

Woessner WW, Poeter EP (2020) Hydrogeologic Properties of Earth Materials and Principles of Groundwater Flow. The Groundwater Project, Guelph, Ontario, Canada

Yang XM, Drury CF, Reynolds WD, Yang JY (2016) How do changes in bulk soil organic carbon content affect carbon concentrations in individual soil particle fractions? Sci Rep 6:1-7. https://doi.org/10.1038/srep27173

Statements and Declarations

This work was supported by the National Institute of Environmental Health Sciences Superfund Research Program project PROTECT (Puerto Rico Testsite for Exploring Contamination Threats) PTE Federal Award Number 5P42ES017198-12 and the West Virginia University Ruby Distinguished Doctoral Fellowship.

The authors have no relevant competing financial or non-financial interests to disclose.

All authors contributed to the study conception and design. Material preparation, data collection, and analysis were performed by Jill Riddell. The first draft of the manuscript was written by Jill Riddell and all authors commented on previous versions of the manuscript. All authors read and approved the final manuscript.

Data Availability

For the purposes of this dissertation, all data and code used in this manuscript can be found in Appendix B. Upon journal acceptance, data will be made publicly available in the GitHub repository for this project: https://github.com/jlriddell12/ButlerCaveSediment.

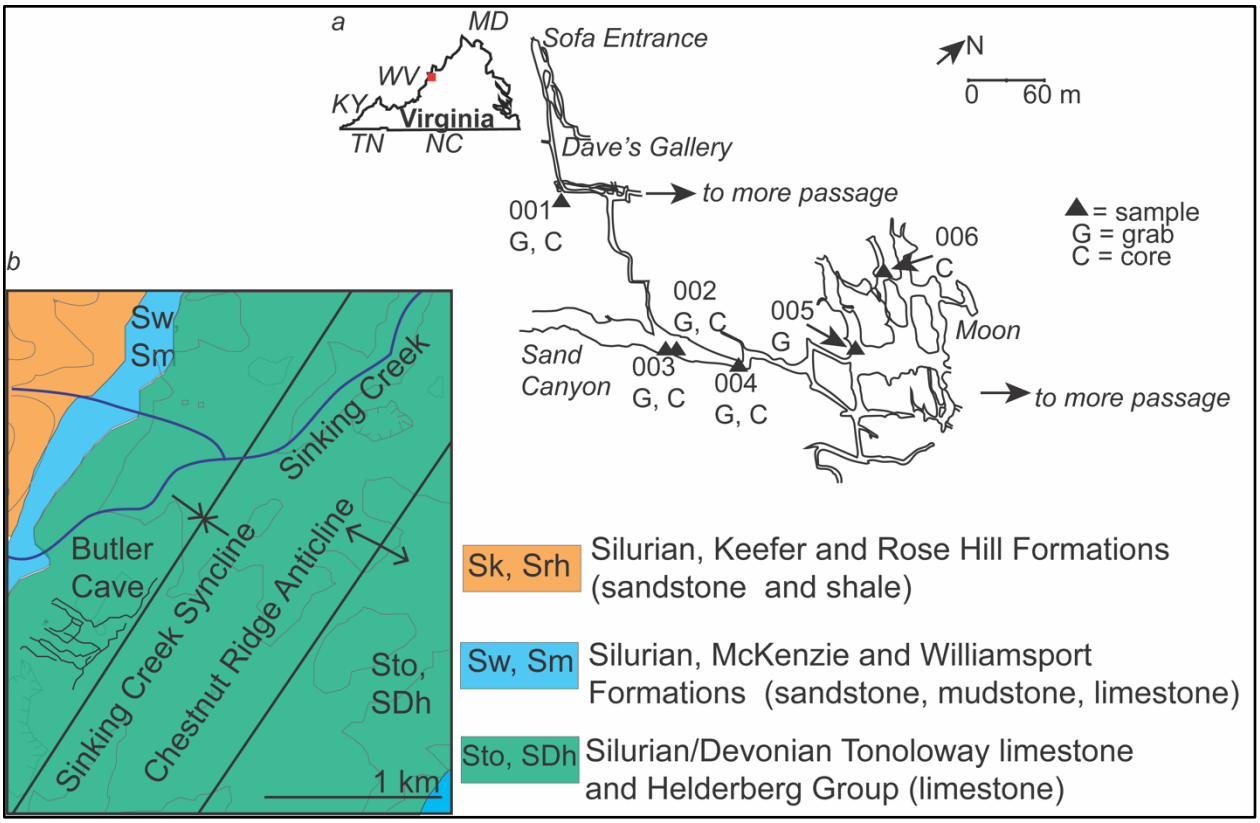

Fig. 1. Location of Butler Cave in VA and cave map with sample locations indicated with a black triangle and location number. Grab and core samples are indicated with letter G and C, respectively (a). Geology of the Butler Cave area of Burnsville Cove. Butler Cave formed along the Sinking Creek syncline in the Tonoloway limestone and larger Helderberg Group, indicated in green (b). Modified from White (2015) and Swezey et. al. (2017).

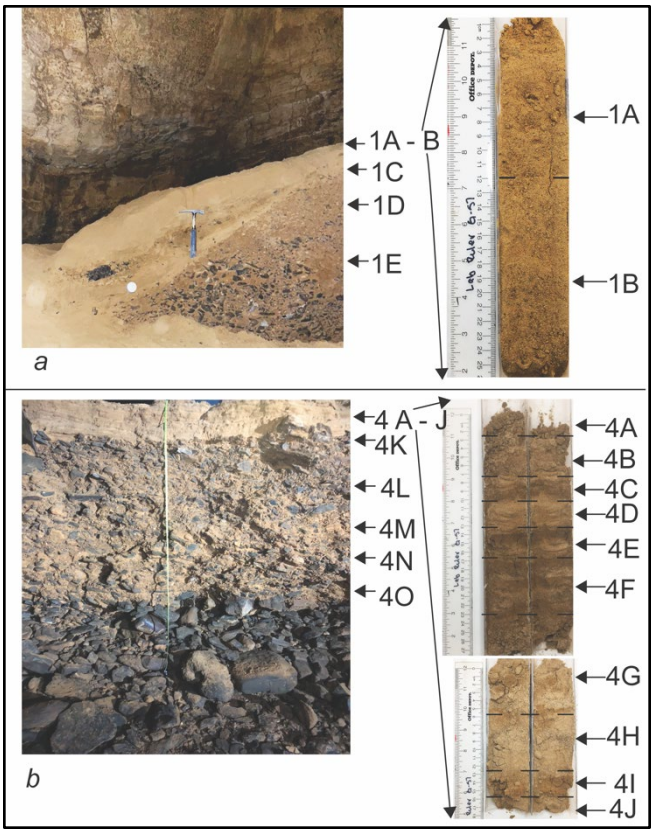

Fig. 2. Sample locations 001 (a) and 004 (b). Location 001 shows a smaller grained cap over a relatively unsorted deposit. The core samples (1A and 1B) represent the sandy cap and the grab samples (1C – 1D) represent the unsorted deposit. The core sample was uniform in color and apparent grainsize and was subsampled in two sections(a). Location 004 shows a sorted bank from finer to coarser grains ~2 m in height. The core samples were subsampled in 10 sections (4A- 4J) and represent the upper layer, which had visible color changes and layering. The grab samples (4K – 4O) represent the lower, larger grained section of the deposit (b).

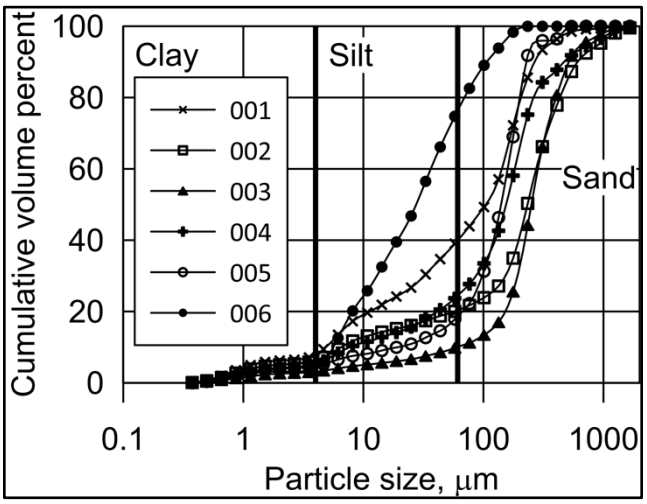

Fig. 3. Cumulative grain size distributions averaged for all samples collected at each location. Locations 001 – 005 are mostly sandy while location 006 is siltier in comparison. Location 006 is furthest from potential sediment entrance points (relative to the other locations), suggesting that sediments are being continually processed as they are transported through the cave. This results in smaller and more uniform grain size distributions with distance from sediment input.

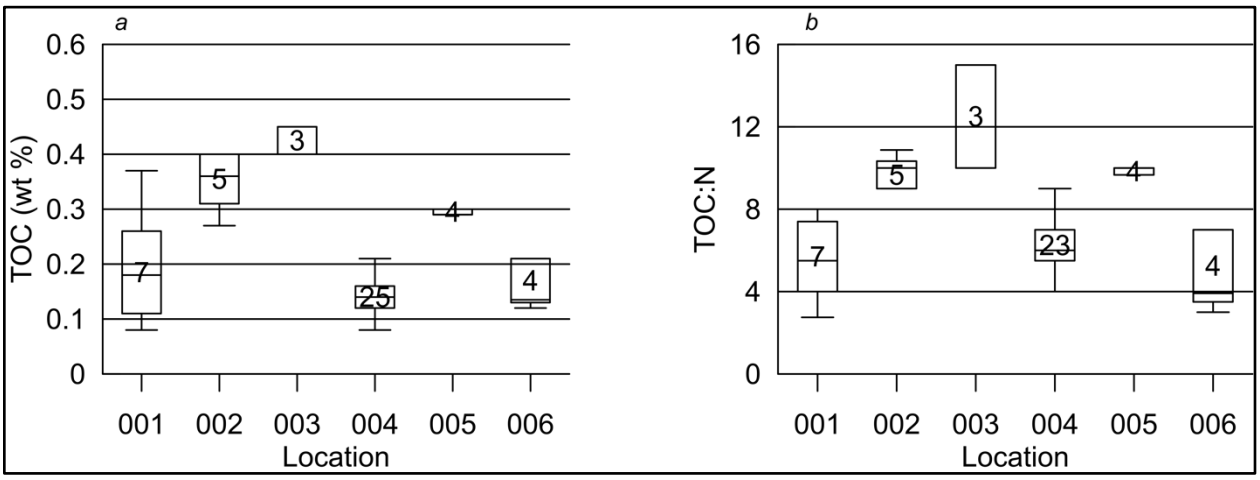

Fig. 4. Box and whisker plot of TOC wt % showing sample size and distribution across the six locations. Locations 001, 004, and 005 include laboratory duplicates (a). Box and whisker plot of TOC:N ratios across the sampling locations with similar distribution as TOC. Location 004 has n = 23 because two samples had TN = 0. Locations 001, 004, and 005 include laboratory duplicates (b).

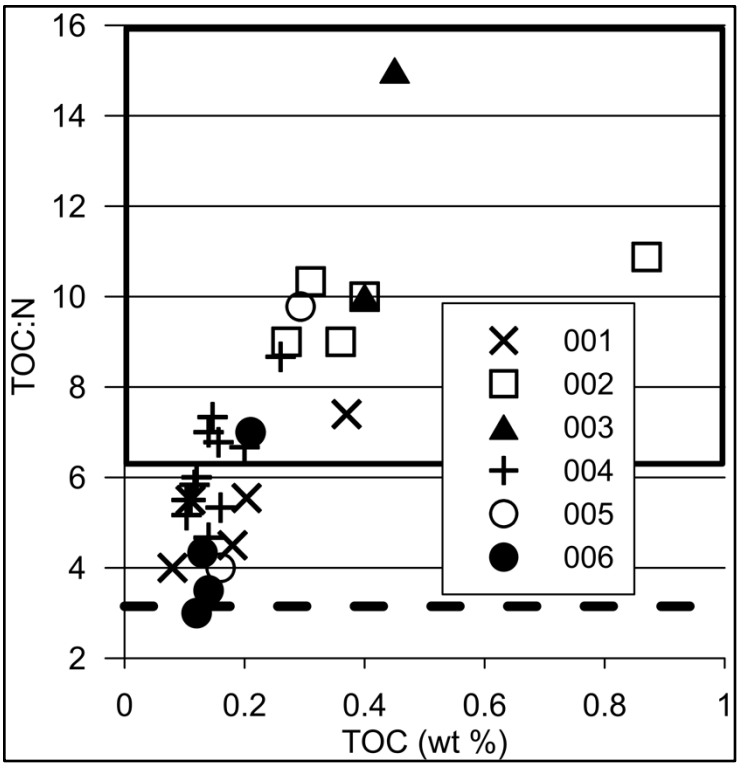

Fig. 5. TOC:N graphed relative to TOC wt % for all analyzed samples. The boxed area from ~6.43 – 16 TOC:N represents the humic and fulvic acid TOC:N range (Rice and MacCarthy 1991) and the dashed line at 3.15 TOC:N represents the amino acid average (Jover et al. 2014). Most samples fall within the TOC:N range reported for humic and fulvic acid, which may be indicative of a terrestrial organic carbon source. Some samples at locations 001, 005, and 006 are near the amino acid average for TOC:N, which may indicate microbial processing of organic carbon at those locations.

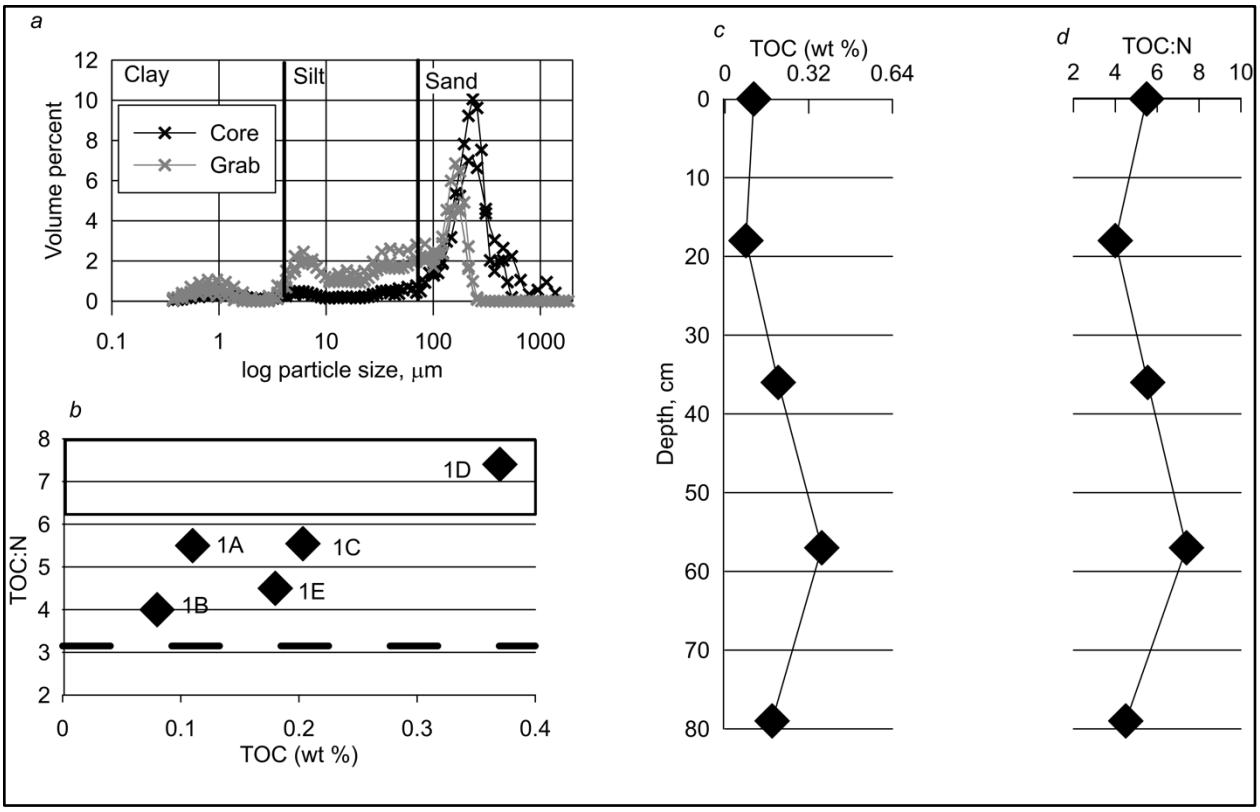

Fig. 6. Grain size percentage of the five samples analyzed at location 001 showing majority sand size grains in the samples, but with grab samples showing more silt, comparatively (a). TOC:N ratios relative to TOC wt % show four out of the five samples between the amino acid TOC:N average (Jover et al. 2014), represented by the dashed line and the humic and fulvic acid TOC:N range (Rice and MacCarthy 1991), represented by the shaded area (b). A general increase in TOC and TOC:N is observed with depth with the exception of the deepest sample, which was observed in the field to consist of very coarse gravel-sized grains (c, d).

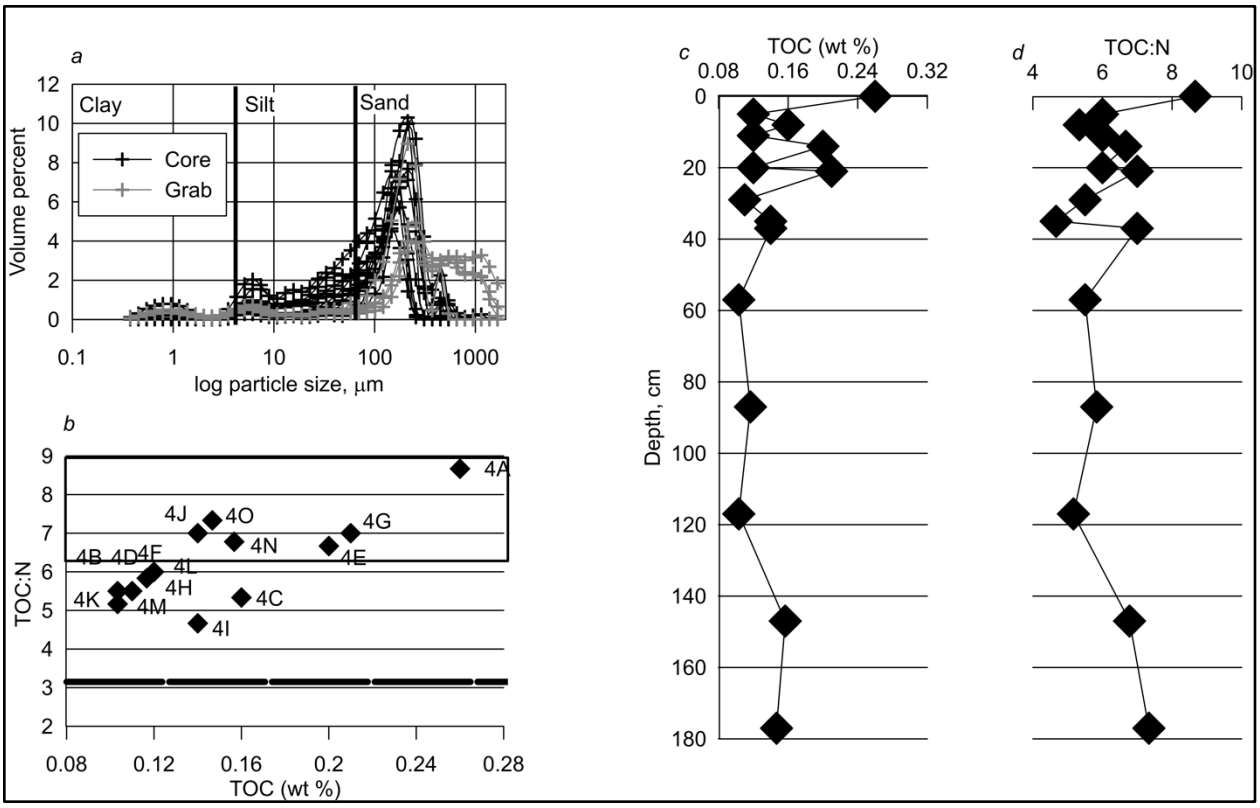

Fig. 7 Grain size percentage of the fifteen samples analyzed at location 004 showing a majority sand size percentage in the samples (a). TOC:N ratios relative to TOC wt % show nine samples between the amino acid TOC:N average (Jover et al. 2014) represented by the dashed line and the humic and fulvic acid TOC:N range (Rice and MacCarthy 1991), represented by the boxed area and six samples within the humic and fulvic acid TOC:N range (b). In the core samples, alternating high and low concentrations of TOC wt % and TOC:N are observed which is consistent with the described interbedded silts and shales of channel facies (c, d).

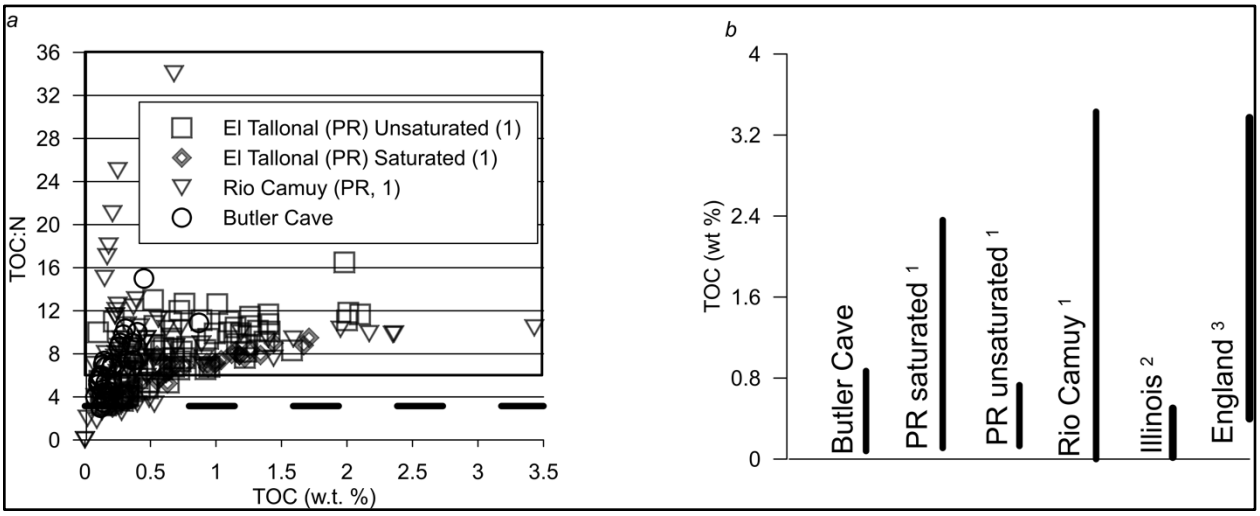

Fig. 8. TOC:N ratios for Butler Cave, El Tallonal Cave, and Rio Camuy Cave. Butler cave (black circles) and unsaturated sediments from El Tallonal Cave (blue squares) show a similar range of TOC:N while Rio Camuy sediments have the largest range of TOC:N and TOC. Dashed line indicates the average amino acid TOC:N (Jover et al. 2014) and the boxed range indicates the humic and fulvic acid TOC:N range (Rice and MacCarthy 1991) (a). TOC wt % ranges for a selection of clastic sediments reported in recent literature. Butler Cave and unsaturated sediments from TAL cave show similar ranges while Rio Camuy and England cave sediments, which were sampled within two and seven years of deposition, respectively, have a similar range of TOC wt % (b). (1) Downey (2020), (2) Panno et. al. (2004), (3) Bottrell (1996).

Table 1 Butler Cave data summary: sample schema, sediment type, particle size fraction, and chemical results for the ≤ 2mm fraction

Location	Facies Represented	Sample Type	Core sample depth, cm [+]	Sample Number	Sediment Type	TOC wt%	N wt%	TOC:N
001	Diamicton	Core	0 – 13	1A	very coarse silty fine sand	0.11	0.02	5.5
		Core	13 – 26	1B	very coarse silty fine sand	0.08	0.02	4.0
		Grab	–	1C	very coarse silty fine sand	0.20	0.04	5.5
		Grab	–	1D	fine sandy very coarse silt	0.37	0.05	7.4
		Grab	–	1E	fine sandy fine silt	0.18	0.04	4.5
002	Channel	Core	0 – 4.5	2A	very coarse silty fine sand	0.31	0.03	10.3
		Core	5 – 9.5	2B	very coarse silty fine sand	0.87	0.08	10.9
		Core	9.5 – 27	2C	very coarse silty fine sand	0.36	0.04	9.0
		Core	27 – 42.5	2D	fine sandy very coarse silt	0.27	0.03	9.0
		Grab	–	2E	fine sandy fine silt	0.40	0.04	10.0
003	Channel	Core	0 – 22	3A	poorly sorted medium sand	0.45	0.03	15.0
		Grab	-	3B	very coarse silty medium sand	0.40	0.04	10.0
004	Channel	Core	0	4A	very coarse silty very fine sand	0.26	0.03	8.7
		Core	1 – 5	4B	very coarse silty fine sand	0.12	0.02	6.0
		Core	5 – 8	4C	fine silty fine sand	0.16	0.03	5.3
		Core	8 – 11	4D	very coarse silty fine sand	0.12	0.02	6.0
		Core	11 – 14	4E	very coarse silty fine sand	0.20	0.03	6.7
		Core	14 – 20	4F	fine silty fine sand	0.12	0.02	6.0
		Core	20 – 21	4G	very coarse silty fine sand	0.21	0.03	7.0
		Core	22 – 30	4H	muddy fine sand	0.11	0.02	5.5
		Core	30 – 45	4I	very coarse silty fine sand	0.14	0.03	4.7
		Core	45 – 47	4J	very coarse silty fine sand	0.14	0.02	7.0
		Grab	–	4K	very coarse silty fine sand	0.10	0.02	5.5
		Grab	–	4L	fine silty medium sand	0.12	0.02	5.8
		Grab	–	4M	fine silty medium sand	0.10	0.02	5.2
		Grab	–	4N	fine silty medium sand	0.16	0.02	6.8
		Grab	–	4O	fine silty medium sand	0.15	0.02	7.3
005*	Channel or slackwater	Grab	–	5A	very coarse silty fine sand	0.29	0.03	9.8
		Grab	–	5B	very coarse silty fine sand	0.16	0.04	4.0
006*	Slackwater	Core	0 – 3	6A	fine sandy very coarse silt	0.21	0.03	7.0
		Core	3 – 9	6B	very fine sandy very coarse silt	0.13	0.03	4.3
		Core	9 – 16	6C	very fine sandy very coarse silt	0.14	0.04	3.5
		Core	16 – 23	6D	very fine sandy very coarse silt	0.12	0.04	3.0

TOC = total organic carbon; TOC:N is the molar ratio between organic carbon and nitrogen. *The facies for these locations have not been previously described in literature and was estimated based on physical description and observation. [+]Core sample depths are relative to the top of the sediment bank where the top = 0 cm. Ranges are given for where the respective sample was collected

Table 2 Comparison of maximum and minimum TOC values across climatic settings

		Highest Reported TOC wt %			Lowest Reported TOC wt %		
Climate	**Location**	**TOC**	**In-situ wetness**	**Sediment Age**	**TOC**	**In-situ wetness**	**Sediment Age**
Temperate	Butler Cave	0.87	Ephemeral cave stream	Unknown	0.08	Unsaturated	~70,000?
Temperate	England	3.37	Unknown	<7 years	0.4	Unknown	<7 years
Temperate	Illinois	0.5	Unknown	Modern	0.02	Unknown	~35,000 B.P.
Tropical	PR TAL unsat.	0.73	Unsaturated	Unknown	0.13	Unsaturated	Unknown
Tropical	PR TAL sat.	2.36	Saturated	Unknown	0.11	Saturated	Unknown
Tropical	PR CAM	3.43	Unsaturated	Modern	BDL	Unsaturated	Modern
Tropical	Brazil 2020	0.12*	Dry season	Unknown	0.004*	Dry season	Unknown
Tropical	Brazil 2016	1.31	Higher soil moisture	Unknown	0.49	Lower soil moisture	Unknown

*These data represent less TOC w.t.% than is expected based on their climate, location, and other data available (Downey, 2020; Panno et. al. 2004; Bottrell, 1996). In-situ wetness refers to various descriptions of the sediment provided by the respective study – e.g. “collected during dry season”; “collected from below water table in saturated conditions”

Table 3 Estimated adsorption coefficients (K_D) and retardation factors (R_F) for selected contaminants based on minimum (min) and maximum (max) TOC value in Butler Cave

Chemical	Source of K_{OC} values	Log K_{OC}	K_D (min)	K_D (max)	R_F min	R_F max	% Increase R_F
carbon tetrachloride, CT	EPA Superfund Guidance	2.18	0.12	1.32	1.63	7.84	381
1,2-dichloroethane, DCE	EPA Superfund Guidance	1.58	0.03	0.33	1.16	2.71	134
dichloromethane, DCM	EPA Superfund Guidance	1.00	0.08	0.09	1.04	1.45	39
diethyl phthalate, DEP	EPA Superfund Guidance	2.91	0.66	7.15	4.40	38.0	763
di(2-ethylhexyl)phthalate, DEPH	NCBI 2022	5.71	408	4440	2111	22950	987
di-n-butyl phthalate, DBP	EPA Superfund Guidance	3.20	1.26	13.7	7.50	71.7	856
tetrachloroethylene, PCE	EPA Superfund Guidance	2.42	0.21	2.31	2.10	12.9	516
trichloroethylene, TCE	EPA Superfund Guidance	1.81	0.05	0.56	1.27	3.89	208

Estimated K_D and R_F values for chemicals frequently detected in Puerto Rico karst (Ghasemizadeh et al., 2015; Padilla et al., 2011). Organic carbon-water partition coefficients (K_{OC}) values were obtained from National Center for Biotechnology Information and the EPA Superfund Soil Screening Guidance Part 5: Chemical Specific Parameters. The minimum (0.08%) and maximum (0.87%) TOC concentrations measured in Butler Cave were used to calculate the minimum and maximum K_D and R_F values. For RF, bulk density and effective porosity were estimated from reported values for sandy sediments (Andersen et. al., 2015; Grabowski et. al., 2011; Stringer et. al., 2016; Woessner et. al., 2020)

CHAPTER THREE

Adherence of nonfunctionalized and carboxylated polystyrene microspheres on a cave sediment: implications for organic contaminants and microplastics in karst systems

Jill L. Riddell[1*], Dorothy Vesper[1], Louis M. McDonald[1]

1 West Virginia University, Morgantown WV

*Corresponding author

ORC ID

Jill Riddell: 0000-003-3485-2896

Dorothy J. Vesper: 0000-0002-29607548

Louis M. McDonald: 0000-0001-8921-8951

Target Journal: Environmental Pollution

Target Submission Date: June 2022

Abstract

Caves provide an accessible window into karst systems by which karst processes can be studied. The role of clastic cave sediments in contaminant fate and transport remains relatively unquantified. Tracer experiments are often used to estimate the mobility of different substances or contaminants in karst aquifers. Recent studies have used polystyrene microspheres as a tracer to estimate bacteria mobility in karst systems given their similar size and surface chemistry to bacteria. These experiments typically resulted in low recovery of microspheres. In this study, the adherence of carboxylated and nonfunctionalized polystyrene microspheres onto a clastic cave sediment was quantified for microsphere dilutions in three water types – deionized water, a 25 mg/L $CaCO_3$ solution, and a karst spring water. Regardless of water type, both types of microspheres adhered to the sediment. Infrared absorbance data of different microsphere-solution-sediment mixtures indicated the potential presence of sediment minerals and microspheres in the solution. Analysis of solution pH and infrared spectra suggested pH and mineral constituents of the sediment are the most important factors in microsphere adherence. Using the adherence data, estimated K_{OC} values for both types of microspheres were calculated and were in the same ranges as phthalates, a known contaminant in karst aquifers that is also considered a plastic, like polystyrene. The chemical and physical commonalities between microspheres and organic and microplastic (MP) contaminants warrant further investigation of microspheres as a proxy for contaminants in sediment-contaminant experiments. The results of these experiments suggest that consideration of MPs adhered to sediments should be considered when quantifying MP contamination in karst systems.

Keywords – microspheres, cave sediments, adherence, microplastics

1.0 Introduction

Karst systems are geologic landscapes defined by their solutional features such has sinkholes, caves, springs, and sinking streams. Aquifers that form in these settings can store and transport large amounts of water and estimates suggest that these aquifers provide some amount of drinking water to over 25% of the global population (Ford and Williams 2007, Maupin and Barber 2005). Because of this, the contamination of karst systems by organic contaminants has been well documented and researched for several decades (Crawford and Ulmer, 1994; Ewers et al., 2012; Ewers et al., 1991; Ghasemizadeh et al., 2015; Loop and White, 2005; Padilla et al., 2011; Vesper et al., 2003; Vesper, 2002; White et al., 2018). These contaminants can exist in aqueous or non-aqueous phases and be denser or lighter than water (Loop and White, 2005; Schwarzenbach et al., 2003; Vesper et al., 2003). A notable library of literature exists regarding the fluid movement of these contaminants and their geochemical interactions through karst systems. Recently, attention has turned to evaluating and quantifying emerging contaminants in these systems like microplastics (MPs).

MPs are chemically organic solid particles < 5 mm in diameter that are derived from the production and breakdown of primary plastic materials (Corami et al., 2020; Prata et al., 2019; Zhou et al., 2019). MPs have become ubiquitous in the environment and present a challenging environmental pollution problem due to their ability to be the sorbate for organic contaminants and metals and carry those contaminants into other systems (Petersen and Hubbart, 2021). The presence of MPs in karst systems remains relatively unquantified. Two recent studies, one in a show cave in Italy (Balestra and Bellopede, 2021; Panno et al., 2019) and one in the karst region of Illinois, USA (Panno et al., 2019) detected measurable amounts of MPs in karst sediments (Balestra and Bellopede, 2021) and karst groundwater (Panno et al., 2019), respectively. Still, the surface chemical interactions between MPs and karst sediments as well as the larger role of karst sediments in contaminant fate and transport remains relatively unquantified.

Caves provide an accessible window into the larger karst aquifer system. Particularly, clastic cave sediments (sediments that are washed into a cave from the surface or sediments resultant from breakdown or erosion of the cave wall) are a useful and abundant resource in understanding the role of karst aquifer sediments in contaminant fate and transport. Karst aquifers, with their solutionally-enhanced permeability, have the capacity to transport sediments, especially during high-velocity events, like floods and hurricanes. During these events, sediments can be washed

into a karst system (Doehring and Vierbuchen, 1971; Herman et al., 2008) while existing sediments can be re-mobilized and transported within the system or to outlet points such as springs (Herman et al., 2008; Mahler, 1999). The characteristics of sediments and their mobility through karst aquifers has been used to understand historic hydrologic and paleoclimate conditions (Doehring and Vierbuchen, 1971; Gale, 1984) and karstification of the system (Ford and Ewers, 1978; Van Gundy and White, 2009). Sediments can also be a contaminant themselves and act as a carrier of adsorbed contaminants through karst systems (Frimmel et al., 2007; Goeppert and Goldscheider, 2019; Goeppert and Hoetzl, 2009; Mahler et al., 2007; Mahler, 1999; McCarthy and Zachara, 1989).

The processing and transport of aquifer sediments through the system has important implications for particle movement over a range of sizes (~1 nm – 10 μm) through karst aquifers. Different types of particles that exist in karst aquifers include mineral precipitates, natural organic matter, biological material such as bacteria (Goeppert and Goldscheider, 2019), and MPs (Balestra and Bellopede, 2021; Panno et al., 2019). Contaminants, like bacteria, are often in this size range and the adsorption of organic or metal contaminants onto sediment particles can create particles in this size range as well (McCarthy and Zachara, 1989). The storage and movement of these particles through karst aquifers is of particular interest due to the variable hydraulic conditions and geochemical parameters of karst aquifers (Goeppert and Hoetzl, 2009).

The adsorption of organic compounds on to a sediment is positively correlated to the amount of organic carbon in the sediment (Schwarzenbach et al., 2003). Caves, and by extension karst, systems are oligotrophic, < 2 mg/L organic carbon, (Barton and Jurado, 2007). Much research has focused on quantifying organic carbon in speleothems (Banks et al., 2010; Buczynski and Chafetz, 1991; Folk and Chafetz, 1983; Melim et al., 2008; Melim et al., 2001) and dissolved organic carbon in karst waters (Birdwell and Engel, 2010; Husic et al., 2017; Simon et al., 2010). Quantifying concentrations of organic carbon in clastic cave sediments has only recently begun to receive this same attention (Bottrell, 1996; de Paula et al., 2020; de Paula et al., 2016; Downey, 2020; Panno et al., 2004). Quantification of organic carbon content in clastic cave and karst systems is essential in understanding the sediment-contaminant chemical interactions.

Tracer experiments, where a substance is injected at one point in the system and measured at another point, are commonly conducted in karst aquifers to understand the aquifer geometry and the movement of aqueous phase liquids through the system (Kass, 1992). This technique

frequently uses dissolved tracers like dyes or salts (Kass, 1992). Tracers are often separated into conservative and reactive tracers (Kass, 1992). Conservative tracers are those tracers that do not react with their surroundings and whose concentrations remain relatively unchanged as the material moves through the system (Cao, 2020). Conservative tracers include salts, hydrogen and oxygen isotopes, and some dyes (Cao, 2020 and Kass, 1992). Reactive tracers are those tracers that do react with the aquifer surroundings and are used to understand different biological, geochemical, or geobiochemical reactions in aquifers (Cao, 2020). These tracers include charged particles, sediments, non-aqueous phase liquids, and some dyes. The type of tracer dedicates the shape of breakthrough curves with conservative tracers typically having the earliest breakthrough curve and highest peaks, compared to reactive tracers with later peak breakthrough and shorter peaks (Cao, 2020).

Particle tracer experiments, used to understand how sediment, bacteria, or other solids move through the system, commonly use natural particles, like sediments, or engineered particles, like microspheres. Polystyrene microspheres are manufactured particles ranging from <1 μm– 1,000 μm and can be made with a variety of surface charges and fluorescent tags which influence their chemical behavior and the method by which they are detected. Due to their similar size to bacteria, polystyrene microspheres have been used in a variety of tracer experiments to understand pathogenic microbe motility in karst aquifers (Auckenthaler et al., 2002; Bandy, 2016; Flynn and Sinreich, 2010; Goeppert and Goldscheider, 2011; Goldscheider et al., 2003; Goppert and Goldscheider, 2008; Harvey et al., 1989; Harvey et al., 2008; Sinreich et al., 2009). Recovery of microspheres in these experiments has ranged from 0 – 57%; low recoveries are often attributed to adsorption of the microspheres onto sediments or mineral surfaces. Some research has attempted to describe and quantify microsphere adsorption as it relates to bacterial adsorption (Sinreich et al., 2009), but few studies have quantified microsphere adsorption onto karst sediments and directly compared those results to field experiments. Further, few studies have explored the potential for microspheres to act as a surrogate chemical for specific characteristics of organic contaminants or MPs.

Microspheres, especially in the case of polystyrene (a benzene ring with a hydrocarbon chain), are a microplastic. They are chemically organic which make them a candidate for use as a surrogate for organic particles and MPs in laboratory experiments. The microspheres can be obtained with different surface chemistries and functional group configurations which can be

matched to the same on organic contaminants. Functional groups, like carboxyl groups, participate in acid-base reactions and can introduce a degree of hydrophilicity (Schwarzenbach et al., 2003) to the organic molecule to which it is attached. Microspheres with functional groups ("functionalized") and without functional groups ("non-functionalized") will be expected to react differently under the same natural or experimental conditions. Experiments using functionalized and non-functionalized microspheres can be used to estimate chemical behavior in different settings or under different chemical conditions.

Adsorption is the removal of a dissolved or aqueous compound by the solid phase constituents. The sorbate, or the compound being removed, is usually ionic to molecular in size while the sorbent, or the solid phase constituent (typically soil or sediment), is much larger – usually micron to millimeter in size. For the experiments described here, the microspheres are the sorbate, not dissolved, and are much larger in size than an ion or molecule, in this case 1-μm. The sediments are the sorbent, they are < 2 mm in size, and also solid. Due to the similar size and solid phase of both the sorbent and the sorbate, the term adherence will be used to describe any potential attachment of the microspheres onto the sediment.

The purpose of this study was to: i) conduct batch adherence experiments to determine if polystyrene microspheres adhere to clastic cave sediments and quantify any adherence; ii) conduct a preliminary investigation into how the microspheres adhere to the sediments; and, iii) use the results of the adherence experiments to estimate the adsorption coefficients (K_D) and organic carbon-water partitioning coefficients (K_{OC}) of microspheres to compare to known organic contaminants. Batch adherence experiments were carried out for carboxylated (functionalized) and nonfunctionalized 1.0 μm polystyrene microspheres in three different types of experimental solutions (deionized water, a calcium-carbonate solution, and a karst spring water) using a composite sediment from a cave. Both types of microspheres adhered to the sediments in all experiments. Infrared absorbance data of different microsphere-solution-sediment mixtures indicated the potential presence of sediment minerals and microspheres in the solution. Estimated K_{OC} values for both types of microspheres were in the same ranges as phthalates, a known contaminant in karst aquifers that is also considered a plastic, like polystyrene.

2.0 Methods

To quantify microsphere adherence to the sediments, batch sorption experiments were conducted with techniques adapted from the USEPA Technical Resource Document for Batch Type Procedures (Roy et al., 1991) which describes batch experimental techniques for testing the sorption capacity of different soils with ionic and organic compounds. In the experiments described here, a single, composite cave sediment was the sorbent and microspheres were chosen as the sorbate.

2.1 Sediment Preparation and Analysis

The clastic cave sediment was collected in bulk using stainless steel instruments from Dropping Lick Cave in Monroe County, WV, a cave typical of the valley and ridge karst system in central Appalachia (Bausher, 2018). This cave is formed in the Beekmantown Formation, an Ordovician dolostone and limestone unit. The sediment was air dried in a dark room for ~72 hours. Upon collection, the cave sediments were above the active cave stream. After air drying the sediment was combined (gentle breaking apart of large clumps and light grinding) and sieved to < 2 mm, which represents the active fraction (particles that are sand sized or smaller). Particles in this size range have increased surface area and are responsible for surface chemistry interactions within a sediment profile . This composite sediment was used in all the experiments to hold constant the effects on pH and ionic strength from the sediment on the microsphere solutions.

Particle size distribution for the < 2 mm fraction of sediments was measured by further air-drying samples in a fume hood, mixing the sediments in a 1:1.5 sediment to 5% Calgon® mass ratio solution, and shaken at 70 rotations per minute (RPM) on a rotary shaker for ~ 24 hours. Particle size was measured using a Beckman Coulter single wavelength LS13-320 particle size analyzer at Bucknell University, measuring from 0.4 μm – 2,000 μm. The particle size data are reported in volume percent and the raw data were organized in R and processed using the GRADISTAT program (Blott and Pye, 2001) to determine volume percent of sand, silt, and clay. Nine aliquots of the homogenized sediment were analyzed for particle size.

A portion of sediment was also oven dried to calculate percent moisture to determine the oven-dried mass equivalent weight during the experiments. Seven replicates of sediment were analyzed for total carbon (TC) and total inorganic carbon (TIC). For TC analysis, samples were air-dried for 24 hours, lightly homogenized using an agate mortar and pestle, and subsequently

oven-dried at 60 C for 24 hours. TC was measured on a Carlo Erba NA1500 CNHS elemental analyzer at the University of Florida Stable Isotope Mass Spectroscopy Laboratory in Gainesville, Florida. TC is determined by measuring the CO_2 in a sample after it is combusted and the oxygen and water are removed. TIC was measured by acidifying the sediment in an N_2 environment and quantifying the degassed CO_2 using an UIC 5017 CO_2 coulometer. TOC is determined as the difference between TC and TIC. TC, TIC, and TOC are reported as a weight percent (wt %) by sample.

2.2 Microsphere selection

Polystyrene 1.0 μm yellow-green (YG) fluorescent (excitation = 441nm, emission = 486 nm) carboxylated microspheres (CMS) and non-functionalized microspheres (NFMS) microspheres were selected for these experiments (Polysciences, Inc., Warrington PA; respective item numbers 15702-10 and 17154-10). Polystyrene is a synthetic aromatic hydrocarbon polymer consisting of a hydrocarbon chain attached to a benzene ring (Fig. 1a). Polystyrene is used commonly in a variety of plastic and foam goods and was chosen as the base material for these experiments due to its affordability and relative chemical inertness in water. The CMS are modified with a carboxyl (COOH) functional group attached to the hydrocarbon chain (Fig. 1b) which, theoretically, alters the chemical properties and behavior of the CMS in solutions. Both types of microspheres are polar compounds and can participate in hydrogen bonding which will influence adherence. Carboxyl groups are proton donors with an acid dissociation constant (pK_a) around pH = 5 (Wade, 2006) and can participate in ionic bonding. (In the case of polystyrene, this value may increase due to the hydrocarbon chain in the polystyrene structure, Vysotsky et al., 2020). This happens when the hydrogen ion is released from the COOH group and a negatively charged surface (COO^-) is created when the carboxyl group is introduced to a fluid at pH = 5 or higher. This negatively charged surface creates an opportunity for surface chemical interaction, or adherence, between the CMS and other particles in the same fluid. The NFMS microspheres, lacking the carboxyl functional group, should be less likely to interact with sediments in the same way as CMS, and should be relatively more inert than the CMS. However, the hydrocarbon chain on the polystyrene molecules can still participate in some level of adherence or chemical attraction with other materials through hydrogen bonding or Van der Waals forces. Further, the hydrophobicity of the benzene ring will drive both molecules out of solution and encourage adherence.

2.3 Experimental Design and Data Analysis

Both types of microspheres were obtained in a 2.5% aqueous suspension in 10-mL quantities at a concentration of 4.55 x 10^{10} particles/mL. Because of these high concentrations in small volumes, serial dilution of ~5,000x was done to create a new stock solution of each microsphere type so that the spheres could be accurately counted during each stage of the experiments. It was also necessary to create an adequate volume of experimental solutions. Further dilutions of varying concentrations were made from these new stocks for the adherence experiments. For each sphere type, three sets of experimental dilutions were made to match the experiments: 1) organic free, deionized water (DI), 2) a 25-mg/L $CaCO_3$ solution, and 3) a representative karst water collected from a tufa spring to provide a total of six experimental types (2 microsphere types x 3 solution types). The karst water was collected from a tufa spring in southwestern Pennsylvania and analyzed for major anions and cations according to EPA Methods 200.7 and 300.0, respectively, at the West Virginia University National Resource Center for Coal and Energy.

Each of the six experimental solution types was then diluted again to create up to 14 different initial solutions per experiment with varying concentrations of microspheres (Fig. 2). These concentrations of microspheres were mixed with the representative sediment to measure the adherence of each type of microspheres onto the sediment under the three different dilution conditions (DI water, $CaCO_3$ solution, representative karst water). The different solution conditions allow for the assessment of the role of pH and $CaCO_3$ concentration on adherence. The DI water has negligible ionic strength and no dissolved ions, like calcium; the $CaCO_3$ solution has 25 mg/L calcium; and the karst water has dissolved concentrations of calcium, magnesium, and other ions with high ionic strength (Table 1).

The sediment to solution ratio and equilibration time were determined via the methods described in Roy et. al. (1991) for ionic solutes and through evaluation of preliminary data to determine microsphere counting consistency. The CMS can participate in ionic bonding due to the COOH group, so this method was selected for consistency across the experiments.
The initial solutions of microspheres were mixed in a 1:20 ratio (~1.25 g sediment to ~25 mL solution) of sediment to solution in amber glass vials. The fluorescent properties of the microspheres increase their likelihood to degrade in fluorescent lighting so amber glass vials and the darkest possible laboratory lighting was used to minimize degradation. After mixing, the

solutions were rotated on a rotary shaker (at 70 rotations per minute, RPM) for four hours (equilibration time) to ensure thorough mixing of solutions. Afterwards, the solutions were centrifuged at 1,000 RPM on a Beckman Coulter Allegra X-30 series centrifuge to separate the supernatant from the sediment mixtures. The supernatant (equilibrium solution) was then pipetted into a clean amber glass container for storage until analysis.

The initial and equilibrium solutions were analyzed on BD LSR Fortessa Analyzer flow cytometer at the West Virginia University Flow Cytometry and Single Cell Core Facility. This instrument counts cells and particles in a fluid stream. The instrument uses fluorescence activated cell sorting to sort particles of interest - in this case 1 um YG – as the sample flows past an excitation source (laser). This instrument can detect up to twelve fluorochromes. Since the microspheres are imbued with YG dye, they are easily detected by the 488 nm laser on the instrument. The emitted fluorescence is detected by a forward scatter (FCS) diode and the resulting particle information is reported. All particle events, that is all the target particles, or "beads", in a sample are counted. This provides an exact count of microspheres in 50 μL of solution, from this the equilibrium and initial concentrations of microspheres (sph) per mL (sph/mL) are determined.

2.4 Determination of sediment:solution ratio and equilibration time

The sediment:solution ratio refers to the grams of sediment relative to the milliliters of microsphere solution and the equilibration time refers to the time the solutions are allowed to mix on the rotating shaker. For NFMS and CMS experiments were carried out for sediment:solution ratios at 1:4, 1:10, 1:20, 1:40, 1:60; 1:100: 1:200: and 1:500. For both sphere types, equilibration times of 1, 24, 48, and 72 hours were evaluated. Based on preliminary data, a ratio of 1:20 and equilibration time of 4 hours was chosen for the following experiments to reflect the potential ratio that would be observed in a natural setting. These parameters resulted in adhered microspheres that is consistent with previously reported field experiments and allows for comparison of different microsphere behavior under the same conditions (data for this process can be found in the Supplementary Data section of this paper).

2.5 Data Evaluation

The microsphere counts from the flow cytometer were used to calculate the adhered concentration of microspheres, sph/g, relative to the mass of sediment used according to Equation 1.

$$Ad\ conc\ \left(\frac{sph}{g}\right) = \left(init\ \frac{sph}{mL} - equil\ \frac{sph}{mL}\right) \times \frac{volume\ solution(mL)}{mass\ sediment\ (g)} \quad \text{Equation 1.}$$

Where ad conc is the adhered concentration, init is the initial solution concentration and equil is the equilibrium solution concentration. The adhered concentration was graphed against the equilibrium concentration to create adsorption isotherms. Adsorption isotherms are simply graphical representations of the amount of solute (in this case, microspheres) adsorbed onto a sorbent (in this case, sediment) relative to the equilibrium concentration of the solute. The slope of the line of these graphs indicates the K_D which describes the average bulk removal of the sorbate from solution by the sorbent. The graphical models and data were compared using an f-statistic and p-value.

The fraction of organic carbon of the sediment was calculated based on the organic carbon content determined via the CNS analyzer described above. From this, the soil K_{OC} was calculated:

$$K_{OC} = \frac{K_D}{f_{\ OC}} \quad \text{Equation 2.}$$

Because sorption or adherence occurs via partition into soil or sediment organic matter (Schwarzenbach et al., 2003), K_D values are highly variable based on the organic carbon content of the soil or sediment. Normalizing K_D values to organic carbon content by calculating K_{OC} allows for a better comparison between the same substances in different media. K_{OC} is still a measure of substance mobility, and the mobility of several known organic contaminants are often reported in K_{OC} to remove the influence of the sediment chemistry. While K_{OC} is typically reported for aqueous compounds and not solids, the K_{OC} of the microsphere solutions was calculated in order to have a similar parameter to compare to other compounds. The calculated K_D and K_{OC} values for the microsphere experiments were compared to the known K_{OC} values of contaminants in karst aquifers (such as chlorinated solvents, volatile organic compounds, and plastics) to estimate the potential for the microspheres to act as a surrogate for these contaminants in future experiments.

2.6 FTIR-ATR spectroscopy analysis of sediment and microsphere solutions

Fourier transform infrared spectroscopy (FTIR) via attenuated total reflectance (ATR) infrared (IR) absorbance spectra were collected using a Nicolet Magna-IR 560 FTIR Spectrometer at the University of Arizona. Spectra of the highest concentrations of microspheres in the DI and 25 mg/L $CaCO_3$ and solution-sediment controls (no microspheres) were obtained by placing 1 mL of solution on a Ge internal reflection element (IRE) cell. Samples were subjected to an incident beam angle of 45°. Spectra data were baseline corrected and the water signature subtracted using OMNIC processing software. IR bands were identified in OMNIC and statistical analysis of processed spectra were done in ChemoSpec (Hanson, 2019) in R. Functional group assignments were made based on reported functional group assignments for similar compounds in the spectroscopic literature.

Hierarchical cluster analysis (HCA) was done using ChemoSpec on the FTIR spectra to calculate "distances" between samples, or spectra. In this method, samples that are similar to one another are clustered together (Varmuza and Filzmoser, 2009). The results are reported as a dendrogram and suggest some correlation in samples that cluster together. A classical principal component analysis (PCA) was also done on the spectra using ChemoSpec again, to determine if any spectra samples could be explained by the same components (Varmuza and Filzmoser, 2009). These analyses were applied in two ways: grouping the spectra by microsphere type (NFMS and CMS) and grouping the spectra by water treatment type (DI and $CaCO_3$, spectra were not collected on the karst water group). Together, these analyses may reveal if microsphere type or water treatment type influence IR-bands. To determine if any specific IR bands had greater influence in the components of the PCA analysis, s-plots were created in ChemoSpec. These plot the correlation frequency of each variable and its PCA score against the covariance of the same variable-score combination. The result is an s-shaped plot in which the most influential variables (in this case IR-bands) are in the lower-left and upper-right regions of the plot.

2.7 Electron microscopy

Back-scattered electron images (BSE) were collected from the sediments and microsphere-sediment solutions on a Hitachi S-4800 cold-field emission gun scanning electron microscope (FE-SEM) at the Kuiper Imaging Facility at the University of Arizona in Tucson, AZ. An accelerating voltage of 15.0 kV and a working distance of 8 mm were used to obtain the BSE images. The stock microsphere solutions and sediment-microspheres pictures were imaged at

varying levels of magnification. Samples were freeze dried and coated in 5 nm of platinum by ion sputter to generate conductivity. This analysis was able to directly observe microspheres on or near sediment surfaces.

3.0 Results

3.1 Sediment analysis of the active fraction, < 2mm

The aliquots analyzed for particle size ranged from 35 – 61 % sand and 39 – 65% silt. All aliquots were classified as poor to poorly sorted; samples with < 50% sand were classified as very fine sandy very coarse silt (n = 3) and samples with > 50% sand were classified as very coarse silty very fine sand (n = 6). Concentrations of wt % TC, TIC, and TOC ranged from 1.07 – 1.18%, 0.16 – 0.60%, and, 0.57 – 0.91%, respectively. Reaction time of the TIC analyses indicated that dolomite or another slow reacting carbonate was present (J. Curtis, personal communication, March 23, 2020). Since the sediments were collected from a cave that formed in dolostone-containing unit it is likely dolomite is an important carbonate mineral in the sediments. The TOC ranges measured for these sediments are in the same ranges as those reported for unsaturated clastic cave sediments (Bottrell, 1996; de Paula et al., 2020; de Paula et al., 2016; Downey, 2020; Panno et al., 2004). Consistency in the grain size percentage of the sediments indicate that the sediments were well homogenized and sediment controls on pH and ionic strength in the solution will be constant in each experimental scenario.

3.2 Adherence of NFMS and CMS

For both microsphere types in all solutions, correlation was observed between the adhered and equilibrium concentrations, indicating adherence did occur. The strongest relationships ($R^2 > 0.9$) were observed in NFMS in karst water and CMS in DI and 25 mg/L $CaCO_3$ solution. For NFMS, three adherence experiments in DI water, three experiments in 25 mg/L $CaCO_3$ solution, and three experiments in the karst water were carried out.

The percent of NFMS removed from the initial solution ranged from 49.1 – 88.2% (Table 2). For all DI (and subsequent experiments) only the linear range of adherence was observed due to the low concentration of microspheres required to be accurately counted by the flow cytometer. The calculated adsorbed spheres/g concentration was compared to a modeled linear fit via an f-test and resulted in a significant fit value ($p < 0.01$). However, some R^2 values of the linear fits were < 0.5 so these significant f-test results may be skewed by the low sample number

in some experiments. The slope of the linear models was considered to be the estimated K_D value which averaged 37.1 $\pm$ 12 (Fig 3a). The calculated K_{OC} values based on these K_D values averaged 5.16 x 10^3 $\pm$ 1.7 x 10^3. The percent of NFMS removed from the initial to the equilibrium solutions in the 25 mg/L $CaCO_3$ solution averaged 60.3% (Table 2). These experiments were also fitted with a linear model (Fig 3b) and the f-test statistic also showed a significant ($p < 0.01$) for the three experiments. Across the three experiments, the K_D values averaged 25.3 $\pm$ 15 and the K_{OC} values averaged 3.52 x 10^3 $\pm$ 2.0 x 10^3. In the three experiments using the karst water for the microsphere dilutions, percent removal of NFMS from the initial solutions increased to 93.5%, a 29% and 55% increase in removal compared to the DI solution and 25 mg/L $CaCO_3$ solution experiments, respectively. The linear model fits in the karst water experiments were less robust than in the DI and $CaCO_3$ experiments (Fig. 3c). However, in these karst water experiments the K_D values averaged 247 $\pm$ 71 and the K_{OC} values averaged 3.01 x 10^4 $\pm$ 6.60 x 10^3. The increase in adhered microspheres and the order-of-magnitude increase in K_{OC} in the karst water experiments compared to the DI and 25 mg/L $CaCO_3$ experiments, indicate that increasing dissolved mineral content or other chemical parameters are driving adherence of NFMS onto these sediments under the specified parameters.

For the CMS, four experiments in DI water were conducted. Here, linear model fits (Fig. 3d) had an overall higher average R^2 than the DI experiments for NFMS and still had significant f-test statistic results ($p < 0.01$). The average percent removal of CMS in microspheres (64%) was lower than the DI experiments for NFMS. The average K_D and K_{OC} values for the CMS in DI water were on the same order of magnitude as for the NFMS at 40.4 $\pm$ 21 and 5.60 x 10^3 $\pm$ 2.9 x 10^3, respectively. For CMS in 25mg/L $CaCO_3$ solution experiments, R^2 values indicate the strongest linear relationship between equilibrium spheres/mL and adsorbed spheres/g (Fig. 3e) of any of the experiments reported here (Table 2). Yet, the average percent removal of CMS initial solutions was the lowest of all the experiments reported here at 55.5%. The average K_D and K_{OC} values remained in the same order of magnitude for all experiments reported thus far at 28.8 $\pm$ 16 and 4.01 x 10^3 $\pm$ 2.2 x 10^3, respectively. Finally, for the CMS in karst water solutions, the average R^2 of the linear models was the lowest of all the experiments reported here (Table 1). However, the average percent removal of CMS from the initial solutions was the second highest for the all the experiments reported here at 88.8%. The average K_D and K_{OC} values were an order of magnitude higher than for CMS in the DI and 25 mg/L $CaCO_3$ solutions, at 232 $\pm$ 158 and

$3.22 \times 10^4 \pm 2.2 \times 10^4$, respectively. This same increase was also observed in the NFMS in the karst water. The greater removal of NFMS and CMS in the karst water experiments indicates that some chemical parameter of the karst water is driving increased adherence. It should be noted that the true adherence pattern of NFMS and CMS is likely not linear, and the linear pattern observed here is due to the relatively low microsphere concentration necessary for the instrument to count. Regardless, the purpose of these experiments was to determine if microspheres were adhering to the karst sediments under different experimental conditions and the results suggest that adherence is occurring.

3.3 FTIR-ATR and SEM

Solid polystyrene has characteristic IR bands from 1550 – 1610 cm^{-1} associated with the C=C stretch, from 1550 – 1750 cm^{-1} associated with the C=O stretch, from 2800 – 3060 cm^{-1} associated with C-H stretch in aliphatic and aromatic arrangements, and from 3610 – 3645 cm^{-1} associated with O-H stretch of hydroxyl groups (Al-Kadhemy et al., 2016; Hermán et al., 2015). IR bands from 1550 – 1750 cm-^{1} can also be associated with the C=O of COOH groups. The FTIR spectra of the dried sediment used in these experiments had IR bands at 1040 and 1110 cm^{-1} which are associated with Si-O stretch in quartz and other silicate minerals; and at 3420 and 3620 cm^{-1} associated with the O-H stretch of hydroxide groups in clay minerals or aqueous compounds (Bandopadhyay, 2010; Jozanikohan and Abarghooei, 2022). Microsphere-sediment-solution spectra had IR bands at 1040, 1110, 1540 (NFMS only), 1700, 2850, 2920, and ~3330 cm^{-1} (Fig. 4c, d). Functional group assignments for these are IR bands can be found in Table 3.

The appearance of IR bands at 2850 cm^{-1} and 2920 cm^{-1} in the microsphere-sediment-solution mixtures (but their absence in the sediment spectra) indicate some effect of the microspheres on the sediment spectra. In solid polystyrene, IR bands in this range are associated with C-H stretch of aliphatic or aromatic structures. The hydrocarbon chain of the polystyrene could be interacting with some mineral surface in the sediment. IR bands at 1540 cm^{-1} and 1700 cm^{-1} in the microsphere-sediment-solution mixtures and their absence in the dried sediment spectra, also suggest some bond activity in the C=C bonds of the polystyrene and the sediments. The characteristic Si-O stretch IR bands are apparent in the dry sediment spectra and in the microsphere-sediment-solution mixtures. No difference in spectra was observed in the DI treatment and $CaCO_3$ treatment and signature IR bands of calcite and dolomite were not observed in the sediment spectra or microsphere mixtures spectra.

SEM images were able to identify the possible effects of COOH groups on the exterior of the CMS (Fig. 5a). These structures appear to contribute to an ordered arrangement of CMS in their undiluted form (Fig. 5b). SEM images of microsphere and sediment mixtures identified microspheres on the sediment matrix (Fig. 5c). Microspheres were also observed to have some sediment material on their surfaces as well (Fig. 5d).

These results clearly demonstrate that microspheres adhere to the clastic cave sediment regardless of water type. The COOH group did not result in stronger adherence of the CMS to the sediment. However, different surface chemistry interactions could be responsible for the adherence of each type of microsphere where the COOH group is responsible for a different chemical bond interaction in the CMS that is not present NFMS. The adherence of NFMS may be driven by the benzene ring or hydrocarbon chain structure of the polystyrene.

4.0 Discussion

4.1 The role of pH and $CaCO_3$ on adherence

A controlling factor of the surface chemistry interactions of the microspheres and sediment is the pH of the solution, and to some degree, the alkalinity of the solution. The changes in pH and alkalinity as contributed by the addition of sediments and microspheres will vary with the concentration of each and the initial pH solution. Further, ionic strength and dissolving species contributed by the sediment will also change the pH of the solution and ultimately sediment-microsphere interactions. Though this is a complicated and non-linear relationship, some inferences can be made with data presented here. The adherence of both types of spheres is likely being controlled by the pH of the different solution types (DI, 25 mg/L $CaCO_3$, and the karst water), the contribution of pH and ionic strength changes from the sediment, and, for the CMS, the pK_a of the COOH functional group.

The effects of DI water on mineral surfaces can be difficult to estimate due to the low ionic strength of DI water. The microspheres may have contributed some IS or alkalinity to the solutions reported here. Regardless of these effects, the DI experiments had similar K_D results as the other two water types. In the DI water experiments, the average pH of the DI water was 5.62 and the addition of the sediment to the water increased the average pH to 8.04 (Fig. 6a) after mixing on the rotator for four hours. For the initial solutions, or those solutions that just consisted of DI water and varying concentrations of NFMS or CMS, the pH decreased (Fig.

6a). A greater decrease in pH was observed in NFMS initial solutions than CMS. For the equilibrium solutions (solutions with DI, sediment, and microspheres), the pH increased in each case (Fig 6a). The pH only exceeded 8.04 in CMS equilibrium solutions with low concentrations. This indicates that some property of the sediment is resulting in an increase in pH and some property of the microspheres in contributing to a decrease in pH. The CMS had a larger pH range than the NFMS in both the initial and equilibrium solutions. This range of CMS pH was correlated to the number of microspheres in solution where a higher concentration of microspheres was associated with lower pH. This could be a result of the dissociation of the H^+ from the COOH since the pH values were >5, the pK_a of COOH. Thus, the more CMS in a solution, would result in a higher concentration of H^+ and therefore a lower pH. These negatively charged COO^- surfaces could also be a driving factor in microsphere adherence with any positively charged surface on the sediments. However, adherence of NFMS was also observed in DI solution and could be due to other intermolecular forces such as hydrogen bonding or Vander Waals forces.

In the 25 mg/L $CaCO_3$ experiments, the initial pH of the $CaCO_3$ solution was higher than the DI solution at 7.27 but the addition of the sediment decreased the average pH of the solution to 6.24 (Fig. 6b). The initial solutions of NFMS and CMS had lower average pH ranges than the equilibrium solutions (solutions with microspheres and sediment). The CMS solutions had a larger a pH range overall than the NFMS solutions and both microsphere types generally exhibited the same pattern of pH ranges as in the DI solution experiments but at an overall lower average pH except for the initial NFMS solutions (Fig 6b). For the karst water experiments, the average pH ranges of all microsphere solutions (initial and equilibrium) were between 7.57 – 8.45 (Fig. 6c). The pH of the karst water averaged 8.30 and the pH of the water after the addition of the sediment was 8.05. These ranges of pH are much smaller than in the DI and 25 mg/L $CaCO_3$ solutions (the dissolved concentration of Ca^{2+} in the karst water was 74.0 mg/L) and is likely due to the pH buffering capacity of karst waters, or it's resistance to change in pH resultant from the carbonate chemical reaction system. Some buffering is likely also responsible for the pH changes in the 25 mg/L $CaCO_3$ solution experiments as well.

The relative concentration of COO^- in solution increases above pH 5 while the relative concentration of COOH decreases above pH 5 (Fig. 7). All of the solutions reported here were generally above pH 5 but the increasing concentration of COO^- at higher pH values could be a

contributing factor in the increase in adherence of CMS spheres in the karst waters relative to the DI and 25mg/L $CaCO_3$ solutions. This does not explain the same increase that was observed in NFMS. While several intermolecular forces, buffering capacity, and mineral surfaces in the sediment are likely working in concert to drive microsphere adherence under the different experimental parameters, these results show the role of pH changes drive by COOH dissociation and $CaCO_3$ buffering capacity in microsphere adherence.

4.2 IR spectra peaks and bonding locations

Hierarchical component analysis (HCA), principial component analysis (PCA), and standard loading of covariance and correlation were done in Chemospec (Hanson et. al. 2022) for different groupings of the IR spectral data. Data were grouped based on microsphere type (NFMS, CMS) and then on solution type (DI, 25 mg/L $CaCO_3$). HCA based on microsphere type clustered together the equilibrium and sediment control solutions for both types of microspheres and the initial solutions were clustered separately (Fig. 8a). This indicates the sediment had a greater effect on the spectra peaks (and thus bond changes of the components in solution) than did microsphere type. PCA analysis based on microsphere type only explained 78% of the data with two components and considerable overlap was observed between the groups (Fig. 8b). The PCA analysis produces loadings which provide information on which spectral frequencies, in this case wavenumber, are affecting the PCA scores. A plot of the correlation score of each wavenumber for each solution against the covariance of the same score for each wavenumber shows that 1050 cm^{-1}, 1040cm^{-1}, 3360 cm^{-1}, 1200 cm^{-1} and 1230 cm^{-1} are the most influential wavenumbers on the PCA analysis (Fig. 8c). Interestingly, these wave numbers correspond with the sediment and hydrates or hydroxides present in the solution and not the COOH group or polystyrene structure.

The same statistical analyses were repeated by grouping the IR spectral data based on solution type rather than microsphere type. The HCA analysis for this group clustered the same solutions together where equilibrium and sediment solutions were clustered and initial solutions were a separate cluster (Fig. 9a). In this case, the $CaCO_3$ solution was included since the water IR spectra could be subtracted from the solution. The results also indicate that the addition of sediment maybe be the most dominant variable in microsphere IR spectra. The PCA analysis again only explained 67% of the data with much overlap in the solution types (Fig. 9b). PCA plots identified the initial CMS solution in DI as a potential outlier. The PCA s-plot for this

group identified 1050 cm^{-1}, 2930 cm^{-1}, 3360 cm^{-1}, and 1230 cm^{-1} as the most influential wavenumbers on the PCA scores (Fig. 9c). These wavenumbers potentially correspond with the mineral components of the sediment and aliphatic chains of the polystyrene structure.

Previously reported data on the mineralogy of the sediments showed that quartz was the dominant mineral in these sediments (Riddell, unpublished) followed by clay or other silicate minerals, amorphous materials, and dolomite. While the data presented here cannot definitively determine if microspheres are adhering to mineral surfaces or organic particles in the sediment, the effects of the mineral and the solution chemistry on mineral surfaces are likely influencing adherence. The increasing ionic strength, pH, and alkalinity from the DI through the karst water result in differently charged surface areas and dissolve minerals that will drive adherence of the microspheres. Further experimentation and analyses is required to determine the preferred adherence site of microspheres (mineral or organic) and the effects of solution chemistry on adherence.

However, these data, when combined with the pH data for each solution type show that the solution chemistry and mineral components of the sediment are likely driving microsphere adherence onto the sediments. This illustrates the importance of understanding the solution and sediment chemistry of the geologic media when using microspheres as an experimental surrogate for other chemicals. When exploring the behavior of MPs in the environment, these data support the necessity of a robust chemical characterization of the environment in which the MPs are found.

4.3 Comparison to microsphere field tracer experiments

Of the many microsphere tracer experiments reported in karst aquifers, the percent recovery of microspheres is most often reported for functionalized microspheres as these microspheres are often used to mimic bacteria motility in karst aquifer. The percent of unrecovered microspheres in these studies can be compared to the percent of adhered microspheres reported here to compare laboratory and field behavior of microspheres as the percent unrecovered is considered to represent any microspheres that adhered to aquifer sediments or rock matrix. Bandy et. al. (2016) used 1.0 um YG CMS to trace karst aquifers in central and western Kentucky with regard to E. coli motility. Bandy reported 88.7% unrecovered microspheres which is comparable to the average percent of adhered microspheres for NFMS (93.5%) and CMS (88.8%) reported here. A study in the northern Alps (Goeppert and

Goldscheider, 2011) underlain by a carbonate conglomerate aquifer used 1.0 um YG and red microspheres to estimate the mobility of fecal indicator bacteria through the aquifer and discharging at springs throughout the system (Goeppert and Goldscheider, 2011). The percent unrecovered YG and red microspheres was 43% and 94.9% respectively. These values are comparable to the percent adhered microspheres for NFMS in 25 mg/L CaCO3 solutions (55.7%) and NFMS and CMS in karst water solutions (93.5% and 88.8%). Yet another study in the Biscayne aquifer, a notable karst system, used various sizes of functionalized microspheres to estimate the transport of cryptosporidium cysts, a common bacterial groundwater contaminant, through the system (Harvey et. al., 2008). This study reported unrecovered rates of microspheres at 94.2%, 96.1%, and 97.1% which is, again, comparable to the percent adhered microspheres for NFMS and CMS karst water solutions reported here. The studies cited here speculated that the low recovery of their microsphere tracers was due to adsorption of the microsphere on to aquifer sediments or rock matrix and this is supported by the results of the experiments reported here. The retardation (R_F) of the microspheres in the reported tracer studies was not directly reported but estimated retardation of the NFMS and CMS can be estimated. R_F is directly related to the fraction of organic carbon, bulk density, and effective porosity of the substrate the material is traveling through. For the R_F estimates of the NFMS and CMS, the f_{OC} was directly measured and the bulk density and effective porosity was estimated from values for sandy sediments reported in Andersen et. al. (2015), Grabowski et. al. (2011), Stringer et. al. (2016), and Woessner et. al. (2020). Estimated R_F for NFMS ranged from 132 – 1277 and 150 – 1200 for CMS, with the highest value for both microsphere types being in the karst water experiment solutions (Table 4).

4.4 Microspheres as a surrogate tracer for organic contaminants and MPs

While microspheres maybe similar in size to bacteria, they are organic compounds and may be a more suitable surrogate for organic contaminants. The potential for organic compounds to adsorb on to sediments and soils and be stored can mean that karst sediments can act as a potential sink for organic contaminants. Furthermore, threshold transport events can cause sediments to be dislodged from karst aquifers and transported out of the system (Herman 2005; Doehring, 1971). Any associated contamination can then be reintroduced to the surface and potential ecological receptors, thereby making karst aquifer sediments a source for contamination as well. The mobility of organic contaminants through a sediment or soil is

measured by their K_{OC} value. Documented organic contaminants in karst aquifers include trichloroethylene (TCE), tetrachloroethylene (PCE), and various phthalates including DEHP, DEP, and DBP (Padilla, Ghisamizdeh). The reported K_{OC} values for these contaminants range from 64.3 (TCE) to 510,000 (DEHP) as reported by the EPA Superfund Soil Screening Guidance Part 5: Chemical Specific Parameters. The estimated K_{OC} values for NFMS and CMS here ranged from $10^3 – 10^4$ and was in the same range as phthalates ($10^2 – 10^5$), which are in plastic.

Polystyrene is a material used in the production of plastic and foam goods, so it is possible, given the K_{OC} range of the polystyrene microspheres, that these microspheres could be used as a surrogate material to understand the behavior of organic contaminants or MPs in different soils and sediments. Emerging research on MPs has documented their presence in karst settings (Balestra and Bellopede, 2021; Panno et al., 2019). Balestra and Bellopede (2021) developed a method to extract MPs from cave sediments using a density separation which accounted for the variation in density of different polymers. This study quantified different sizes and shapes of MPs in the sediments. The data presented in this current study show that microspheres readily adsorb to sediments regardless of solution chemistry yet the adherence or adsorption of MPs has rarely, if ever, been reported for cave sediments. The density separation technique presented by Balestra and Bellopede (2021) may result in underestimation of MPs in cave sediments if adhered MPs are not completely divorced from the sediments. Panno et. al. (2019) reported a concentration for 15.2 particles/L in karst waters from aquifers in Illinois, USA. Sediments were not considered in that study, nor was the surface chemistry of the plastic particles that were identified. The current study presented here indicates that, depending on surface chemistry, microspheres (or MPs with similar surface chemistry as microspheres) could be driven out of solution and adhere to sediments. Reporting MP concentrations in only water in karst systems is likely an underestimation of MP contamination in the entire system. Although MP contaminants are not uniform in shape and size like the engineered microspheres, which could affect their surface chemistry interactions with various geologic media, their likelihood to be adhered onto sediments should be considered when quantifying MP contamination in karst systems.

5.0 Conclusions

Microsphere tracer experiments in karst aquifers have been historically used to understand the movement of bacteria through the aquifers given their similarity in sizes. However, the tracer studies report consistently low recovery of the microspheres and attribute this to adsorption of microspheres onto aquifer sediments or matrix. Here, the adherence of two types of microspheres onto a clastic cave sediment was successfully measured in laboratory batch experiments under different experimental conditions. The resultant data allowed for the estimated calculation of K_D, K_{OC}, and R_F values that were used to compare against the known values of organic contaminants. The microspheres adhered to the sediments regardless of water type and microsphere type. The highest K_{OC} values were calculated in the karst water experiments, suggesting that this experimental parameter results in the most adherence of microspheres. The K_{OC} values of the microspheres was in the same range as phthalates (another type of plastic). Analysis of the pH of each solution and the infrared spectra of microsphere-sediment-solutions indicate the pH and the mineral content of the sediment are primary drivers of microsphere adherence to these sediments. The potential for microspheres to be used to understand surface chemistry interactions between organic contaminants or MPs and different soils and sediments warrants further exploration based on the results reported here. The estimation of MP contamination in the environment should consider adhered MPs in sediment and soils in addition to MPs concentration in water.

6.0 References

Al-Kadhemy, M. F. H., Rasheed, Z. S., and Salim, S. R., 2016, Fourier transform infrared spectroscopy for irradiation coumarin doped polystyrene polymer films by alpha ray: Journal of Radiation Research and Applied Sciences, v. 9, no. 3, p. 321-331. https://doi.org/10.1016/j.jrras.2016.02.004

Auckenthaler, A., Raso, G., and Huggenberger, P., 2002, Particle transport in a karst aquifer: natural and artificial tracer experiments with bacteria, bacteriophages and microspheres: Water Science Technology, v. 43, no. 3, p. 9.

Balestra, V., and Bellopede, R., 2021, Microplastic pollution in show cave sediments: First evidence and detection technique: Environmental Pollution, v. 292, p. 9. https://doi.org/10.1016/j.envpol.2021.118261

Bandopadhyay, A. K., 2010, Determination of quartz content for Indian coals using an FTIR technique: International Journal of Coal Geology, v. 81, no. 1, p. 6. https://doi.org/10.1016/j.coal.2009.10.018

Bandy, A. M., 2016, Mobility of *Escherichia coli* within Karst Terrains, Kentucky, USA [Doctor of Philosophy: University of Kentucky.

Banks, E. D., Taylor, N. M., Gulley, J., Lubbers, B. R., Giarrizzo, J. G., Bullen, H. A., Hoehler, T. M., and Barton, H. A., 2010, Bacterial Calcium Carbonate Precipitation in Cave Environments: A Function of Calcium Homeostasis: Geomicrobiology Journal, v. 27, no. 5, p. 444-454. https://doi.org/10.1080/01490450903485136

Barton, H. A., and Jurado, V., 2007, What's Up Down There? Microbial Diversity in Caves: Microbe, v. 2, p. 132-138.

Bausher, E. A., 2018, Qualitative and quantitative analysis of carbonate waters in the Peters Mountain Region of Monroe County, WV, Master of Science, West Virginia University,137 p.

Birdwell, J. E., and Engel, A. S., 2010, Characterization of dissolved organic matter in cave and spring waters using UV–Vis absorbance and fluorescence spectroscopy: Organic Geochemistry, v. 41, no. 3, p. 270-280. https://doi.org/10.1016/j.orggeochem.2009.11.002

Blott, S. J., and Pye, K., 2001, GRADISTAT: a grain size distribution and statistics package for the analysis of unconsolidated sediments: Earth Surface Processes and Landforms, v. 26, no. 11, p. 1237-1248. https://doi.org/10.1002/esp.261

Bottrell, S. H., 1996, Organic carbon concentrations profiles in recent cave sediments: Records of agricultrual pollution or diagenesis?: Environmental Pollution, v. 91, no. 3, p. 8. https://doi.org/10.1016/0269-7491(95)00064-x

Buczynski, C., and Chafetz, H. S., 1991, Habit of bacterially induced precipitates of calcium carbonate and the influence of medium viscosity on mineralogy: Journal of Sedimentary Petrology, v. 61, p. 226-233.

Cao, V., Schafer, M., Taherdangkoo R., and Licha T., 2020, Solute Tracers for hydrogeological applications: a short review and future prospects: Water, v. 12, p. 653. https://doi.org/10.3390/212030653

Corami, F., Rosso, B., Bravo, B., Gambaro, A., and Barbante, C., 2020, A novel method for purification, quantitative analysis and characterization of microplastic fibers using Micro-FTIR: Chemosphere, v. 238, p. 124564. https://doi.org/10.1016/j.chemosphere.2019.124564

Crawford, N., C, and Ulmer, C., S, 1994, Hydrogeologic investigations of contaminant movement in karst aquifers of a train derailment near Lewisburg, Tennessee: Environmental Geology, v. 21, p. 12.

de Paula, C. C. P., Bichuette, M. E., and Seleghim, M. H. R., 2020, Nutrient availability in tropical caves influences the dynamics of microbial biomass: Microbiologyopen, v. 9, no. 7, p. e1044. https://doi.org/10.1002/mbo3.1044

de Paula, C. C. P., Montoya, Q. V., Rodrigues, A., Bichuette, M. E., and Seleghim, M. H. R., 2016, Terrestrial filamentous fungi from Gruta do Catão (São Desidério, Bahia, Northeastern Brazil) show high levels of cellulose degradation: Journal of Cave and Karst Studies, v. 78, no. 3, p. 208-217. https://doi.org/10.4311/2016mb0100

Doehring, D. O., and Vierbuchen, R. C., 1971, Cave development during a catastrophic storm in the Great Valley of Virginia: Science, v. 174, p. 3.

Downey, A. R., 2020, Physical and chemical properties of clastic sediments from two caves in the northern karst region of Puerto Rico M.Sc. Graduate Theses, Dissertations, and Problem Reports, Master of Science in Geology, West Virginia University 157 p.

Ewers, R., O, White, K., A, and Fuller, J., F, 2012, Contaminant plumes and pseudo plumes in karst aquifers: Carbonate Evaporite, v. 27, p. 7.

Ewers, R. O., Duda, A. J., Estes, E. K., Idstein, P. J., and Johnson, K. M., 1991, The transmission of light hydrocarbon contaminants in limestone (karst) aquifers, Third Conference on Hydrology, Ecology, Monitoring, and Management of Ground Water in Karst Terranes: Nashville, TN, p. 20.

Flynn, R. M., and Sinreich, M., 2010, Characterisation of virus transport and attenuation in epikarst using short pulse and prolonged injection multi-tracer testing: Water Res, v. 44, no. 4, p. 1138-1149. Contaminant plumes and pseudo plumes in karst aquifers

Folk, R. L., and Chafetz, H. S., 1983, Pisoliths (Pisoids) in Quaternary Travertines of Tivoli, Italy, Coated Grains, p. 474-487. https://doi.org/10.1007/978-3-642-68869-0_41

Ford, D. C., and Ewers, R. O., 1978, The development of limestone cave systems in the dimensions of length and depth: Canadian Journal of Earth Sciences, v. 15, p. 16. https://doi.org/10.1139/e78-186

Frimmel, F. H., von der Kammer, F., and Flemmin, H.-C., 2007, Colloidal Transport in Porous Media, New York, Springer.

Gale, S. J., 1984, The hydraulics of conduit flow in carbonate aquifers: Journal of HYdrology, v. 70, p. 19. https://doi.org/10.1016/0022-1694(84)90129-X

Ghasemizadeh, R., Yu, X., Butscher, C., Hellweger, F., Padilla, I., and Alshawabkeh, A., 2015, Equivalent Porous Media (EPM) Simulation of Groundwater Hydraulics and Contaminant Transport in Karst Aquifers: PLoS One, v. 10, no. 9, p. e0138954. https://doi.org/10.1371/journal.pone.0138954

Goeppert, N., and Goldscheider, N., 2011, Transport and variability of fecal bacteria in carbonate conglomerate aquifers: Ground Water, v. 49, no. 1, p. 77-84. https://doi.org/10.1111/j.1745-6584.2010.00741.x

Goeppert, N., and Goldscheider, N., 2011, Improved understanding of particle transport in karst groundwater using natural sediments as tracers: Water Res, v. 166, p. 115045. https://doi.org/10.1016/j.watres.2019.115045

Goeppert, N., and Hoetzl, H., 2009, Precise method for continuous measurement of fluorescent microspheres during flow: Hydrogeology Journal, v. 18, no. 2, p. 317-324. https://doi.org/10.1007/s10040-009-0517-0

Goldscheider, N., Hötzl, H., Käss, W., and Ufrecht, W., 2003, Combined tracer tests in the karst aquifer of the artesian mineral springs of Stuttgart, Germany: Environmental Geology, v. 43, no. 8, p. 922-929. https://doi.org/10.1007/s00254-002-0714-9

Goppert, N., and Goldscheider, N., 2008, Solute and colloid transport in karst conduits under low- and high-flow conditions: Ground Water, v. 46, no. 1, p. 61-68. https://doi.org/10.1111/j.1745-6584.2007.00373.x

Hanson, B. A., 2019, An introduction to ChemoSpec: DePauw University.

Harvey, R. W., George, L. H., Smith, R. L., and LeBlanc, D. R., 1989, Trasnport of microspheres and indigenous bacteria through a sandy aquifer: results of natural- and forced-gradient tracer experiments: Environmental Science and Technology, v. 23, p. 6. https://doi.org/10.1021/es00178a005

Harvey, R. W., Metge, D. W., Shapiro, A. M., Renken, R. A., Osborn, C. L., Ryan, J. N., Cunningham, K. J., and Landkamer, L., 2008, Pathogen and chemical transport in the karst limestone of the Biscayne aquifer: 3. Use of microspheres to estimate the transport of potential of *Cryptosporidium parvum* oocysts: Water Resources Research, v. 44, no. 12. https://doi.org/10.1029/2007WR006060

Herman, E. K., Toran, L., and White, W. B., 2008, Threshold events in spring discharge: Evidence from sediment and continuous water level measurement: Journal of Hydrology, v. 351, no. 1, p. 98-106. https://doi.org/10.1016/j.jhydrol.2007.12.001

Hermán, V., Takacs, H., Duclairoir, F., Renault, O., Tortai, J. H., and Viala, B., 2015, Core double–shell cobalt/graphene/polystyrene magnetic nanocomposites synthesized by in situ sonochemical polymerization: RSC Advances, v. 5, no. 63, p. 51371-51381. https://doi.org/10.1039/c5ra06847a

Husic, A., Fox, J., Agouridis, C., Currens, J., Ford, W., and Taylor, C., 2017, Sediment carbon fate in phreatic karst (Part 1): Conceptual model development: Journal of Hydrology, v. 549, p. 179-193. https://doi.org/10.1016/j.jhydrol.2017.03.052

Jozanikohan, G., and Abarghooei, M. N., 2022, The Fourier transform infrared spectroscopy (FTIR) analysis for the clay mineralogy studies in a clastic reservoir: Journal of Petroleum Exploration and Production Technology, p. 14. https://doi.org/10.1007/s13202-021-01449-y

Kass, W., 1992, Tracing Technique in Geohydrology, Rotterdam, Netherlands, A.A. Balkema.

Loop, C., M, and White, W., B, 2005, A Conceptual Model for DNAPL Transport in Karst Ground Water Basins: Groundwater, v. 39, no. 1. https://doi.org/10.1111/j.1745-6584.2001.tb00357.x

Mahler, B. J., Valdes, D., Musgroves, M., and Massei, N., Nutrient migration in carbonate aquiferes in response to storms: a comparison of two geologically contrasting aquifers, *in* Proceedings 2007 GSA Denver Annual Meeting2007.

Mahler, B. J., Lynch, L; Bennett, P.C., 1999, Mobile sediment in an urbanizing karst aquifer: implications for contaminant transport: Environmental Geology, v. 39, no. 1, p. 14. https://doi.org/10.1007/S002540050434

McCarthy, J. F., and Zachara, J. M., 1989, Subsurface transport of contaminants:mobile colloids in the subsurface environment may alter the transport of contaminants: Environmental Science and Technology, v. 23, no. 5, p. 7.

Melim, L. A., Northup, D. E., Spilde, M. N., Jones, B., Boston, P. J., and Bixby, R. J., 2008, Reticulated filaments in cave pool speleothems: Microbe or mineral?: Journal of Cave and Karst Studies, v. 700, no. 3, p. 135-141. https://doi.org/10.7939/R3J38KZ7V

Melim, L. A., Shinglman, K. M., Boston, P. J., Northup, D. E., Spilde, M. N., and Queen, J. M., 2001, Evidence for microbial onvolvement in pool finger precipitation, Hidden Cave, New Mexico: Geomicrobiology Journal, v. 18, p. 311-329. https://doi.org/10.1080/01490450152467813

Padilla, I., Irizarry, C., and Steele, K., 2011, Historical contamination of groundwater resources in the north coast aquiferes of Puerto Rico: Rev Dimens, v. 3, p. 7-12.

Panno, S. V., Curry, B. B., Wang, H., Hackley, K. C., Liu, C.-L., Lundstrom, C., and Zhou, J., 2004, Climate change in southern Illinois, USA, based on the age and δ13C of organic matter in cave sediments: Quaternary Research, v. 61, no. 3, p. 301-313. https://doi.org/10.1016/j.yqres.2004.01.003

Panno, S. V., Kelly, W. R., Scott, J., Zheng, W., McNeish, R. E., Holm, N., Hoellein, T. J., and Baranski, E. L., 2019, Microplastic contamination in karst groundwater systems: Groundwater, v. 57, no. 2, p. 189 - 196. https://doi.org/10.1111/gwat.12862

Petersen, F., and Hubbart, J. A., 2021, The occurrence and transport of microplastics: The state of the science: Sci Total Environ, v. 758, p. 12. https://doi.org/10.1016/j.scitotenv.2020.143936

Prata, J. C., Reis, V., Matos, J. T. V., da Costa, J. P., Duarte, A. C., and Rocha-Santos, T., 2019, A new approach for routine quantification of microplastics using Nile Red and automated software (MP-VAT): Sci Total Environ, v. 690, p. 1277-1283. https://doi.org/10.1016/j.scitotenv.2019.07.060

Roy, W., R, Krapac, I., G, Chou, S., F, J, and Griffin, R., A, 1991, Technical Resource Document: Batch-type procedures for estimating soil adsorption of chemicals, *in* Survey, I. S. G., ed.: Champagne, Illinois, U.S. Environmental Protection Agency.

Schwarzenbach, R. P., Gschwend, P. M., and Imboden, D. M., 2003, Environmental Organic Chemistry, Hoboken, New Jersey, Wiley and Sons.

Simon, K., Pipan, T., Ohno, T., and Culver, D., 2010, Spatial and temporal patterns in abundance and character of dissolved organic matter in two karst aquifers: Fundamental and Applied Limnology / Archiv für Hydrobiologie, v. 177, p. 81-92. https://doi.org/10.1127/1863-9135/2010/0177-0081

Sinreich, M., Flynn, R., and Zopfi, J., 2009, Use of particulate surrogates for assessing microbial mobility in subsurface ecosystems: Hydrogeology Journal, v. 17, no. 1, p. 49-59. https://doi.org/10.1127/1863-9135/2010/0177-0081

Van Gundy, J. J., and White, W. B., 2009, Sediment flushing in Mystic Cave, West Virginia, USA, in response to the 1985 Potomac Valley Flood: International Journal of Speleology, v. 38, no. 2, p. 7. http://dx.doi.org/10.5038/1827-806X.38.2.2

Varmuza, K., and Filzmoser, P., 2009, Introduction to multivariate statistical analysis in chemometrics, Boca Raton, Florida, CRC Press.

Vesper, D., J, Loop, C., M, and White, W. W., 2003, Contaminant transport in karst aquifers: Speleogenesis and Evolution of Karst Aquifers, v. 1, no. 2, p. 11.

Vesper, D. J., 2002, Transport and storage of trace metals in a karst aquifer: An example from Fort Campbell, Kentucky PhD: The Pennsylvania State University.

Vysotsky, Y. B., Kartashynska, E. S., Vollhardt, D., and Fainerman, V. B., 2020, Surface pKa of Saturated Carboxylic Acids at the Air/Water Interface: A Quantum Chemical Approach: The Journal of Physical Chemistry C, v. 124, no. 25, p. 13809-13818. https://doi.org/10.1021/acs.jpcc.0c03785

Wade, L. G., 2006, Organic chemistry, Upper Saddle River, N.J., Pearson Prentice Hall.

White, W. B., Herman, J. S., Herman, E. K., and M., R., 2018, Karst Groundwater Contamination and Public Health, Cham, Switzerland, Springer International, Advances in Karst Science.

Zhou, Y., Liu, X., and Wang, J., 2019, Characterization of microplastics and the association of heavy metals with microplastics in suburban soil of central China: Sci Total Environ, v. 694, p. 133798. https://doi.org/10.1016/j.scitotenv.2019.133798

Acknowledgements

The authors would like to acknowledge Dr. Jon Chorover, Dr. Robert Root, Dr. Yaniv Olshansky, and Dr. Bryan Moravec, all of the University of Arizona, for their help in preparing

and analyzing samples for FTIR analysis. We would also like to acknowledge Autum Downey for her assistance in collecting the sediment and processing the particle size data and Dr. Ellen Herman and the Bucknell University for allowing us to use their instrumentation.

Statements and Declarations

This work was supported by the National Institute of Environmental Health Sciences Superfund Research Program project PROTECT (Puerto Rico Testsite for Exploring Contamination Threats) PTE Federal Award Number 5P42ES017198-12 and the West Virginia University Ruby Distinguished Doctoral Fellowship. The authors have no relevant competing financial or non-financial interests to disclose. All authors contributed to the study conception and design. Material preparation, data collection, and analysis were performed by Jill Riddell. The first draft of the manuscript was written by Jill Riddell and all authors commented on previous versions of the manuscript. All authors read and approved the final manuscript.

Data Availability

For the purposes of this dissertation, all data and code used in this manuscript can be found in Appendix C. Upon journal acceptance, data will be made publicly available in the GitHub repository for this project: https://github.com/jlriddell12/microsphereadherence.

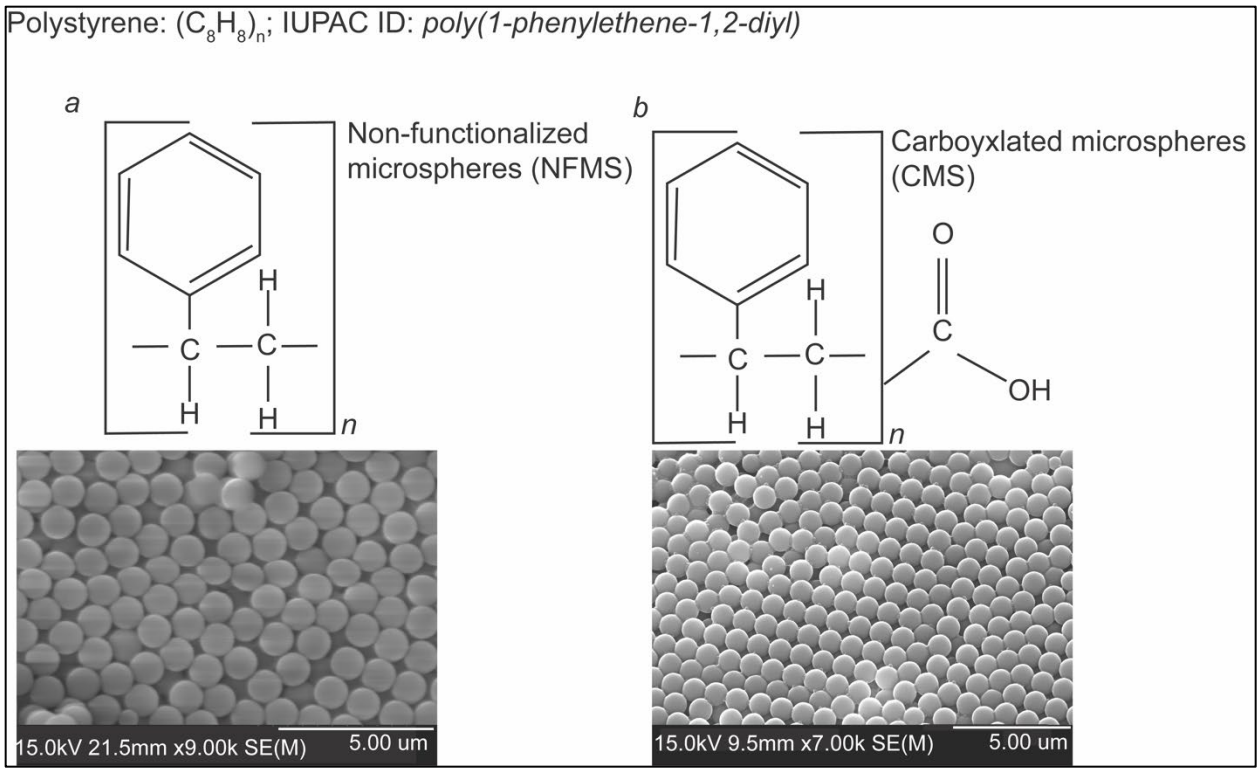

Fig. 1. Chemical structure of polystyrene microspheres and SEM image of NFMS (a). Chemical structure of COOH group and SEM image of CMS (b). The CMS exhibit a more ordered alignment than the NFMS due to interactions of the COOH functional groups on each CMS.

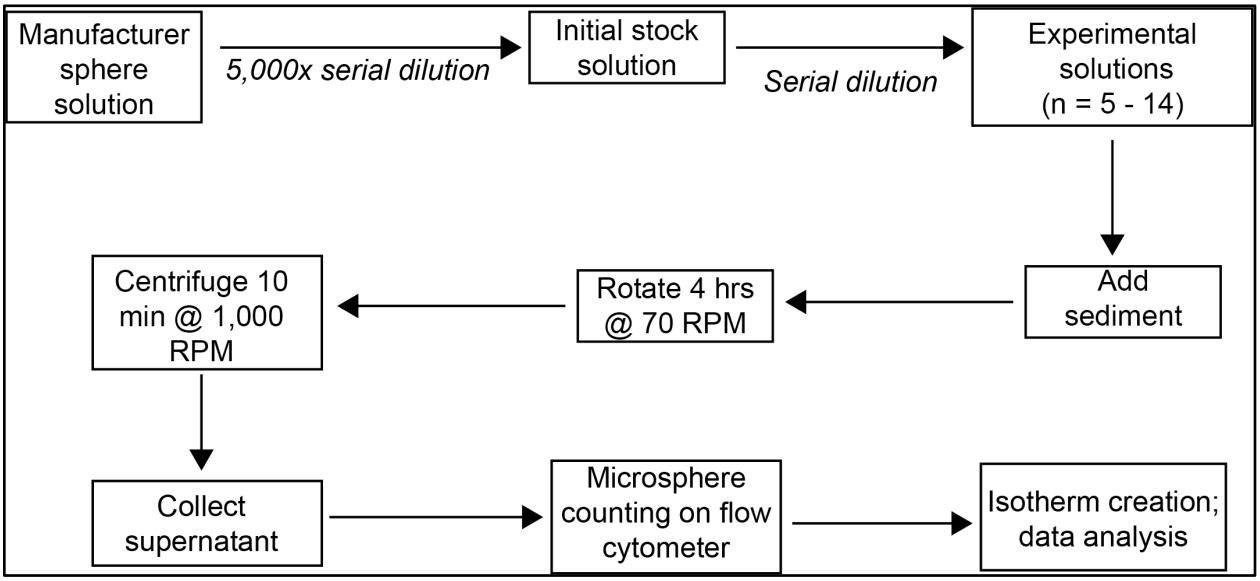

Fig. 2. Flow chart of experimental design and solution preparation.

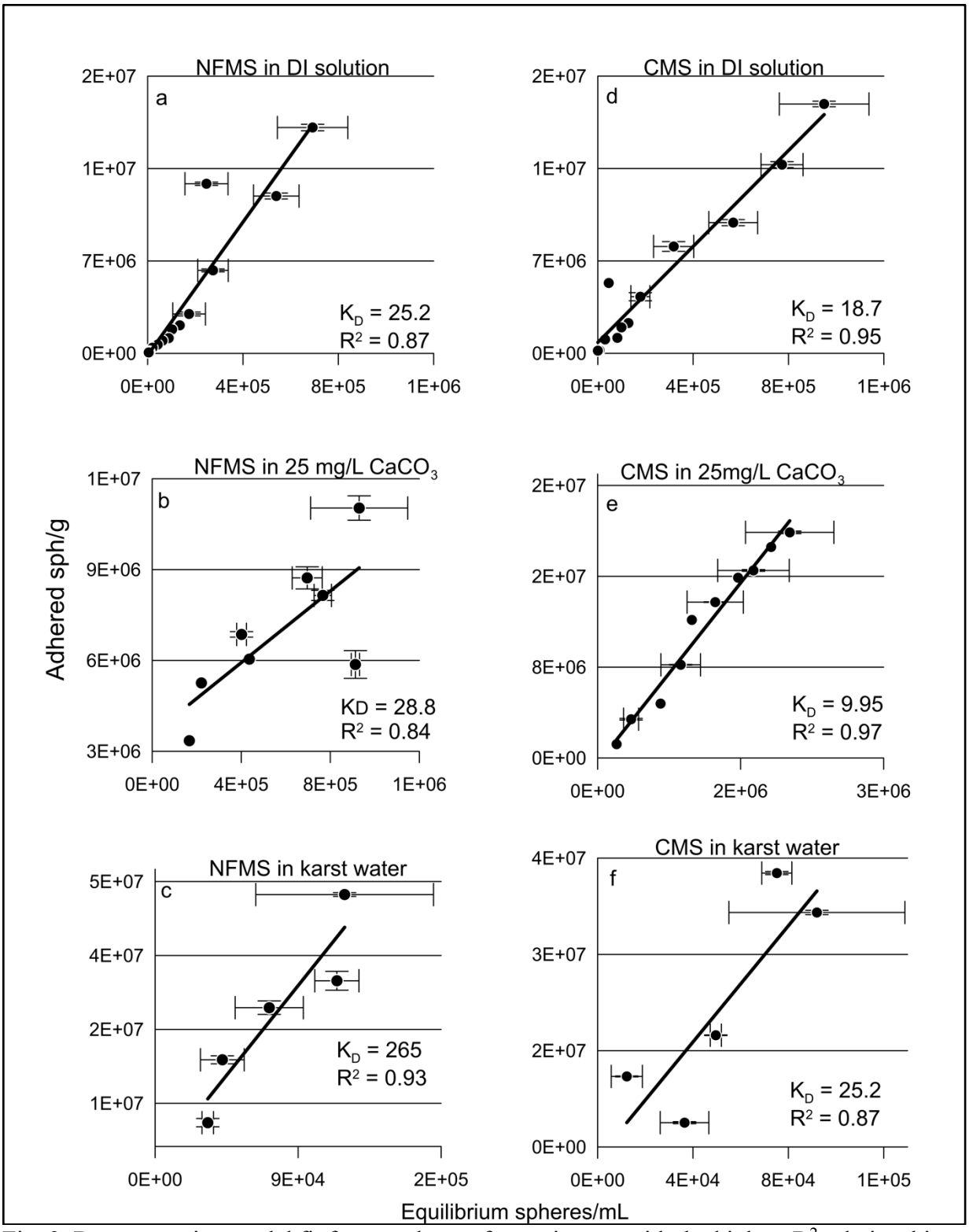

Fig. 3. Representative model fit from each set of experiments with the highest R^2 relationship represented for each experiment type. NFMS solutions all show a strong linear relationship (a-c) with the strongest relationship being observed in karst water (c). CMS also have strong linear relationships (d-f) which strongest relationship observed in 25mg/L $CaCO_3$ solutions.

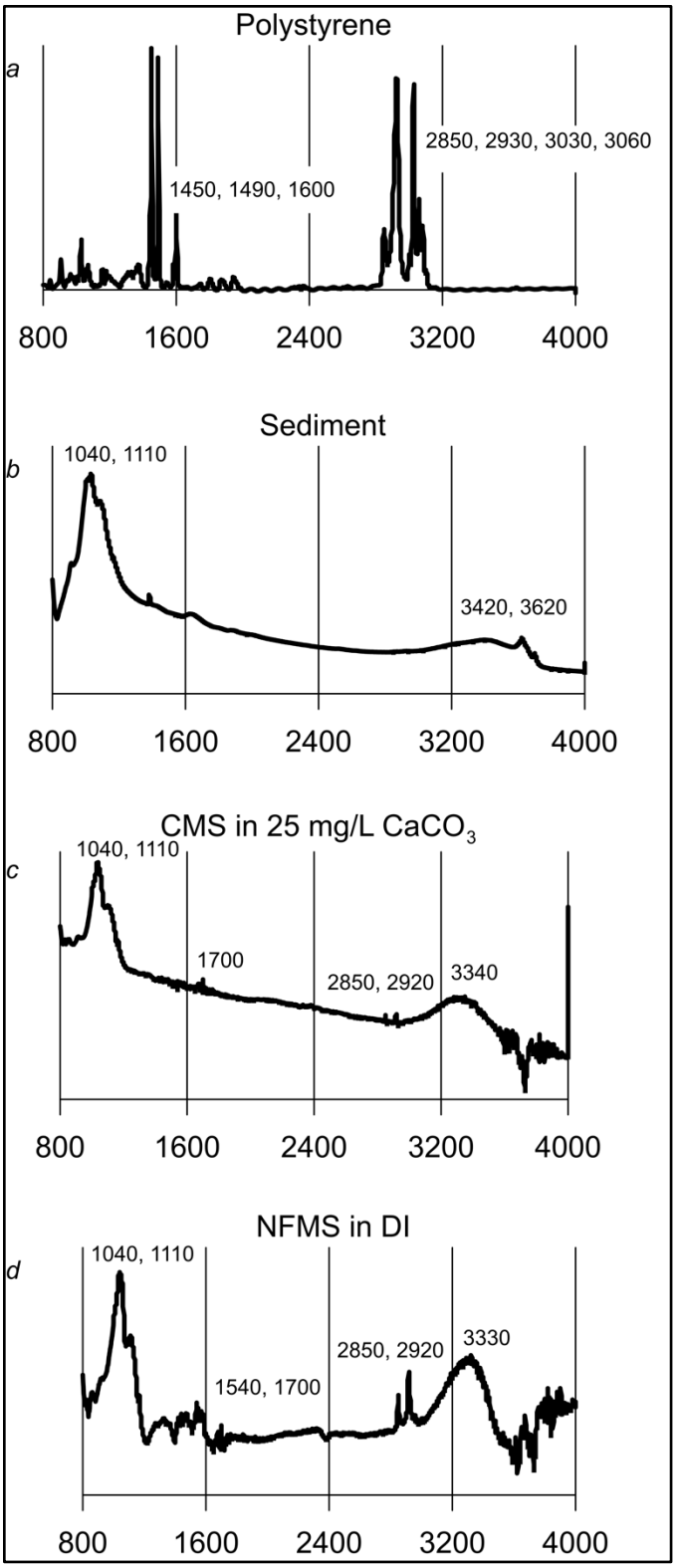

Fig. 4. FTIR spectra for polystyrene solid (a); the sediment used in these experiments (b); and the CMS and NFMS in different water treatments with sediment (c, d). IR bands signature of polystyrene and quartz or silicate minerals are evident in the NFMS and CMS mixtures.

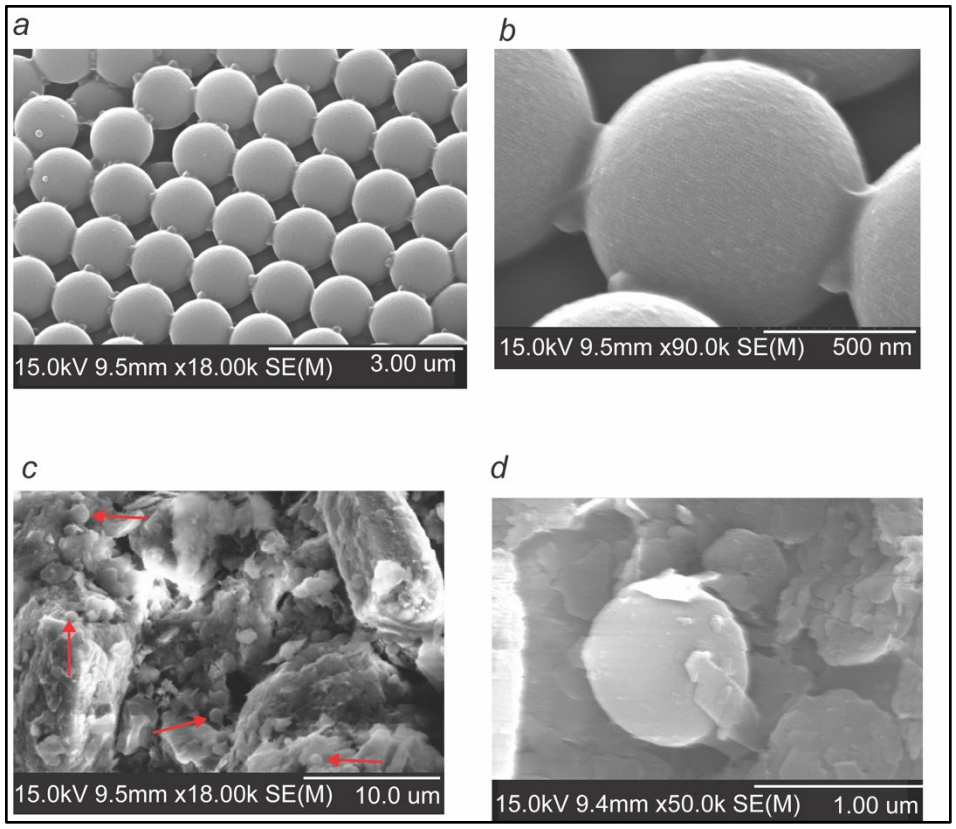

Fig. 5. SEM images of CMS showing an ordered arrangement of spheres due to the COOH group on the surface (a). Higher magnification image of a, showing detail of possible COOH attachment of CMS (b). CMS and sediment mixture at equilibrium. Possible CMS are indicated by red arrows (c). CMS sphere in sediment with some sediment material adhered to the outside of the sphere (d).

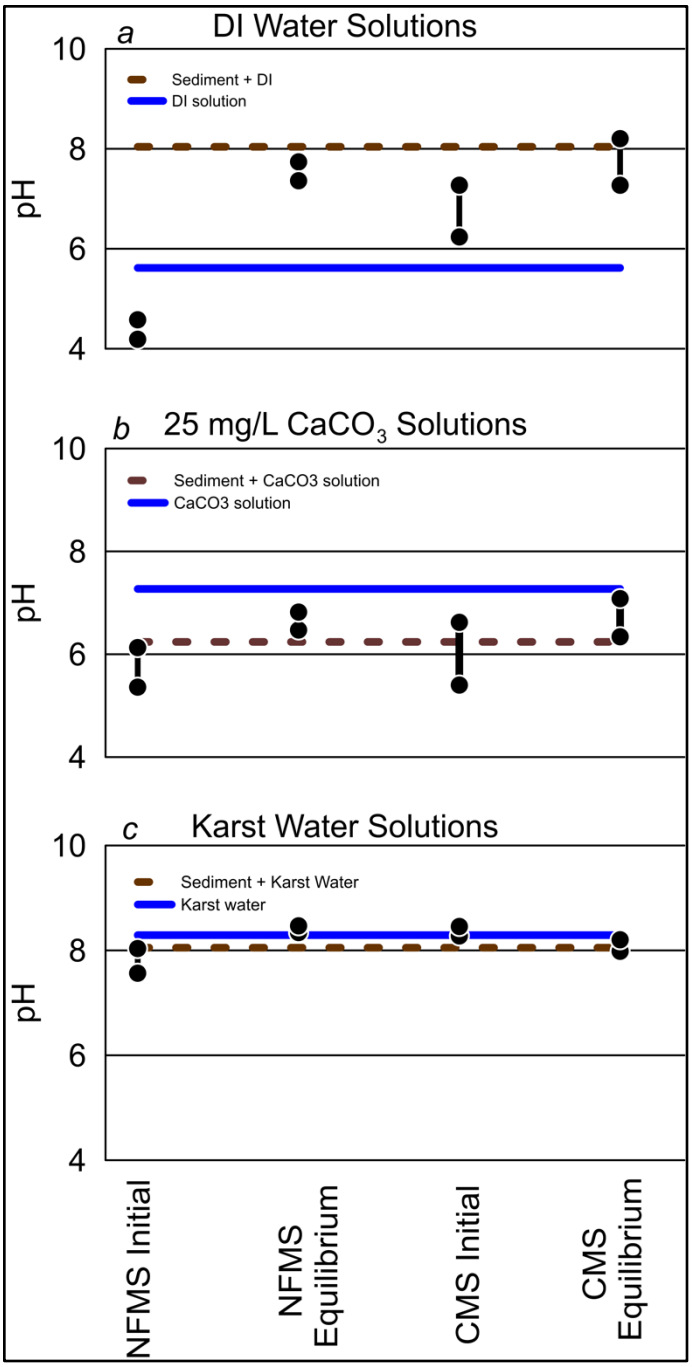

Fig. 6. Effect of $CaCO_3$ and pH on microsphere adherence. The pH ranges represent the minimum and maximum pH across the indicated solution. With increasing Ca content, the pH ranges of all microsphere types becoming smaller, indicating a control on microsphere adherence, possibly due to the buffering capacity of carbonate waters.

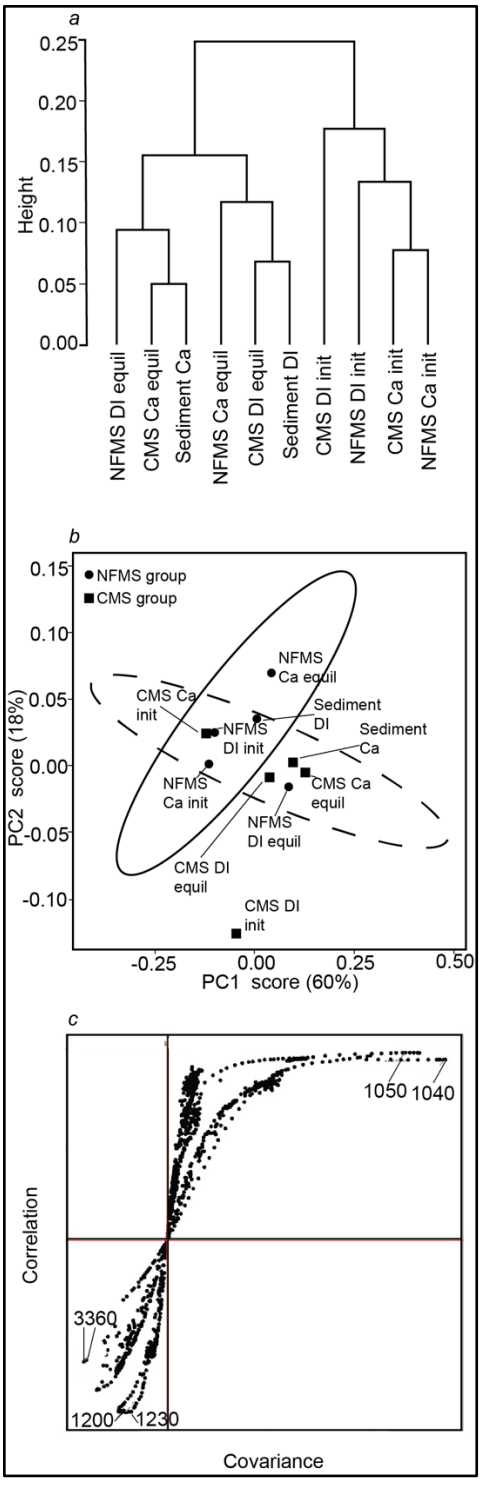

Fig. 8. HCA of IR spectra divided into groups based on microsphere type, NFMS and CMS (a) where init = initial solution, equil = equilibrium solution, and Ca = 25mg/L $CaCO_3$ solutions. The initial CMS solution does not cluster with any other solution. PCA plot using two scores for microsphere types (b). Confidence ellipses representing NFMS (solid) and CMS (dotted) are at the 95% confidence interval. Points outside the ellipses are potential outliers. PCA loadings plot showing the most influential IR spectra wavenumbers on the PCA analysis (c).

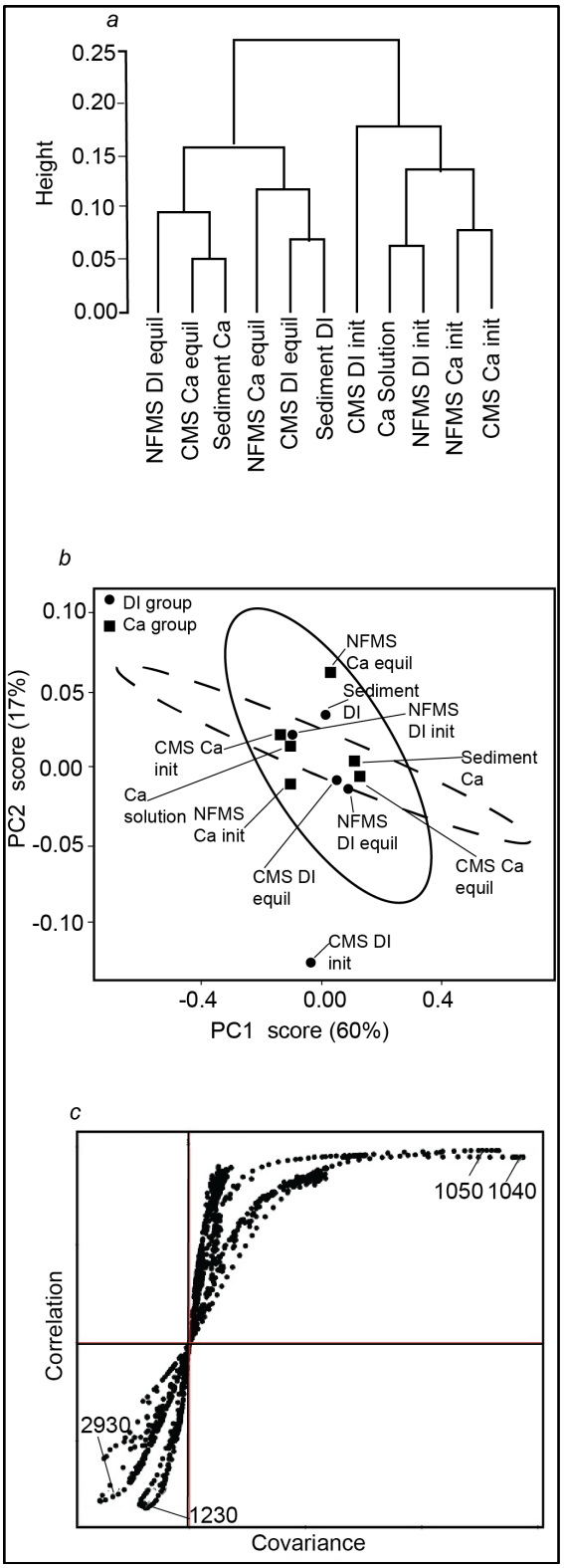

Fig. 9. HCA of IR spectra divided when divided into groups based on solution type, DI and 25 mg/L $CaCO_3$(a) where init = initial solution, equil = equilibrium solution, and Ca = 25mg/L $CaCO_3$ solutions. PCA plot using two scores for microsphere types (b). Confidence ellipses again indicate

that the initial CMS solution in DI is a potential outlier. PCA loadings plot showing the most influential IR spectra wavenumbers on the PCA analysis (c).

Table 1. Chemistry of water types used in microsphere dilutions

Parameter	DI water	25 mg/L $CaCO_3$	Karst water
pH	5.62	7.27	8.30
Mg (mg/L)	0	0	32.9
Ca (mg/L)	0	25	74.0
Ionic strength (mol/L)	-	5.38×10^{-4}	1.03×10^{-3}
Alkalinity (meq/L)	-	7.52×10^{-5}	0.99
CBE (%)	-	73.2	-0.53

Basic solution chemistry of water types used in microsphere dilutions. Ionic strength of the $CaCO_3$ solution was unable to be measured. Increasing pH due to the increasing amount of calcium carbonate in the solutions is clearly noted. The 25 mg/L $CaCO_3$ solution was achieved by cooling the DI water that the $CaCO_3$ was added to increase solubility and working with the solution in temperatures below 25 C. Ionic strength, alkalinity, and charge balance error (CBE) were modeled the USGS aqueous geochemical modeling software PHREEQC.

Table 2. Linear fit results of adherence experiments

NFMS					CMS				
Solution (n)	K_D	K_{OC}	R^2	% Removed	Solution (n)	K_D	K_{OC}	R^2	% Removed
DI (13)	25.2	3.50E3	0.87	49.1	DI (13)	18.2	2.52E3	0.95	58.4
DI (14)	32.9	4.56E3	0.78	66.9	DI (14)	21.4	2.98E3	0.86	49.2
DI (5)	53.3	7.42E3	**0.39**	88.2	DI (5)	54.6	7.58E3	0.44	76.2
					DI (5)	67.2	9.33E3	0.79	72.9
Solution (n)	K_D	K_{OC}	R^2	% Removed	Solution (n)	K_D	K_{OC}	R^2	% Removed
25 mg/L (8)	5.91	8.21E2	0.56	40.9	25 mg/L (10)	9.50	1.32E3	0.97	31.5
25 mg/L (5)	41.3	5.74E3	0.66	73.2	25 mg/L (5)	28.1	3.91E3	0.96	67.7
25 mg/L (5)	28.8	3.99E3	0.84	66.9	25 mg/L (5)	48.9	6.79E3	0.97	67.9
Solution (n)	K_D	K_{OC}	R^2	% Removed	Solution (n)	K_D	K_{OC}	R^2	% Removed
karst water (5)	152	2.11E4	0.75	92.5	karst water (5)	452	6.28E4	0.73	93.6
karst water (5)	265	3.68E4	0.93	93.5	karst water (5)	156	2.17E4	0.20	92.5
karst water (5)	323	3.23E4	0.86	94.4	karst water (5)	87.4	1.21E4	**0.07**	93.6

Results from adherence experiments of each microsphere and solution type where n = number of solutions analyzed in that experiment. NFMS = non-functionalized microspheres, CMS = carboxylated microspheres, K_D = adsorption coefficient, K_{OC} = organic-carbon water partition coefficient. Even with in instances of poor linear correlation (bolded) the percent of microspheres removed from solution is still considerable. K_D were calculated based on the average f_{OC} of the collected sediments, 0.0072.

Table 3. Functional group assignments based on IR band observations microsphere-sediment-solution spectra

IR band	Functional group assignment
1040	Si-O stretch, quartz or silicate minerals[1,2]
1110	Si-O stretch, quartz or silicate minerals[1,2]
1540	C=C or C=O stretch, polystyrene[3,4]
1700	C=C or C=O stretch, polystyrene[3,4]
2850	C-H stretch (aliphatic or aromatic), polystyrene[3,4]
2930	C-H stretch (aliphatic or aromatic), polystyrene[3,4]
3200 - 3360	O-H stretch[1,2,3,4]

IR band assignments are related to the minerals in the sediment and the polystyrene structure of the microspheres. [1]Bandopadhyay, 2010; [2]Jozanikohan and Abarghooei, 2022; [3]Al-Kadhemy et al., 2016; [4]Hermán et al., 2015.

Table 4. Estimated adherence properties of microspheres through an aquifer

Microsphere and solution	Average K_D	Estimated R_F
NFMS DI solutions	26.4	137
NFMS 25 mg/L $CaCO_3$ solutions	25.3	132
NFMS karst water solutions	247	1277
CMS DI solutions	40.4	210
CMS 25 mg/L $CaCO_3$ solutions	28.8	150
CMS karst water solutions	232	1200

Estimated retardation of the microspheres through the karst system from where the sediments were collected based on K_D values from linear model fits. Estimated bulk density and effective porosity for sandy sediments was used in the calculation of retardation factors based on values from Andersen et. al., 2015; Grabowski et. al., 2011; Stringer et. al., 2016; and Woessner et. al., 2020.

Conclusions

Caves have long represented an entity through which cultural and scientific exploration and research has taken place (Addesso et al., 2022; Goldberg and Sherwood, 2006). With the growth of speleological science in the mid-19th century (Shaw, 1992), cave science developed into an independent field of study. With this development, the importance of caves as a recorder of paleoenvironments and geologic history and processes was recognized. The ability of caves to provide a window into larger karst system has been recognized and used to research a number of karst-groundwater-cave related processes (Sasowsky and Mylroie, 2007; White, 1988; White et al., 2018) but the role of clastic cave sediments has only recently begun to receive attention in regard to their role in karst processes and contaminant fate and transport (Herman et al., 2008; Lynch et al., 2007; Mahler, 1999).

The chemical components of clastic cave sediments are essential to understanding how sediments are transported and stored in the karst aquifer and for exploring chemical interactions between sediments and other particles, like contaminants. The mineralogy and organic carbon content are the chemical components that are likely most responsible for sediment-particle interactions but quantitative reports of these values in cave sediments remain underreported. Together, the three studies presented in this dissertation quantified the chemical components and organic carbon content of a cave sediment in southern WV; quantified the organic carbon content relative to depositional facies of cave sediment in VA; and quantified the adherence of a plastic-based microsphere particle onto a cave sediment. The data collected in this research provided clues to sediment provenance and transport in karst settings (Chapter 1) and describe the range and type of carbon in cave systems and the potential importance of that carbon in contaminant retardation (Chapter 2). This research also applied a practical analytical technique to explore the chemical interactions with a cave sediment and an organic, plastic based microparticle (Chapter 3) which allowed for preliminary discussion on the relationships between sediments and different types of contaminants in karst aquifers.

This dissertation illustrates the importance of quantifying the mineralogical components of clastic cave sediments using an array of analytical techniques. It also demonstrates the importance of sediment in karst processes. Future work in cave sediment research should take care to analyze different sediment facies for chemical components when attempting to describe the overall characteristics of the sediment. Research in karst contaminant fate and transport

should consider sediment-contaminant interaction when exploring emerging contaminants like microplastics. Cave sediments are abundant, and caves provide a window in the karst system. The work presented in this dissertation demonstrates their usefulness when investigating karst systems and processes.

Addesso, R., De Waele, J., Cafaro, S., and Baldantoni, D., 2022, Geochemical characterization of clastic sediments sheds light on energy sources and on alleged anthropogenic impacts in cave ecosystems: International Journal of Earth Sciences, v. 111, no. 3, p. 9.

Goldberg, P., and Sherwood, S. C., 2006, Deciphering human prehistory through the geoarcheological study of cave sediments: Evolutionary Anthropology: Issues, News, and Reviews, v. 15, no. 1, p. 20-36.

Herman, E. K., Toran, L., and White, W. B., 2008, Threshold events in spring discharge: Evidence from sediment and continuous water level measurement: Journal of Hydrology, v. 351, no. 1-2, p. 98-106.

Lynch, F. L., Mahler, B. J., and Hauwert, N. N., 2007, Provenance of suspended sediment discharged from a karst aquifer determined by clay mineralogy, *in* Sasowsky, I. D., and Mylroie, J. E., eds., Studies of cave sediments: physical and chemical records of paleoclimate: New York, NY, Springer, p. 83 - 94.

Mahler, B. J. L., L; Bennett, P.C., 1999, Mobile sediment in an urbanizing karst aquifer: implications for contaminant transport: Environmental Geology, v. 39, no. 1, p. 14.

Sasowsky, I. D., and Mylroie, J. E., 2007, Studies of cave sediments: physical and chemical records of paleoclimate, New York, NY, Springer.

Shaw, T. R., 1992, History of cave science, Sydney Speleological Society, 338 p.:

White, W. B., 1988, Geomorphology and Hydrology of Karst Terrains, New York, New York, Oxford University Press.

White, W. B., Herman, J. S., Herman, E. K., and M., R., 2018, Karst Groundwater Contamination and Public Health, Cham, Switzerland, Springer International, Advances in Karst Science.

Appendix A: Data for Dropping Lick Cave

Table A1. Particle size data for Dropping Lick Cave

Replicate	Classification	%Sand	%Silt	%Clay	Total
DLBULK-09	very coarse silty very fine sand	50.3	49.7	0	100
DLBULK-12	very fine sandy very coarse silt	34.9	65	0	99.9
DLBULK-13	very fine sandy very coarse silt	48.7	51.1	0	99.8
DLBULK-14	very coarse silty very fine sand	56.7	43.3	0	100
DLBULK-15	very coarse silty very fine sand	60.5	39.4	0	99.9
DLBULK-16	very coarse silty very fine sand	56.6	43.3	0	99.9
DLBULK-17	very fine sandy very coarse silt	39.2	60.7	0	99.9
DLBULK-18	very coarse silty very fine sand	52.1	47.8	0	99.9
DLBULK-19	very coarse silty very fine sand	52.7	47.3	0	100

Table A2. Summarized qXRD data for Dropping Lick Cave

Mineral	Replicate Number	Total %	Normalized Mineral %
Chlorite	1	3.3	3.96
Quartz	1	56.8	68.11
Dolomite	1	5.8	6.95
Calcite	1	7	8.39
Orthoclase	1	3.5	4.20
Amorphous	1	7	8.39
Chlorite	2	4.7	5.62
Quartz	2	43.8	52.33
Dolomite	2	3.1	3.70
Orthoclase	2	2.7	3.23
Amorphous	2	29.4	35.13
Quartz	3	50.4	64.70
Dolomite	3	7.1	9.11
Orthoclase	3	4.2	5.39
Amorphous	3	16.2	20.80
Chlorite	4	3.4	4.33
Quartz	4	60.5	77.07
Dolomite	4	4.4	5.61
Orthoclase	4	5.6	7.13
Amorphous	4	4.6	5.86
Chlorite	5	2.6	3.27
Quartz	5	55.8	70.10
Dolomite	5	4.3	5.40
Orthoclase	5	4.8	6.03
Amorphous	5	12.1	15.20
Quartz	6	57.3	70.83
Dolomite	6	3.7	4.57
Orthoclase	6	5.8	7.17
Amorphous	6	14.1	17.43

Table A3. Total carbon, TIC, TOC and f_{OC} for Dropping Lick Cave

Replicate	TC wt %	TIC wt %	TOC wt %	f_{OC}
DLBULK-001	1.17	0.60	0.57	0.0057
DLBULK-002	1.18	0.54	0.64	0.0064
DLBULK-003	1.15	0.41	0.74	0.0074
DlBULK-004	1.08	0.40	0.68	0.0068
DLBULK-005	1.12	0.41	0.71	0.0071
DLBULK-006	1.13	0.33	0.80	0.008
DLBULK-007	1.07	0.16	0.91	0.0091

Table A4. Digested elemental chemistry for Dropping Lick Cave

Replicate	Al mol/L	Ca mol/L	Fe mol/L	K mol/L	Mg mol/L	Si mol/L	Ti mol/L
DLBULK01	2.35E-01	2.12E-01	3.65E-01	1.58E-02	2.42E-01	2.52E-02	8.19E-04
DLBULK02	2.55E-01	1.89E-01	3.77E-01	1.62E-02	2.23E-01	2.66E-02	7.94E-04
DLBULK03	2.17E-01	1.84E-01	3.49E-01	1.43E-02	2.11E-01	1.33E-02	7.39E-04
DLBULK04	2.29E-01	2.16E-01	3.63E-01	1.54E-02	2.27E-01	2.26E-02	8.27E-04
DLBULK05	2.17E-01	1.95E-01	3.60E-01	1.46E-02	2.17E-01	1.00E-02	7.89E-04
DLBULK06-	2.22E-01	2.17E-01	3.43E-01	1.52E-02	2.47E-01	2.56E-02	8.17E-04
DLBULK07	2.33E-01	2.05E-01	3.54E-01	1.54E-02	2.35E-01	1.45E-02	7.56E-04
DLBULK08	2.38E-01	2.07E-01	3.60E-01	1.56E-02	2.33E-01	2.66E-02	8.31E-04

Table A5. EDS atomic percentages for Dropping Lick Cave

Replicate	Al atomic %	Ca atomic %	Fe atomic %	K atomic %	Mg atomic %	Si atomic %	Ti atomic %
DLBULK01	1.77	0.11	1.09	0.34	0.17	24.99	-
DLBULK02	7.29	0.31	2.92	1.53	0.73	18.93	-
DLBULK03	4.94	-	2.24	2.54	0.46	23.1	0.3
DLBULK04	6.73	0.77	2.09	1.27	0.71	12.26	-
DLBULK05	4.5	-	1.09	1.8	0.26	25.25	-
DLBULK06	6.44	0.78	2.84	1.02	0.69	10.75	-

Appendix B: Data for Butler Cave

Table B1. Sample Location and Description

Location	Facies Represented	Sample Types	Sample Names	Simplified Sample Name
BTC-001	Diamicton	Core	BTC-001-C1-1 (0 – 13 cm*)	1A
		Core		1B
		Grab	BTC-001-C1-2 (13 – 26 cm)	1C
		Grab		1D
		Grab	BTC-001-G1	1E
			BTC-001-G2	
			BTC-001-G3	
BTC-002	Channel	Core	BTC-002-C1-1 (0 – 4.5 cm)	2A
		Core		2B
		Core	BTC-002-C1-2 (5 – 9.5 cm)	2C
		Core		2D
		Grab	BTC-002-C1-3 (9.5 – 27 cm)	2E
			BTC-002-C2-1 (0 – 15.5 cm)	
			BTC-002-G1	
BTC-003	Channel	Core	BTC-003-C1-1 (0 – 22 cm)	3A
		Grab	BTC-003-G1	3B
BTC-004	Channel	Core	BTC-004-C1-1 (0 cm)	4A
		Core	BTC-004-C1-2 (1 – 5 cm)	4B
		Core	BTC-004-C1-3 (5 – 8 cm)	4C
		Core	BTC-004-C1-4 (8 – 11 cm)	4D
		Core	BTC-004-C1-5 (11 – 14 cm)	4E
		Core		4F
		Core	BTC-004-C1-6 (14 – 20 cm)	4G
		Core		4H
		Core	BTC-004-C2-1 (0 cm)	4I
		Core	BTC-004-C2-2 (1 – 8 cm)	4J
		Grab	BTC-004-C2-3 (8 – 15 cm)	4K
		Grab	BTC-004-C2-4 (15 – 17 cm)	4L
		Grab		4M
		Grab	BTC-004-G1	4N
		Grab	BTC-004-G2	4O
			BTC-004-G3	
			BTC-004-G4	
			BTC-004-G5	
BTC-005	Channel/Slackwater	Grab	BTC-005-G1	5A
		Grab	BTC-005-G2	5B
BTC-006	Slackwater	Core	BTC-006-C1-1 (0 – 3 cm)	6A
		Core	BTC-006-C1-2 (3 – 9 cm)	6B

	Core	BTC-006-C1-3 (9 – 16 cm)	6C
	Core	BTC-006-C1-4 (16 – 23 cm)	6D

Sampling schema, names, and depths in the core where subsamples were collected.

Table B2. Data Summary for Butler Cave

Location	Sample Location	Sample Name	Simplified Sample Number	Sediment Type	% Sand	% Silt	%Clay	TC w.t. %	TOC w.t.%	N w.t.%	C:N
Butler Cave	BTC-001	BTC-001-C1-1	1A	very coarse silty fine sand	85.1	10.7	4.3	0.11	0.11	0.02	5.5
Butler Cave	BTC-001	BTC-001-C1-2	1B	very coarse silty fine sand	86	10.7	3.3	0.08	0.08	0.02	4.0
Butler Cave	BTC-001	BTC-001-G1	1C	very coarse silty fine sand	51.3	41.8	6.9	0.25	0.20	0.04	5.5
Butler Cave	BTC-001	BTC-001-G2	1D	fine sandy very coarse silt	45.3	51.3	3.4	0.43	0.37	0.05	7.4
Butler Cave	BTC-001	BTC-001-G3	1E	fine sandy fine silt	38.4	48.9	12.7	0.42	0.18	0.04	4.5
Butler Cave	BTC-002	BTC-002-C1-1	2A	very coarse silty fine sand	85.1	10.7	4.3	0.31	0.31	0.03	10.3
Butler Cave	BTC-002	BTC-002-C1-2	2B	very coarse silty fine sand	86	10.7	3.3	0.87	0.87	0.08	10.9
Butler Cave	BTC-002	BTC-002-C1-3	2C	very coarse silty fine sand	51.3	41.8	6.9	0.36	0.36	0.04	9.0
Butler Cave	BTC-002	BTC-002-C2-1	2D	fine sandy very coarse silt	45.3	51.3	3.4	0.27	0.27	0.03	9.0
Butler Cave	BTC-002	BTC-002-G1	2E	fine sandy fine silt	38.4	48.9	12.7	0.40	0.40	0.04	10.0
Butler Cave	BTC-003	BTC-003-C1-1	3A	poorly sorted medium sand	91.4	6.1	2.5	0.45	0.45	0.03	15.0

Table B2. Data Summary for Butler Cave

Location	Sample Location	Sample Name	Simplified Sample Number	Sediment Type	% Sand	% Silt	%Clay	TC w.t. %	TOC w.t.%	N w.t.%	C:N
Butler Cave	BTC-003	BTC-003-G1	3B	very coarse silty medium sand	89.2	8.5	2.4	0.63	0.40	0.04	10.0
Butler Cave	BTC-004	BTC-004-C1-1	4A	very coarse silty very fine sand	60.2	39.9	0	0.31	0.26	0.03	8.7
Butler Cave	BTC-004	BTC-004-C1-2	4B	very coarse silty fine sand	54.4	12.3	3.5	0.13	0.12	0.02	6.0
Butler Cave	BTC-004	BTC-004-C1-3	4C	fine silty fine sand	53.9	36.7	9.3	0.17	0.16	0.03	5.3
Butler Cave	BTC-004	BTC-004-C1-4	4D	very coarse silty fine sand	85.2	10.6	4.2	0.12	0.12	0.02	6.0
Butler Cave	BTC-004	BTC-004-C1-5	4E	very coarse silty fine sand	52.7	46.8	0.5	0.20	0.20	0.03	6.7
Butler Cave	BTC-004	BTC-004-C1-6	4F	fine silty fine sand	83.7	11.9	4.4	0.12	0.12	0.02	6.0
Butler Cave	BTC-004	BTC-004-C2-1	4G	very coarse silty fine sand	66.6	31.2	2.3	0.23	0.21	0.03	7.0
Butler Cave	BTC-004	BTC-004-C2-2	4H	muddy fine sand	89.5	6.8	3.7	0.11	0.11	0.02	5.5

Table B2. Data Summary for Butler Cave

Location	Sample Location	Sample Name	Simplified Sample Number	Sediment Type	% Sand	% Silt	%Clay	TC w.t. %	TOC w.t.%	N w.t.%	C:N
Butler Cave	BTC-004	BTC-004-C2-3	4I	very coarse silty fine sand	74.5	20.8	4.7	0.14	0.14	0.03	4.7
Butler Cave	BTC-004	BTC-004-C2-4	4J	very coarse silty fine sand	80.1	15.3	4.5	0.14	0.14	0.02	7.0
Butler Cave	BTC-004	BTC-004-G1	4K	very coarse silty fine sand	84.7	11.1	4.2	0.11	0.10	0.02	5.5
Butler Cave	BTC-004	BTC-004-G2	4L	fine silty medium sand	79	14.7	6.3	0.17	0.12	0.02	5.8
Butler Cave	BTC-004	BTC-004-G3	4M	fine silty medium sand	82.1	12.4	5.4	0.17	0.10	0.02	5.2
Butler Cave	BTC-004	BTC-004-G4	4N	fine silty medium sand	84.2	11.9	3.9	0.19	0.16	0.02	6.8
Butler Cave	BTC-004	BTC-004-G5	4O	fine silty medium sand	84.1	11.6	4.4	0.16	0.15	0.02	7.3
Butler Cave	BTC-005	BTC-005-G1	5A	very coarse silty fine sand	82.4	13.8	3.8	0.31	0.29	0.03	9.8
Butler Cave	BTC-005	BTC-005-G2	5B	very coarse silty fine sand	82.4	13.9	3.8	0.16	0.16	0.04	4.0
Butler Cave	BTC006	BTC-006-C1-1	6A	fine sandy very coarse silt	38.5	51.2	10.2	0.25	0.21	0.03	7.0
Butler Cave	BTC-006	BTC-006-C1-2	6B	very fine sandy very coarse silt	27	72.3	0.7	0.13	0.13	0.03	4.3
Butler Cave	BTC006	BTC-006-C1-3	6C	very fine sandy very coarse silt	16.2	83.8	0	0.14	0.14	0.04	3.5

Table B2. Data Summary for Butler Cave

Location	Sample Location	Sample Name	Simplified Sample Number	Sediment Type	% Sand	% Silt	%Clay	TC w.t. %	TOC w.t.%	N w.t.%	C:N
Butler Cave	BTC006	BTC-006-C1-4	6D	very fine sandy very coarse silt	21	77.4	1.5	0.12	0.12	0.04	3.0
Butler Cave	BTC-001	BTC-001-C1-1	1A	very coarse silty fine sand	85.1	10.7	4.3	0.11	0.11	0.02	5.5

Table B2. Data Summary for Butler Cave

Location	Sample Location	Sample Name	Simplified Sample Number	Sediment Type	% Sand	% Silt	% Clay	Notes
Butler Cave	BTC-001	BTC-001-C1-1	1A	very coarse silty fine sand	85.1	10.7	4.3	
Butler Cave	BTC-001	BTC-001-C1-2	1B	very coarse silty fine sand	86	10.7	3.3	
Butler Cave	BTC-001	BTC-001-G1	1C	very coarse silty fine sand	51.3	41.8	6.9	
Butler Cave	BTC-001	BTC-001-G2	1D	fine sandy very coarse silt	45.3	51.3	3.4	
Butler Cave	BTC-001	BTC-001-G3	1E	fine sandy fine silt	38.4	48.9	12.7	
Butler Cave	BTC-002	BTC-002-C1-1	2A	very coarse silty fine sand	85.1	10.7	4.3	
Butler Cave	BTC-002	BTC-002-C1-2	2B	very coarse silty fine sand	86	10.7	3.3	
Butler Cave	BTC-002	BTC-002-C1-3	2C	very coarse silty fine sand	51.3	41.8	6.9	
Butler Cave	BTC-002	BTC-002-C2-1	2D	fine sandy very coarse silt	45.3	51.3	3.4	
Butler Cave	BTC-002	BTC-002-G1	2E	fine sandy fine silt	38.4	48.9	12.7	
Butler Cave	BTC-003	BTC-003-C1-1	3A	poorly sorted medium sand	91.4	6.1	2.5	
Butler Cave	BTC-003	BTC-003-G1	3B	very coarse silty medium sand	89.2	8.5	2.4	
Butler Cave	BTC-004	BTC-004-C1-1	4A	very coarse silty very fine sand	60.2	39.9	0	
Butler Cave	BTC-004	BTC-004-C1-2	4B	very coarse silty fine sand	54.4	12.3	3.5	

Butler Cave	BTC-004	BTC-004-C1-3	4C	fine silty fine sand	53.9	36.7	9.3	
Butler Cave	BTC-004	BTC-004-C1-4	4D	very coarse silty fine sand	85.2	10.6	4.2	
Butler Cave	BTC-004	BTC-004-C1-5	4E	very coarse silty fine sand	52.7	46.8	0.5	
Butler Cave	BTC-004	BTC-004-C1-6	4F	fine silty fine sand	83.7	11.9	4.4	
Butler Cave	BTC-004	BTC-004-C2-1	4G	very coarse silty fine sand	66.6	31.2	2.3	

Table B2. Data Summary for Butler Cave

Location	Sample Location	Sample Name	Simplified Sample Number	Sediment Type	% Sand	% Silt	% Clay	Notes
Butler Cave	BTC-004	BTC-004-C2-2	4H	muddy fine sand	89.5	6.8	3.7	
Butler Cave	BTC-004	BTC-004-C2-3	4I	very coarse silty fine sand	74.5	20.8	4.7	
Butler Cave	BTC-004	BTC-004-C2-4	4J	very coarse silty fine sand	80.1	15.3	4.5	
Butler Cave	BTC-004	BTC-004-G1-01	4K	very coarse silty fine sand	86	10.2	3.9	
Butler Cave	BTC-004	BTC-004-G1-02	4K	fine silty fine sand	84	11.4	4.5	
Butler Cave	BTC-004	BTC-004-G1-03	4K	very coarse silty fine sand	84	11.6	4.3	
Butler Cave	BTC-004	BTC-004-G1	4K	very coarse silty fine sand	84.7	11.1	4.2	Average of preceeding 3 samples
Butler Cave	BTC-004	BTC-004-G2	4L	fine silty medium sand	79	14.7	6.3	
Butler Cave	BTC-004	BTC-004-G3	4M	fine silty medium sand	82.1	12.4	5.4	

Butler Cave	BTC-004	BTC-004-G4	4N	fine silty medium sand	84.2	11.9	3.9	
Butler Cave	BTC-004	BTC-004-G5	4O	fine silty medium sand	84.1	11.6	4.4	
Butler Cave	BTC-005	BTC-005-G1-01	5A	very coarse silty fine sand	82.7	13.7	3.6	
Butler Cave	BTC-005	BTC-005-G2-01	5A	very coarse silty fine sand	80.8	14.9	4.2	
Butler Cave	BTC-005	BTC-005-G3-01	5A	very coarse silty fine sand	83.7	12.8	3.5	
Butler Cave	BTC-005	BTC-005-G1	5A	very coarse silty fine sand	82.4	13.8	3.8	Average of preceeding 3 samples
Butler Cave	BTC-005	BTC-005-G2	5B	very coarse silty fine sand	82.4	13.9	3.8	
Butler Cave	BTC006	BTC-006-C1-1	6A	fine sandy very coarse silt	38.5	51.2	10.2	
Butler Cave	BTC-006	BTC-006-C1-2	6B	very fine sandy very coarse silt	27	72.3	0.7	
Butler Cave	BTC006	BTC-006-C1-3	6C	very fine sandy very coarse silt	16.2	83.8	0	
Butler Cave	BTC006	BTC-006-C1-4	6D	very fine sandy very coarse silt	21	77.4	1.5	

Table B3.1. Significant Result of Welch's t-test between BTC-001 and BTC-004 Parameters

Parameter	Mean	Parameter	Mean	p-value ($\alpha = 0.05$)
% Sand 001 Core	85.6	% Sand 001 Grab	45.0	8.46E-3
% Silt 001 Core	10.7	% Silt 001 Grab	47.3	6.00E-3
% Sand 004 Core	70.1	% Sand 004 Grab	82.8	2.04E-2
% Silt 004 Core	23.2	% Silt 004 Grab	12.3	4.01E-2
% Sand 001 Core	85.6	% Sand 004 Core	70.1	7.71E-3
% Silt 001 Core	10.7	% Silt 004 Core	23.2	2.13E-2
TOC w.t. % 001 Core	9.50E-2	TOC 004 Core	1.58E-1	4.40E-2
% Sand 001 Grab	45.0	% Sand 004 Grab	82.8	1.03E-2
% Silt 001 Grab	47.3	% Silt 004 Grab	12.3	6.89E-3

Table B3.2. Significant Results of Welch's t-test between BTC and other clastic cave sediments TOC w.t.%

Location	Mean	Location	Mean	p-value ($\alpha = 0.05$)
BTC	2.20E-1	TAL* all samples	7.80E-1	1.41E-19
BTC	2.20E-1	TAL* saturated samples	9.43E-1	2.55E-10
BTC	2.20E-1	TAL* unsaturated samples	6.98E-1	8.15E-13
BTC	2.20E-1	CAM*	4.21E-1	5.18E-3
BTC	2.20E-1	All Puerto Rico samples*	6.69E-1	4.90E-17
BTC	2.20E-1	Illinois**	1.23E-1	1.17E-2
BTC	2.20E-1	England***	1.26	1.27E-4
Illinois**	1.23E-1	All Puerto Rico Samples*	6.69E-1	2.55E-22
England***	1.26	All Puerto Rico Samples*	6.69E-1	1.29E-2
Illinois**	1.23E-1	England***	1.26	5.93E-5
England***	1.26	CAM*	4.21E-1	1.12E-3

*Downey,2020; **Panno et. al., 2004; Bottrell et. al., 1996

R code for particle size analysis

```
setwd("/Volumes/GoogleDrive/My Drive/Butler Cave/")
#set your own workng drive
install.packages("dplyr")
install.packages("tidyverse")
install.packages("readxl")
install.packages("ggplot2")
install.packages("colorspace")
install.packages("scales")
library(dplyr)
library(tidyverse)
library(readxl)
library(ggplot2)
library(colorspace)
library(scales)

#Before going to the next step, make sure you have created a file that is only the particle size
  bins as they appear on the data files
size_file <- "particle_size_bins.txt"
size <- read.delim(size_file, header = FALSE)
size[,2] <- list(NULL)

setwd("/Volumes/GoogleDrive/My Drive/Butler Cave/ParticlesizeR")
#Make sure your text files of data for each sample are stored here

#The following code will combine all text files into one csv

files <- list.files()
bins <- data.frame(size)
row.names(bins) <- bins[1:93,]
bins <- bins[1:93,0]

for (xfile_name in files) {
  x_data <- read.delim(paste0(xfile_name), header = TRUE)
  x_data[,1] <- list(NULL)
  assign(xfile_name, x_data)
  bins <- cbind(bins, get(xfile_name))
}

colnames(bins) <- files
write.csv(bins, file = "BTC.csv")

#You can now use this CVS to copy data into the gradistat program to analyze the samples
```

Appendix C: Data for microsphere adherence

Supplementary Data

Determination of the sediment:solution ratio and equilibration time

The sediment:solution ratio refers to the grams of sediment relative to the milliliters of microsphere solution and the equilibration time refers to the time the solutions are allowed to mix on the rotating shaker. For NFMS and CMS experiments were carried out for sediment:solution ratios at 1:4, 1:10, 1:20, 1:40, 1:60; 1:100: 1:200: and 1:500. For NFMS the, the percent of adhered microspheres across these ratios ranged from 80.2 – 96.15 % with an average percent adhered value of 89.0% ± 5.4. For CMS, the percent of adhered microspheres across these ratios ranged from 73.9 – 99.9% with an average percent of adhered value of 89.2% ± 9.77. Due to the percent adhered range across these ratios being consistent with the percent of unrecovered microspheres reported in microsphere tracer studies (Flynn and Sinreich, 2010; Goeppert and Goldscheider, 2011; Goeppert and Hoetzl, 2009; Harvey et al., 1989; Harvey et al., 1993; Harvey et al., 2008; Sinreich et al., 2009), ratios of 1:4 and 1:100 were selected for equilibration time experiments. For NFMS and CMS in a 1:4 sediment:solution ratio, equilibration times of 1, 24, 48, and 72 hours were evaluated. Percent adhered for both types of microspheres across these equilibration times averaged 99.9% ± 0.01. For NFMS and CMS in a 1:100 sediment:solution ratios, equilibration times of 0.5, 6, 16, 18, and 20 were evaluated. For NFMS, percent adhered microspheres averaged 28.6% ± 35.6 and for CMS, percent adhered microspheres averaged 87.3% ± 5.9. Initial adherence experiments for NFMS in 1:100 and 1:4 ratios at four hours equilibration time resulted in average percent removal of microspheres from the initial solutions of 18.1% ± 7.70 and 49.1% ± 8.07, respectively. In the same conditions for CMS, average percent removal was 18.5% ± 7.1 and 58.4% ± 16. Based on these preliminary data, a ratio of 1:20 and equilibration time of 4 hours was chosen for the following experiments to reflect the potential ratio that would be observed in a natural setting. These parameters resulted in adhered microspheres that is consistent with previously reported field experiments and allows for comparison of different microsphere behavior under the same conditions.

Table C1. CMS equilibration times for 1:4 and 1:500 soil:solution ratio

1:4	Initial Sph/mL	Equil Sph/mL	Vol Soln mL	Mass Sed g	ADS, calc sph/G	%ADS
1	3.72E+06	8.61E+02	30.43	7.608	1.49E+07	99.98
24	3.72E+06	5.28E+02	30.34	7.584	1.49E+07	99.99
48	3.72E+06	4.89E+02	30.33	7.583	1.49E+07	99.99
72	3.72E+06	2.83E+02	30.33	7.583	1.49E+07	99.99
1:500	Initial Sph/mL	Equil Sph/mL	Vol Soln mL	Mass Sed g	ADS, calc sph/G	%ADS
1	3.72E+06	5.84E+05	33.5	0.067	1.57E+09	84.31
4	3.72E+06	4.70E+05	30.5	0.061	1.63E+09	87.37
48	3.72E+06	3.35E+05	30.5	0.061	1.69E+09	91.00
72	3.72E+06	1.05E+06	30.5	0.031	2.63E+09	71.90

Table C2. NFMS equilibration times for 1:4 and 1:500 soil:solution ratio

1:4	Initial Sph/mL	Equil Sph/mL	Vol Soln mL	Mass Sed g	ADS, calc sph/G	%ADS
1	2.23E+06	1.04E+03	30.67	7.668	8.92E+06	99.95
24	2.23E+06	5.06E+02	30.33	7.583	8.92E+06	99.98
48	2.23E+06	3.67E+02	30.34	7.585	8.92E+06	99.98
72	2.23E+06	3.00E+02	30.4	7.585	8.94E+06	99.99
1:500	Initial Sph/mL	Equil Sph/mL	Vol Soln mL	Mass Sed g	ADS, calc sph/G	%ADS
1	2.23E+06	1.51E+05	30	0.06	1.04E+09	93.22
24	2.23E+06	2.18E+03	30.5	0.061	1.11E+09	99.90
48	2.23E+06	2.17E+05	31	0.062	1.01E+09	90.29
72	2.23E+06	7.18E+03	30	0.06	1.11E+09	99.68

Table C3. Sphere adherence data for NFMS experiments in DI

Initial sph/mL	Equilibrium sph/mL	Volume solution m/L	g sediment	Adsorbed sph/g	%Decrease
1.55E+06	6.92E+05	2.50E+01	1.25E+00	1.71E+07	5.53E+01
1.14E+06	5.40E+05	2.53E+01	1.26E+00	1.19E+07	5.25E+01
8.89E+05	2.47E+05	2.50E+01	1.25E+00	1.28E+07	7.22E+01
5.88E+05	2.74E+05	2.49E+01	1.25E+00	6.29E+06	5.34E+01
3.23E+05	1.74E+05	2.50E+01	1.25E+00	2.98E+06	4.62E+01
2.41E+05	1.35E+05	2.52E+01	1.26E+00	2.12E+06	4.41E+01
1.93E+05	1.03E+05	2.54E+01	1.27E+00	1.82E+06	4.70E+01
1.46E+05	8.85E+04	2.47E+01	1.24E+00	1.15E+06	3.94E+01
1.10E+05	6.23E+04	2.49E+01	1.24E+00	9.60E+05	4.35E+01
7.56E+04	4.22E+04	2.48E+01	1.24E+00	6.66E+05	4.41E+01
4.18E+04	2.03E+04	2.55E+01	1.28E+00	4.30E+05	5.15E+01
1.49E+04	8.02E+03	2.55E+01	1.27E+00	1.37E+05	4.62E+01

Initial sph/mL	Equilibrium sph/mL	Volume solution m/L	g sediment	Adsorbed sph/g	%Decrease
2.60E+06	8.55E+05	2.47E+01	1.24E+00	3.49E+07	6.71E+01
2.33E+06	7.19E+05	2.49E+01	1.24E+00	3.23E+07	6.92E+01
2.22E+06	6.48E+05	2.46E+01	1.23E+00	3.15E+07	7.08E+01
1.92E+06	7.50E+05	2.49E+01	1.25E+00	2.35E+07	6.10E+01
1.83E+06	6.16E+05	2.46E+01	1.23E+00	2.42E+07	6.63E+01
1.56E+06	7.28E+05	2.55E+01	1.28E+00	1.66E+07	5.32E+01
1.37E+06	4.26E+05	2.46E+01	1.23E+00	1.89E+07	6.90E+01
1.08E+06	3.84E+05	2.49E+01	1.24E+00	1.39E+07	6.44E+01
8.22E+05	2.26E+05	2.47E+01	1.24E+00	1.19E+07	7.25E+01
6.59E+05	1.59E+04	2.49E+01	1.25E+00	1.29E+07	9.76E+01
1.10E+06	3.72E+05	2.50E+01	1.25E+00	1.45E+07	6.61E+01
2.72E+05	1.04E+05	2.46E+01	1.23E+00	3.37E+06	6.19E+01

Initial sph/mL	Equilibrium sph/mL	Volume solution m/L	g sediment	Adsorbed sph/g	%Decrease
2.85E+06	4.38E+05	2.66E+01	1.33E+00	4.83E+07	8.47E+01
2.08E+06	1.50E+05	2.58E+01	1.29E+00	3.86E+07	9.28E+01
1.23E+06	3.45E+05	2.78E+01	1.39E+00	1.77E+07	7.20E+01
1.09E+06	8.17E+04	2.60E+01	1.30E+00	2.01E+07	9.25E+01
5.70E+05	5.60E+03	2.59E+01	1.30E+00	1.13E+07	9.90E+01

Table C4. Sphere adherence data for NFMS experiments in 25 mg/L $CaCO_3$

Equilibrium (sph)	Initial sph/mL	Equilib Sph/mL	Volume Solution, mL	Sediment, g	Adsorbed, sph/g	% Decrease
4.65E+04	1.48E+06	9.30E+05	2.52E+01	1.26	1.10E+07	3.72E+01
4.56E+04	1.21E+06	9.13E+05	2.54E+01	1.28	5.87E+06	2.45E+01
3.48E+04	1.13E+06	6.96E+05	2.47E+01	1.234	8.73E+06	3.85E+01
3.83E+04	1.17E+06	7.66E+05	2.51E+01	1.255	8.15E+06	3.47E+01
2.01E+04	7.44E+05	4.01E+05	2.53E+01	1.267	6.86E+06	4.61E+01
2.18E+04	7.39E+05	4.36E+05	2.49E+01	1.245	6.04E+06	4.09E+01
1.11E+04	4.84E+05	2.21E+05	2.50E+01	1.251	5.26E+06	5.43E+01
8.34E+03	3.34E+05	1.67E+05	2.45E+01	1.223	3.35E+06	5.01E+01

Equilibrium (sph)	Initial sph/mL	Equilib Sph/mL	Volume Solution, mL	Sediment, g	Adsorbed, sph/g	% Decrease
2.17E+06	4.88E+05	2.51E+01	1.26E+00	3.36E+07	7.75E+01	2.17E+06
2.07E+06	6.74E+05	2.51E+01	1.25E+00	2.79E+07	6.74E+01	2.07E+06
1.48E+06	3.23E+05	2.51E+01	1.26E+00	2.32E+07	7.82E+01	1.48E+06
1.05E+06	3.44E+05	2.54E+01	1.27E+00	1.41E+07	6.72E+01	1.05E+06
4.99E+05	1.22E+05	2.50E+01	1.25E+00	7.54E+06	7.56E+01	4.99E+05

Equilibrium (sph)	Initial sph/mL	Equilib Sph/mL	Volume Solution, mL	Sediment, g	Adsorbed, sph/g	% Decrease
2.44E+06	9.69E+05	2.54E+01	1.27E+00	2.94E+07	6.02E+01	2.44E+06
2.14E+06	6.51E+05	2.50E+01	1.25E+00	2.97E+07	6.95E+01	2.14E+06
1.55E+06	4.88E+05	2.51E+01	1.25E+00	2.13E+07	6.85E+01	1.55E+06
1.13E+06	3.68E+05	2.50E+01	1.25E+00	1.52E+07	6.74E+01	1.13E+06
5.47E+05	1.70E+05	2.50E+01	1.25E+00	7.54E+06	6.89E+01	5.47E+05

Table C5. Sphere adherence data for NFMS experiments in karst water

Equilibrium (sph)	Initial sph/mL	Equilib Sph/mL	Volume Solution, mL	Sediment, g	Adsorbed, sph/g	% Decrease
2.48E+06	2.50E+05	2.54E+01	1.27E+00	4.47E+07	8.99E+01	2.48E+06
1.97E+06	9.87E+04	2.51E+01	1.26E+00	3.73E+07	9.50E+01	1.97E+06
1.29E+06	1.17E+05	2.49E+01	1.25E+00	2.35E+07	9.09E+01	1.29E+06
8.92E+05	7.05E+04	2.51E+01	1.26E+00	1.64E+07	9.21E+01	8.92E+05
4.52E+05	2.51E+04	2.49E+01	1.25E+00	8.55E+06	9.45E+01	4.52E+05

Equilibrium (sph)	Initial sph/mL	Equilib Sph/mL	Volume Solution, mL	Sediment, g	Adsorbed, sph/g	% Decrease
1.49E+05	2.52E+01	1.26E+00	4.49E+07	9.38E+01	1.49E+05	2.52E+01
1.33E+05	2.53E+01	1.27E+00	3.77E+07	9.34E+01	1.33E+05	2.53E+01
1.17E+05	2.58E+01	1.29E+00	2.75E+07	9.21E+01	1.17E+05	2.58E+01
7.25E+04	2.45E+01	1.23E+00	1.84E+07	9.27E+01	7.25E+04	2.45E+01
2.59E+04	2.48E+01	1.24E+00	1.12E+07	9.56E+01	2.59E+04	2.48E+01

Equilibrium (sph)	Initial sph/mL	Equilib Sph/mL	Volume Solution, mL	Sediment, g	Adsorbed, sph/g	% Decrease
2.41E+06	1.19E+05	2.55E+01	1.27E+00	4.59E+07	9.51E+01	2.41E+06
1.71E+06	1.14E+05	2.53E+01	1.26E+00	3.19E+07	9.33E+01	1.71E+06
1.45E+06	7.18E+04	2.50E+01	1.25E+00	2.75E+07	9.50E+01	1.45E+06
9.96E+05	4.23E+04	2.53E+01	1.27E+00	1.91E+07	9.58E+01	9.96E+05
4.76E+05	3.31E+04	2.46E+01	1.23E+00	8.86E+06	9.30E+01	4.76E+05

Table C6. Sphere adherence data for CMS experiments in DI

Initial sph/mL	Equilibrium sph/mL	Volume solution m/L	g sediment	Adsorbed sph/g	%Decrease
1.89E+06	9.50E+05	2.47E+01	1.24E+00	1.89E+07	4.99E+01
1.49E+06	7.73E+05	2.49E+01	1.24E+00	1.43E+07	4.80E+01
1.06E+06	5.68E+05	2.53E+01	1.27E+00	9.90E+06	4.66E+01
7.23E+05	3.18E+05	2.49E+01	1.25E+00	8.09E+06	5.60E+01
3.93E+05	1.79E+05	2.49E+01	1.25E+00	4.29E+06	5.45E+01
3.12E+05	4.59E+04	2.47E+01	1.23E+00	5.33E+06	8.53E+01
2.43E+05	1.28E+05	2.49E+01	1.25E+00	2.29E+06	4.71E+01
1.97E+05	9.92E+04	2.52E+01	1.26E+00	1.97E+06	4.98E+01
1.40E+05	8.18E+04	2.47E+01	1.24E+00	1.17E+06	4.17E+01
8.30E+04	3.04E+04	2.51E+01	1.26E+00	1.05E+06	6.34E+01
1.82E+04	6.96E+03	2.48E+01	1.24E+00	2.26E+05	6.19E+01
1.04E+04	3.80E+02	2.47E+01	1.24E+00	2.01E+05	9.64E+01

Initial sph/mL	Equilibrium sph/mL	Volume solution m/L	g sediment	Adsorbed sph/g	%Decrease
2.71E+06	1.39E+06	2.49E+01	1.24E+00	2.63E+07	4.85E+01
2.60E+06	1.32E+06	2.47E+01	1.24E+00	2.57E+07	4.94E+01
2.32E+06	8.88E+05	2.46E+01	1.23E+00	2.87E+07	6.18E+01
2.28E+06	9.65E+05	2.54E+01	1.27E+00	2.63E+07	5.77E+01
1.94E+06	1.02E+06	2.47E+01	1.23E+00	1.84E+07	4.76E+01
1.75E+06	7.87E+05	2.49E+01	1.24E+00	1.93E+07	5.51E+01
1.54E+06	7.57E+05	2.48E+01	1.24E+00	1.56E+07	5.07E+01
1.14E+06	6.49E+05	2.44E+01	1.22E+00	9.75E+06	4.29E+01
8.27E+05	4.92E+05	2.56E+01	1.28E+00	6.70E+06	4.05E+01
7.58E+05	3.63E+05	2.51E+01	1.26E+00	7.90E+06	5.21E+01
5.48E+05	2.90E+05	2.64E+01	1.32E+00	5.17E+06	4.71E+01
3.02E+05	1.37E+05	2.50E+01	1.25E+00	3.30E+06	5.47E+01
1.52E+05	8.58E+04	2.53E+01	1.27E+00	1.33E+06	4.36E+01
2.89E+04	1.82E+04	2.57E+01	1.29E+00	2.14E+05	3.70E+01

Initial sph/mL	Equilibrium sph/mL	Volume solution m/L	g sediment	Adsorbed sph/g	%Decrease
2.20E+06	3.78E+05	2.58E+01	1.29E+00	3.64E+07	8.28E+01
1.64E+06	4.65E+05	2.65E+01	1.33E+00	2.35E+07	7.17E+01
1.45E+06	3.10E+05	2.51E+01	1.26E+00	2.28E+07	7.87E+01
1.06E+06	3.32E+05	2.51E+01	1.26E+00	1.46E+07	6.87E+01

6.01E+05	1.27E+05	2.56E+01	1.28E+00	9.49E+06	7.89E+01

Initial sph/mL	Equilibrium sph/mL	Volume solution m/L	g sediment	Adsorbed sph/g	%Decrease
2.98E+06	6.55E+05	2.58E+01	1.29E+00	4.64E+07	7.80E+01
2.21E+06	5.11E+05	2.72E+01	1.36E+00	3.39E+07	7.68E+01
1.82E+06	2.88E+05	2.47E+01	1.24E+00	3.07E+07	8.42E+01
3.04E+05	1.92E+05	2.53E+01	1.27E+00	2.25E+06	3.69E+01
6.34E+05	7.42E+04	2.50E+01	1.25E+00	1.12E+07	8.83E+01

Table C7. Sphere adherence data for CMS experiments in 25 mg/L $CaCO_3$

Equilibrium (sph)	Initial sph/mL	Equilib Sph/mL	Volume Solution, mL	Sediment, g	Adsorbed, sph/g	% Decrease
3.14E+06	2.15E+06	2.52E+01	1.26E+00	1.99E+07	3.16E+01	3.14E+06
2.87E+06	1.94E+06	2.50E+01	1.25E+00	1.86E+07	3.24E+01	2.87E+06
2.57E+06	1.74E+06	2.59E+01	1.29E+00	1.65E+07	3.21E+01	2.57E+06
2.37E+06	1.57E+06	2.50E+01	1.25E+00	1.59E+07	3.36E+01	2.37E+06
2.00E+06	1.32E+06	2.59E+01	1.30E+00	1.37E+07	3.43E+01	2.00E+06
1.66E+06	1.05E+06	2.60E+01	1.30E+00	1.22E+07	3.66E+01	1.66E+06
1.34E+06	9.30E+05	2.67E+01	1.34E+00	8.21E+06	3.06E+01	1.34E+06
1.01E+06	7.05E+05	2.52E+01	1.62E+00	4.79E+06	3.03E+01	1.01E+06
5.45E+05	3.74E+05	2.50E+01	1.25E+00	3.41E+06	3.13E+01	5.45E+05
2.73E+05	2.12E+05	2.46E+01	1.23E+00	1.22E+06	2.23E+01	2.73E+05

Equilibrium (sph)	Initial sph/mL	Equilib Sph/mL	Volume Solution, mL	Sediment, g	Adsorbed, sph/g	% Decrease
3.41E+06	1.32E+06	2.51E+01	1.25E+00	4.18E+07	6.12E+01	3.41E+06
2.66E+06	8.85E+05	2.50E+01	1.25E+00	3.54E+07	6.67E+01	2.66E+06
2.03E+06	6.68E+05	2.51E+01	1.25E+00	2.73E+07	6.71E+01	2.03E+06
1.38E+06	4.38E+05	2.52E+01	1.26E+00	1.87E+07	6.81E+01	1.38E+06
6.94E+05	1.72E+05	2.53E+01	1.26E+00	1.04E+07	7.52E+01	6.94E+05

Equilibrium (sph)	Initial sph/mL	Equilib Sph/mL	Volume Solution, mL	Sediment, g	Adsorbed, sph/g	% Decrease
3.34E+06	9.69E+05	2.49E+01	1.24E+00	4.73E+07	7.09E+01	3.34E+06
2.75E+06	9.03E+05	2.49E+01	1.25E+00	3.70E+07	6.72E+01	2.75E+06
2.07E+06	6.31E+05	2.50E+01	1.25E+00	2.88E+07	6.96E+01	2.07E+06
1.42E+06	4.86E+05	2.50E+01	1.25E+00	1.86E+07	6.57E+01	1.42E+06
7.03E+05	2.40E+05	2.50E+01	1.25E+00	9.26E+06	6.59E+01	7.03E+05

Table C8. Sphere adherence data for CMS experiments in karst water

Equilibrium (sph)	Initial sph/mL	Equilib Sph/mL	Volume Solution, mL	Sediment, g	Adsorbed, sph/g	% Decrease
1.92E+06	9.20E+04	2.55E+01	1.28E+00	3.65E+07	9.52E+01	1.92E+06
2.21E+06	7.52E+04	2.69E+01	1.35E+00	4.27E+07	9.66E+01	2.21E+06
9.20E+05	4.96E+04	2.53E+01	1.27E+00	1.74E+07	9.46E+01	9.20E+05
2.26E+05	3.65E+04	2.72E+01	1.36E+00	3.79E+06	8.39E+01	2.26E+05
5.62E+05	1.22E+04	2.46E+01	1.23E+00	1.10E+07	9.78E+01	5.62E+05

Equilibrium (sph)	Initial sph/mL	Equilib Sph/mL	Volume Solution, mL	Sediment, g	Adsorbed, sph/g	% Decrease
6.39E+05	8.67E+04	2.44E+01	1.22E+00	1.10E+07	8.64E+01	6.39E+05
1.41E+06	7.29E+04	2.61E+01	1.31E+00	2.68E+07	9.48E+01	1.41E+06
1.07E+06	5.50E+04	2.53E+01	1.26E+00	2.04E+07	9.49E+01	1.07E+06
8.52E+05	4.83E+04	2.55E+01	1.28E+00	1.61E+07	9.43E+01	8.52E+05
3.02E+05	2.46E+04	2.48E+01	1.24E+00	5.55E+06	9.18E+01	3.02E+05

Equilibrium (sph)	Initial sph/mL	Equilib Sph/mL	Volume Solution, mL	Sediment, g	Adsorbed, sph/g	% Decrease
7.15E+05	1.12E+04	2.50E+01	1.25E+00	1.41E+07	9.84E+01	7.15E+05
1.22E+06	6.08E+04	2.56E+01	1.28E+00	2.32E+07	9.50E+01	1.22E+06
8.81E+05	5.06E+04	2.53E+01	1.27E+00	1.66E+07	9.43E+01	8.81E+05
3.74E+05	6.14E+04	2.53E+01	1.27E+00	6.24E+06	8.36E+01	3.74E+05
2.91E+05	2.72E+04	2.57E+01	1.28E+00	5.27E+06	9.06E+01	2.91E+05

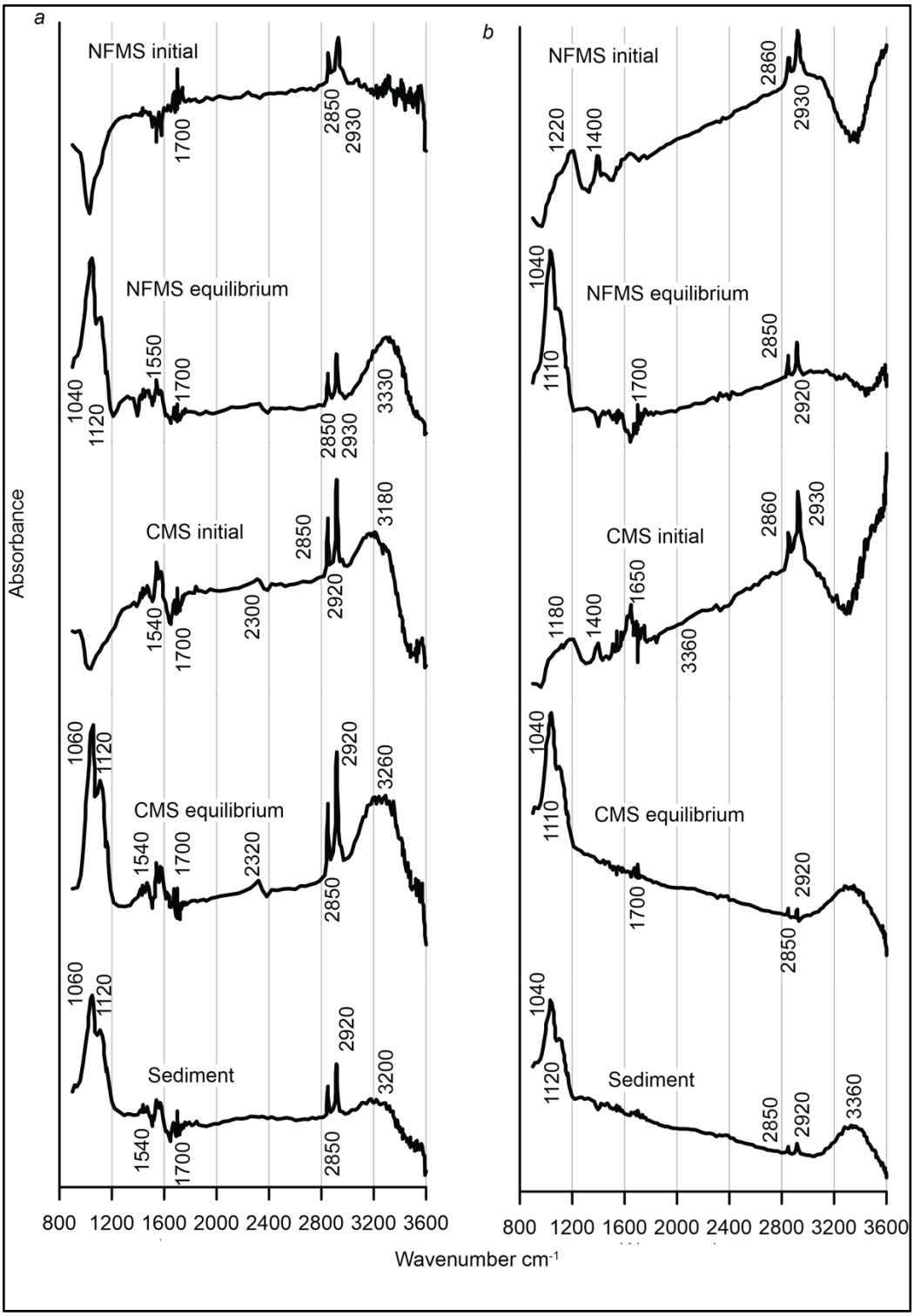

Fig. C1. FTIR spectra of NFMS initial and equilibrium solutions in DI (a) and 25 mg/L $CaCO_3$ (b). These spectra results were used in the statistical analysis.

R code for statistical analysis of FTIR spectra

```
library(baseline)
library(base)
library(R.utils)
library(ChemoSpec)
library(ChemoSpecUtils)
library(dbplyr)
library(knitr)
library(readr)
library(readxl)
library(tidyverse)
library(tidyselect)
library(tidyr)
library(amap)
library(robustbase)
library(pcaPP)

setwd("/Volumes/GoogleDrive/My Drive/Sorp_Data/Paper/FTIR copy/Group1use")

g1 <- files2SpectraObject(
  gr.crit = c("NFMS", "CMS"),
  gr.cols = c("black", "gray"),
  freq.unit = "Wavenumber",
  int.unit = "abosrbance",
  descrip = "no description provided",
  fileEXT = "\\.(csv|CSV)$",
  out.file = "g1_data",
  header = TRUE,
  debug = TRUE,
  sep = ",")

g1data <- loadObject("g1_data.Rdata")
sumSpectra(g1data)
spectraplot <- plotSpectra(g1data, which = c(1, 2, 3, 4, 5, 6, 7, 8, 9, 10),
                           yrange = c(-0.1, 0.1))
spectraplot

g1_base <- baselineSpectra(g1data, int = FALSE, method = "modpolyfit", retC = TRUE)

p1.1 <- surveySpectra(g1_base, method = "iqr", by.gr = FALSE)
p1.1

p1.2 <- p1.1 + ggtitle("Detail of Carbonyl Region") + coord_cartesian(xlim = c(1600, 1800))
p1.2

p1.2a <- p1.1 + ggtitle("Detail of 1000") + coord_cartesian(xlim = c(1000, 1200))
```

```
p1.2a


p1.3 <- p1.1 + ggtitle("Detail of OH Region") + coord_cartesian(xlim = c(3000, 3600))
p1.3

p1.4 <- p1.1 + ggtitle("Detail of 2000 Region") + coord_cartesian(xlim = c(2800, 3000))
p1.4

p1.5 <- surveySpectra(g1_base, int = "iqr", by.gr = TRUE)
p1.5a <- p1.5 + coord_cartesian(xlim = c(1600, 1800))
p1.5a

p1.5b <- p1.5 + coord_cartesian(xlim = c(3000, 3500))
p1.5b

p1.5c <- p1.5 + coord_cartesian(xlim = c(2800, 3000))
p1.5c

HCA <- hcaSpectra(g1_base)

c_g1 <- c_pcaSpectra(g1_base, choice = "noscale")
p1.7 <- plotScores(g1_base, c_g1, pcs = c(1,2), ellipse = "rob", tol = 1)
p1.7

r_g1 <- r_pcaSpectra(g1_base, choice = "noscale")
p1.8 <- plotScores(g1_base, r_g1, pcs = c(1,2), ellipse = "both", tol = 1)
p1.8

p1.9 <- plotScree(c_g1)
p1.9

p1.10 <- plotScree(r_g1)
p1.10

p1.11 <- plotLoadings(g1_base, c_g1, loads = c(1,2), ref = 1)
p1.11

p1.12 <- sPlotSpectra(g1_base, c_g1, pc = 1, tol = .001)
p1.12

library(baseline)
library(base)
library(R.utils)
library(ChemoSpec)
library(ChemoSpecUtils)
```

```
library(dbplyr)
library(knitr)
library(readr)
library(readxl)
library(tidyverse)
library(tidyselect)
library(tidyr)
library(amap)
library(robustbase)
library(pcaPP)

setwd("/Volumes/GoogleDrive/My Drive/Sorp_Data/Paper/FTIR copy/Group2use")

g2 <- files2SpectraObject(
  gr.crit = c("DI", "Ca"),
  gr.cols = c("black", "darkgray"),
  freq.unit = "Wavenumber",
  int.unit = "abosrbance",
  descrip = "no description provided",
  fileEXT = "\\.(csv|CSV)$",
  out.file = "g2_data",
  header = TRUE,
  debug = TRUE,
  sep = ",")

g2data <- loadObject("g2_data.Rdata")
sumSpectra(g2data)
spectraplot2 <- plotSpectra(g2data, which = c(1, 2, 3, 4, 5, 6, 7, 8, 9, 10, 11),
                            yrange = c(-0.1, 0.1))
spectraplot2

g2_base <- baselineSpectra(g2data, int = FALSE, method = "modpolyfit", retC = TRUE)

spectraplot3 <- plotSpectra(g2_base, which = c(1, 2, 3, 4, 5, 6, 7, 8, 9, 10, 11),
                            yrange = c(0, 0.035))
spectraplot3

p2.1 <- surveySpectra(g2_base, method = "iqr", by.gr = FALSE)
p2.1

p2.2 <- p2.1 + ggtitle("Detail of Carbonyl Region") + coord_cartesian(xlim = c(1600, 1800))
p2.2

p2.2a <- p2.1 + ggtitle("Detail of 1000") + coord_cartesian(xlim = c(1000, 1200))
p2.2a
```

```
p2.3 <- p2.1 + ggtitle("Detail of OH Region") + coord_cartesian(xlim = c(3000, 3600))
p2.3

p2.4 <- p2.1 + ggtitle("Detail of 2000 Region") + coord_cartesian(xlim = c(2800, 3000))
p2.4

p2.5 <- surveySpectra(g2_base, int = "iqr", by.gr = TRUE)
p2.5a <- p2.5 + coord_cartesian(xlim = c(1600, 1800))
p2.5a

p2.5b <- p2.5 + coord_cartesian(xlim = c(3000, 3500))
p2.5b

p2.5c <- p2.5 + coord_cartesian(xlim = c(2800, 3000))
p2.5c

HCA <- hcaSpectra(g2_base)

c_g2 <- c_pcaSpectra(g2_base, choice = "noscale")
p2.7 <- plotScores(g2_base, c_g2, pcs = c(1,2), ellipse = "rob", tol = 1)
p2.7

r_g2 <- r_pcaSpectra(g2_base, choice = "noscale")
p2.8 <- plotScores(g2_base, r_g2, pcs = c(1,2), ellipse = "both", tol = 1)
p2.8

p2.9 <- plotScree(c_g2)
p2.9

p2.10 <- plotScree(r_g2)
p2.10

p2.11 <- plotLoadings(g2_base, c_g2, loads = c(1,2), ref = 1)
p2.11

p2.12 <- sPlotSpectra(g2_base, c_g2, pc = 1, tol = .001)
p2.12
```